INFORMATION TO USERS

The most advanced technology has been used to photograph and reproduce this manuscript from the microfilm master. UMI films the text directly from the original or copy submitted. Thus, some thesis and dissertation copies are in typewriter face, while others may be from any type of computer printer.

The quality of this reproduction is dependent upon the quality of the copy submitted. Broken or indistinct print, colored or poor quality illustrations and photographs, print bleedthrough, substandard margins, and improper alignment can adversely affect reproduction.

In the unlikely event that the author did not send UMI a complete manuscript and there are missing pages, these will be noted. Also, if unauthorized copyright material had to be removed, a note will indicate the deletion.

Oversize materials (e.g., maps, drawings, charts) are reproduced by sectioning the original, beginning at the upper left-hand corner and continuing from left to right in equal sections with small overlaps. Each original is also photographed in one exposure and is included in reduced form at the back of the book.

Photographs included in the original manuscript have been reproduced xerographically in this copy. Higher quality 6" x 9" black and white photographic prints are available for any photographs or illustrations appearing in this copy for an additional charge. Contact UMI directly to order.

UMI

University Microfilms International
A Bell & Howell Information Company
300 North Zeeb Road, Ann Arbor, MI 48106-1346 USA
313/761-4700 800/521-0600

Order Number 9103019

Controlling a large flexible structure to mimic a rigid one

Lin, Yeong Ching, Ph.D.

The University of Arizona, 1990

U·M·I

300 N. Zeeb Rd.
Ann Arbor, MI 48106

CONTROLLING A LARGE FLEXIBLE STRUCTURE TO MIMIC A RIGID ONE

by

Yeong Ching Lin

A Dissertation Submitted to the Faculty of the

AEROSPACE AND MECHANICAL ENGINEERING DEPARTMENT

In Partial Fulfillment of the Requirements
For the Degree of

DOCTOR OF PHILOSOPHY

WITH A MAJOR IN MECHANICAL ENGINEERING

In the Graduate College

THE UNIVERSITY OF ARIZONA

1 9 9 0

THE UNIVERSITY OF ARIZONA
GRADUATE COLLEGE

As members of the Final Examination Committee, we certify that we have read the dissertation prepared by Yeong Ching Lin

entitled CONTROLLING A LARGE FLEXIBLE STRUCTURE TO MIMIC A RIGID ONE

and recommend that it be accepted as fulfilling the dissertation requirement for the Degree of Doctor of Philosophy.

Thomas L. Vincent	July 20, 1990 Date
Ara Arabyan	July 20, 1990 Date
Hal S. Tharp	July 20, 1990 Date
	Date
	Date

Final approval and acceptance of this dissertation is contingent upon the candidate's submission of the final copy of the dissertation to the Graduate College.

I hereby certify that I have read this dissertation prepared under my direction and recommend that it be accepted as fulfilling the dissertation requirement.

Dissertation Director	Aug 1, 1990 Date

STATEMENT BY AUTHOR

This dissertation has been submitted in partial fulfillment of requirements for an advanced degree at The University of Arizona and is deposited in the University Library to be made available to borrowers under rules of the Library.

Brief quotations from this dissertation are allowable without special permission, provided that accurate acknowledgement of source is made. Requests for permission for extended quotation from or reproduction of this manuscript in whole or in part may be granted by the head of the major department or the Dean of the Graduate College when in his or her judgment the proposed use of the material is in the interests of scholarship. In all other instances, however, permission must be obtained from the author.

SIGNED: 

DEDICATION

To my parents, Chin Kuei Lin and Yuh Lain Lai

ACKNOWLEDGEMENTS

I wish to express my sincere appreciation to my dissertation director, Professor Thomas L. Vincent, for his advice and guidance regarding both research and professional development throughout the entire period of this study, and for the opportunity to work at the Control Research Laboratory.

I also wish to thank the other members of the examining committee, Dr. Parviz E. Nikravesh, Dr. Ara Arabyan, Dr. Ralph M. Richard and Dr. Donald DaDeppo, for their review of this dissertation. I am especially thankful to Honeywell Inc. for supporting this dissertation.

For many helpful discussions, and for their comments, I would like to thank the members of the Control Laboratory, Zong Yeng Wu, Richard Wilson, Mike R. Hill, Jim Coleman and Christopher J. Comp.

A special thanks to my parents, Chin Kuei Lin and Yuh Lain Lai, and my family for their support and encouragement over these years of graduate study.

TABLE OF CONTENTS

LIST OF ILLUSTRATIONS

LIST OF ILLUSTRATIONS—Continued

LIST OF ILLUSTRATIONS—Continued

LIST OF ILLUSTRATIONS—Continued

LIST OF ILLUSTRATIONS—Continued

LIST OF TABLES

ABSTRACT

Analytical and experimental comparisons are presented for two control laws used in a laboratory structure designed to simulate large space structures. The proposed control laws are based on minimizing the amount of energy imparted to the flexible modes during the maneuver. Structure modeling and various control techniques are discussed. In the proposed modeling procedure, the finite element method is used to describe the equations of motion for a given structure. The main objective of the analysis is to determine optimal actuator locations and the command forces to the actuators such that the structure will follow a desired trajectory while minimizing the internal energy to the flexible modes. The numerical simulations are verified experimentally using a digital implementation of the control laws. Critical issues related to experimental implementation are discussed. A closed-loop control system design which will take care of nonlinearities and uncertain inputs is included in this dissertation.

CHAPTER 1
INTRODUCTION

1.1. Overview

Positioning a flexible structure, such as a space telescope, will generally excite unwanted flexible modes in the structure. Recently, many control systems have been developed for flexible structures to handle the attitude and shape control problems [1-15]. Most control system designs are based on state variable feedback methods or modern control techniques which are generated without regard to the locations of the actuators. No one has yet proposed a general procedure for determining the optimal locations and command forces for a given number of actuators. Also it has been shown that traditional state variable feedback methods may not be satisfactory when applied to the positioning of flexible structures [3, 4]. The objective of this dissertation is to investigate a control design philosophy which, for a given number of actuators, will allow for the positioning of a flexible structure with minimum excitation of internal flexible energy [5].

The control design presented here is based on the modal analysis of a flexible structure which determines actuator locations and open-loop control forces needed to produce the desired motion. An open-loop design based on the modal analysis is more effective for positioning since it is used to determine the actuator location and the open-loop control force that minimizes the amount of energy going into the flexible modes. Indeed, if it is possible to position the flexible structure so that no energy goes into the flexible modes, the flexible structure will behave as a rigid

one. The problem as formulated here is non-traditional since the location of the actuators is considered to be part of the total control design.

The theoretical procedure is described as follows. Since a flexible structure is a continuous system, it will have an infinite number of flexible modes. By modeling the flexible structure in terms of a finite number of differential equations, one will be approximating the continuous system in terms of a finite number of modes which are based on small deflection and small rotation with respect to the neutral surface. The degree of accuracy depends on the order of the model. Suppose, for example, the model has r rigid body modes and f flexible modes. Then, in order to arbitrarily position the structure, at least r actuators are needed. With only r actuators used to position the structure, there will be some spillover into the flexible energy in the system. In order to avoid this with the r + f degree of freedom system, one could use r + f actuators to move the system as a rigid body; hence, no energy would be imparted into flexible modes. The model becomes more accurate as f $\rightarrow \infty$, but this would be an impractical way of removing all of the flexible energy. However, this procedure does suggest a practical way of eliminating a large portion of the imparted flexible energy associated with positioning the structure. In particular, using r + q (where $q < f$) actuators as will be demonstrated here, it is possible to either suppress q flexible body modes or to suppress a combination of modes so as to minimize total flexible energy input. A procedure is developed to select actuator location and force input such that either selective modes are suppressed or the amount of flexible energy is minimized.

A flexible structure is considered to be an m% mimic of a rigid one if less than (100 − m)% of the energy used to position the structure goes into the flexible

modes. The main objective is to make m as large as possible for a given number of actuators and positioning requirement.

Applications of such a control philosophy are numerous. For example, power and weight factors for flexible structures, such as satellites and space stations, are critical. Those structures could be built using lighter and more flexible materials and still behave as nearly rigid bodies under this control technology. In industry, current control techniques require very rigid structures which in turn require massive and powerful components and drivers. Lighter, more flexible structures could perform the same manufacturing tasks cheaper and more efficiently using the control design philosophy presented here.

In this work, the problem of actuator-placement optimization will be discussed in detail. Two optimization criteria will be considered, each reflecting the energy remaining in the system after an open-loop control. In addition, the impact of modal truncation on the actuator-placement problem is considered.

The advantages of the approach are demonstrated by a one-dimensional spring-mass system in Chapter 2. The basic concepts are introduced and the importance of actuator placement is demonstrated. Also the proposed method is compared with a classical approach based on linear-quadratic design. The methods developed are comparatively simple to use and implement.

In Chapter 3, the theoretical development for a three dimensional structure is discussed. In this chapter the optimal locations of actuators and the command forces for any given flexible structure are obtained. Here the solutions for large rotational motion is not provided. In order to satisfy linear elastic theory the

proposed methods must be applied only to systems where the nonlinear effect is small. For nonlinear systems, the proposed method is still valid, but an extra controller is needed to take care of the nonlinearity.

The optimal procedure for determining the actuator-placement and control forces to position a thin plate is presented in Chapter 4. An example introduces the modeling of a continuous structure by the finite element method. The procedure developed in Chapter 3 is used to determine the optimal locations of actuators.

An experimental comparison of the results obtained in Chapter 4 is given in Chapter 5. The experimental setup is discussed and experimental results are compared with computer simulations.

In Chapter 6, a summary of the work and conclusions are given. Several methods to deal with uncertainty are discussed. Some prospective research topics are also stated.

1.2. Background

The location of actuators for the control of flexible structures remains an important question which has received much attention in the last decade. The approaches to resolving the problem are nearly as numerous as the investigators who have addressed it [10-26]. But as yet, a general procedure to determine the placement of actuators and corresponding command forces for each actuator has not been developed.

Juang and Rodriguez (1979) proposed choosing actuator locations to minimize a quadratic performance functional based on the steady state solution of the

optimal control. Aidarous and Gevers (1976) obtained optimal actuator placement solutions by optimizing locations after obtaining an optimal feedback control law which depends on the actuator locations. The common method to determine the actuator locations presented by these authors can be described as follows: consider a system with dimension n, which is governed by a set of ordinary differential equations of the form

$$\mathbf{M}\ddot{\mathbf{q}}(t) + \mathbf{K}\mathbf{q}(t) = \mathbf{U}(t) \tag{1.1}$$

where $\mathbf{M}$ and $\mathbf{K}$ are mass and stiffness matrices respectively and $\mathbf{U}(t)$ is the generalized force vector. Equation (1.1) can also be represented by a standard form

$$\dot{\mathbf{x}} = \mathbf{A}\mathbf{x}(t) + \mathbf{B}\mathbf{u}(t), \tag{1.2}$$

where

$$\mathbf{x} = \begin{bmatrix} \mathbf{q} \\ \dot{\mathbf{q}} \end{bmatrix}.$$

We wish to choose $\mathbf{u}(t)$ so as to minimize the cost criterion:

$$J = \int_0^\infty (\mathbf{x}^T\mathbf{Q}\mathbf{x} + \mathbf{u}^T\mathbf{R}\mathbf{u})dt, \tag{1.3}$$

where $\mathbf{Q}$ is an arbitrary positive semidefinite matrix, and $\mathbf{R}$ is an arbitrary positive definite matrix. Then the optimal control has a feedback form

$$\mathbf{u}(t) = -\mathbf{R}^{-1}\mathbf{B}^{\mathrm{T}}\mathbf{K}(t)\mathbf{x}(t) \tag{1.4}$$

where

$$\dot{\mathbf{K}}(t) = -\mathbf{K}\mathbf{A} - \mathbf{A}^{\mathrm{T}}\mathbf{K} + \mathbf{K}\mathbf{B}\mathbf{R}^{-1}\mathbf{B}^{\mathrm{T}}\mathbf{K} - \mathbf{Q}. \tag{1.5}$$

It is apparent from (1.5) that the actuator location information, inherent in $\mathbf{B}$, influences the optimal control law described by (1.4).

The method outlined above requires solving a single 2n×2n Riccati equation (1.5). The optimal solution will be obtained after the model is simulated under different combinations of **B**. To avoid solving a 2n×2n Riccati equation, Baruh and Meirovitich [25, 26] found that by use of a design technique known as Independent Modal Space Control (IMSC), the actuator locations have no influence on the feedback control law. They suggest that the actuator location is therefore unimportant when IMSC is used.

The IMSC approach has a significantly smaller computational requirement, since it requires the solution of n decoupled 2×2 Riccati equations rather than 2n×2n Riccati equations. They suggest that each mode can be controlled by one actuator. This has raised some serious questions [4] such as how many actuators need be used to control an n dimensional system and how to choose **Q** and **R** to obtain an optimal solution. Also, when the control forces are bounded, the system stability is not guaranteed. Besides, the optimal solution is changed by choosing different cost criterions.

These approaches [6-26] focus on trying different cost functions. This only allows for a comparison of different locations, it does not solve the actuator-placement problems. To position a flexible structure by means of actuators, three main problems must be solved: (1) how many actuators should be used, (2) where they should be placed, and (3) what control law should be used.

1.3. Design Concepts

The location of the actuators on a flexible structure is important because poor location of actuators will result in an unnecessary amount of energy in the

flexible modes after the maneuver takes place. Then it takes more time to damp out the internal energy remaining in the system. The proposed control design minimizes not only the time required to maneuver the structure to a target, but also the amount of energy imparted to the flexible modes during the large motion.

The total time required to perform the maneuver represents one of the primary performance requirements to be satisfied by the control design. According to the maximum principle, one can show that the quickest way to perform a rigid body slew maneuver is with bang-bang control [2-5, 20-22]. With large control forces, the slew is quick, but large forces may impart an excessive amount of energy into the flexible modes. Therefore, a tradeoff exists between maneuvering time and energy imparted to the flexible modes.

Figure 1.1 illustrates a possible slew control system design [3, 4, 20-26]. The open-loop command is used in conjunction with a closed-loop control. The sensors and actuators are collocated. A maneuvering command force designed to position an equivalent rigid body to a final specified configuration is applied in an open-loop mode. In addition, a closed-loop control force is applied to provide damping and precise positioning during the maneuver, as well as to facilitate settling of vibratory motion after the completion of the slew maneuver. The command signal for the feedback loop controller is the rigid body response corresponding to the positions where the sensors are located. Thus, the error signal in this phase is the difference between the calculated rigid body displacements and velocities and the actual displacements and velocities at the positions where the sensors are located.

This project focuses on the open-loop design which involves the location of actuators and the command forces [5] rather than on the closed-loop controller design, which will be discussed in the last chapter.

In summary, the basic idea for designing the open-loop controller is to first obtain an open-loop control law which would properly position the structure as if it were indeed a rigid body. If the location of each actuator and the command of each is calculated correctly, then the more actuators used, the less energy imparted to the flexible modes.

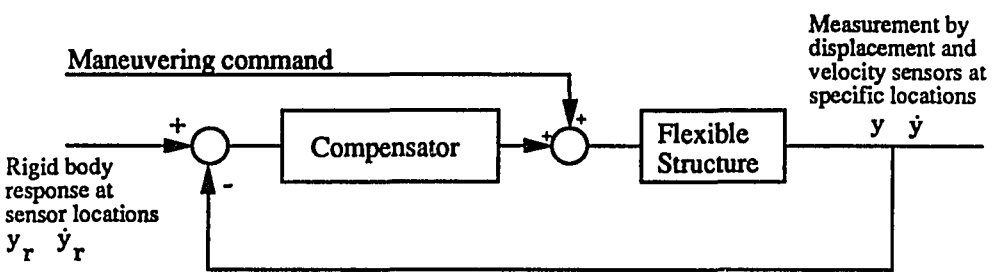

Figure 1.1 Slew Control System.

CHAPTER 2
ONE DIMENSIONAL PROBLEM - SPRING MASS SYSTEMS

In this chapter, an alternate approach to the design of controllers for positioning and damping of a simple spring-mass system will be introduced. The approach taken is to design a controller which uses open-loop positioning followed by closed-loop control for damping. By doing so, we can avoid the conflicting requirements problem associated with traditional state variable feedback design. The open-loop portion of the control is based on optimal control theory, which allows for control saturation. In particular, during this phase of the control, the time to position is minimized. This results in a bang-bang type of control. Once the system has been positioned, the controller switches to a closed-loop phase. The particular closed-loop control used here is based on energy methods and is not a full state variable feedback design. The method is illustrated using a low-order spring-mass example, and the results are compared with an LQ (linear-quadratic) design [2-4].

2.1. Equations of Motion

Consider the four mass-spring flexible system shown in Figure 2.1. The masses, connected by linear springs, are strung on a frictionless rod which may rotate at an angular rate of ω relative to an inertial frame. The system is to be moved to the right 5 meters along the rod, resulting in the same rest configuration within one second. The open-loop maneuvering command input for each of the following cases will be such that an equivalent rigid body would be positioned according to the above specifications. The cases considered below assume $\omega = 0$.

According to the Newton's law, the equations of motion for this system can be written as

$$\mathbf{M}\ddot{\mathbf{y}} + \mathbf{K}\mathbf{y} = \mathbf{B}\mathbf{u}, \tag{2.1}$$

where $\mathbf{y} = [y_1, y_2, y_3, y_4]^T$ is a 4-dimensional generalized displacement vector, $\mathbf{u} = [u_1, u_2, u_3, u_4]^T$ is a 4-dimensional control vector, $\mathbf{M}$ is a diagonal mass matrix of the form

$$\mathbf{M} = \begin{bmatrix} 0.01 & 0.00 & 0.00 & 0.00 \\ 0.00 & 0.02 & 0.00 & 0.00 \\ 0.00 & 0.00 & 0.01 & 0.00 \\ 0.00 & 0.00 & 0.00 & 0.01 \end{bmatrix},$$

$\mathbf{K}$ is a symmetric stiffness matrix of the form

$$\mathbf{K} = \begin{bmatrix} 2.00 & -1.00 & -1.00 & 0.00 \\ -1.00 & 2.00 & -1.00 & 0.00 \\ -1.00 & -1.00 & 3.00 & -1.00 \\ 0.00 & 0.00 & -1.00 & 1.00 \end{bmatrix},$$

and $\mathbf{B}$ is a diagonal actuator placement matrix of the form

$$\mathbf{B} = \begin{bmatrix} b_1 & 0 & 0 & 0 \\ 0 & b_2 & 0 & 0 \\ 0 & 0 & b_3 & 0 \\ 0 & 0 & 0 & b_4 \end{bmatrix}.$$

The control input to the system will be by means of actuators located on the various masses. The placement matrix $\mathbf{B}$ is used to specify whether an actuator is located on a particular mass or not. In particular, b_i will have the value of zero or one. If $b_i = 0$, then there is no actuator on mass i. The actuators are assumed to produce generalized forces subject to control bounds of the form

$$|u_i| \leq 1.0, \qquad i = 1, 2, 3, 4. \tag{2.2}$$

The control law for the actuator is chosen to satisfy the minimum time control law for a rigid body of mass equal to the total mass of the system. This

results in bang-bang control with a minimum time of 1 second. For example, if $b_2 = 1$, then

$$u_2 = \begin{cases} 1 & \text{if } 0 \leq t \leq 0.5; \\ -1 & \text{if } 0.5 < t \leq 1.0; \\ 0 & \text{elsewhere.} \end{cases} \tag{2.3}$$

2.2. Computer Simulations

Now, we consider the response of the system under a single actuator located on mass 2 ($b_1 = 0, b_2 = 1, b_3 = 0, b_4 = 0$). Fig. 2.2(a) gives a graphic representation of the vibrations of each mass about the respective target positions. Fig. 2.2(b) illustrates the time history of the energy in the system. It is clear that some elastic energy remains in the system after the slew has been applied. The total energy in the system is composed of rigid body energy E_r and elastic energy E_e. Note that the rigid body energy increases to a maximum and then decreases to zero as the control force switches sign. During this same time interval, the elastic energy varies with time until the end of the control cycle. After one second, the elastic energy remains constant.

Compare these results with another single-actuator design. Mass 4 is actuated by the same command force. Figures 2.3(a) and 2.3(b) show the displacement response of each of the masses and the energy time history. It is obvious that different positions of the actuator result in different response and system energy. Case 1 provides a better result than case 2 because the energy in the elastic modes is much less. As a matter of fact, it can be shown that case 1 is the best location and case 2 the worst when using only one actuator.

Consider now using two actuators with energy suppression as the criteria for determining the locations of actuators and the command forces for each actuator.

The method for determining the open-loop command forces will be discussed in Chapter 3. The actuators are placed on mass 2 and mass 4. The open loop command to each of the actuators must be recalculated so that the same rigid body result is obtained while giving minimum energy to the flexible modes. The optimum situation is when masses 2 and 4 are actuated with ± 0.7033 and ± 0.2967 Newtons respectively. Figures 2.4(a) and 2.4(b) represent the response of the system and the energy time history. We see that the oscillations about the final position are smaller. The final amount of elastic energy in the system after the maneuver is also considerably less. The procedure may be continued by using the same criteria to determine the location for 3 actuators. Here, masses 2, 3, 4 are actuated with ± 0.5882, ± 0.1661, and ± 0.2457 Newtons respectively. Figures 2.5(a) and 2.5(b) illustrate the response of the system and the energy history. It is obvious that 3 actuators give much better results than 2 actuators when the actuators are placed properly. Of course, when 4 actuators are used there is no flexible energy remaining in the system after the position takes place, as illustrated in Figures 2.6(a) and 2.6(b). For this case, the optimum situation is when all four masses are actuated with ± 0.2, ± 0.4, ± 0.2 and ± 0.2 Newtons respectively

We know we could move this system as a rigid body when four actuators are used. But this is not our design philosophy. We want to use less then 4 actuators and achieve the same performance. For example, we could use two actuators to maneuver the system and, when the system reached the desired position, we could use the closed-loop control to damp out the rest energy in the system. Consider two actuators located on mass 2 and mass 4. The open-loop forces are as described

above. The closed-loop feedback is of the form [2-4, 23, 24]

$$u_2 = -0.1\dot{y}_2 - 2(y_2 - 5)$$
$$u_4 = -0.1\dot{y}_1 \tag{2.3}$$

after the positioning phase took place. The results are illustrated in Figs. 2.7(a), (b), and (c). For this particular case, very little positioning control is needed. The majority of the control action is by the first actuator, as shown in Fig. 2.7(a), resulting in the damped response illustrated in Fig. 2.7(b), with the energy profile illustrated in Fig. 2.7(c). Note from Fig. 2.7(b) and Fig. 2.7(c) that only little energy remains in the system after 1 second and the system appears to be in steady state after about 2.0 seconds.

2.3. Linear-quadratic Design

We will compare the performance of the above controllers based on the LQ design. Since the LQ design approach does not specifically address the actuator location, we begin by assuming one controller on mass 2 and one on mass 4 ($b_1 = 0, b_2 = 1, b_3 = 0, b_4 = 1$). In order to apply the state space LQ method, we have to obtain the equivalent state space representation of (2.1). There will be 8 state variables, $\mathbf{x} = [x_1 \dots x_8]^T$. By letting $x_i = y_i$ and $x_{4+i} = \dot{y}_i$ for i=1,...,4, we have the system

$$\dot{\mathbf{x}} = \begin{bmatrix} \mathbf{0} & \mathbf{I_4} \\ -\mathbf{M}^{-1}\mathbf{K} & \mathbf{0} \end{bmatrix} \mathbf{x} + \begin{bmatrix} \mathbf{0} \\ \mathbf{M}^{-1}\mathbf{B} \end{bmatrix} \mathbf{u}. \tag{2.4}$$

To get a correspondence as close as possible between the LQ method used above, we take as the performance the sum of the total system energy and the total control action as follows [2-4]:

$$J = \int_0^\infty \{\mathbf{x}^T \begin{bmatrix} \mathbf{K} & \mathbf{0} \\ \mathbf{0} & \mathbf{M} \end{bmatrix} \mathbf{x} + {u_2}^2 + {u_4}^2\} dt. \tag{2.5}$$

Using standard techniques to solve the matrix Ricatti equation associated with this system yields a state variable feedback of the form

$$u_2 = \mathbf{h_1}^T\mathbf{x}, u_4 = \mathbf{h_2}^T\mathbf{x}, \tag{2.6}$$

where

$$\mathbf{h_1}^{\mathrm{T}} = [-.3221 \quad .7688 \quad -.6323 \quad .2677 \quad -.0344 \quad .2237 \quad -.0063 \quad .0136]$$

$$\mathbf{h_2}^{\mathrm{T}} = [.6275 \quad .2224 \quad -1.6873 \quad .8979 \quad .0011 \quad .0273 \quad -.0505 \quad .1667].$$

This yields a controlled system with closed-loop eigenvalues

$$\lambda_1 = -0.4560$$

$$\lambda_{2,3} = -1.7796 \pm 19.6541i$$

$$\lambda_{4,5} = -2.8980 \pm 14.9161i$$

$$\lambda_{6,7} = -5.9945 \pm 9.0582i$$

$$\lambda_8 = -6.0539.$$

In order to satisfy the maximum force requirement, the LQ control law as given by equation (2.6) is modified using saturation control of the form

$$\mathbf{u} = \begin{cases} -1 & \text{if } -\mathbf{h}^T\mathbf{x} < -1.0; \\ -\mathbf{h}^T\mathbf{x} & \text{if } |\mathbf{h}^T\mathbf{x}| \leq 1.0; \\ 1 & \text{if } -\mathbf{h}^T\mathbf{x} > 1.0. \end{cases} \tag{2.7}$$

This response of (2.4) under bounded control law (2.7) yields the response shown in Figs. 2.8(a), (b), (c). The response of the modified LQ controller compares favorably with the proposed open-loop + closed-loop design in that the system settles to the equilibrium position in about 3 seconds. However, if we choose $\mathbf{Q} = \mathbf{I}$, then Figs. 2.9(a), (b), (c) show the system reaches the equilibrium position in about 5 seconds.

2.4. Discussion

While this example illustrates that the two different control approaches can result in comparable performance, it should be noted that the overhead requirements in terms of state space information required for the LQ controller are much larger(8 state variables required versus 3). This difference in information requirements will increase with an increase in system complexity.

It has been shown that the control constraint imposes severe restrictions on the LQ design. Because the control forces are bounded, the system may become unstable [2, 3]. One way to avoid the saturating control obtained here would be to put a greater penalty on the use of control in the performance index (2.5). However, by so doing a larger time period is required before the system will settle to the steady state final position.

The simple spring-mass system considered here shows the advantages of the proposed control design. No state information is needed for the open-loop portion of the control. Nevertheless, employing internal energy suppression during this portion of the control results in reasonable positioning with less internal energy in the system than one would have otherwise. After the positioning phase, a closed-loop design based on internal energy dissipation results in an effective overall design. In particular, the amount of state information required to implement the controller is less than that required by other state space methods. This feature becomes even more pronounced as the dimension of the system is increased.

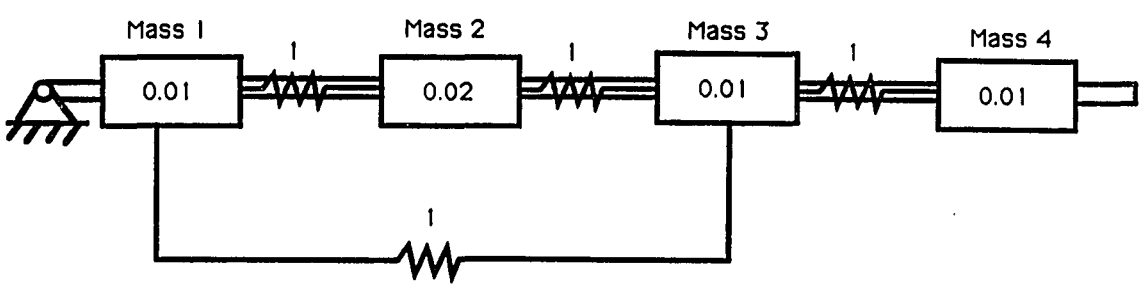

Figure 2.1 Spring-Mass Example

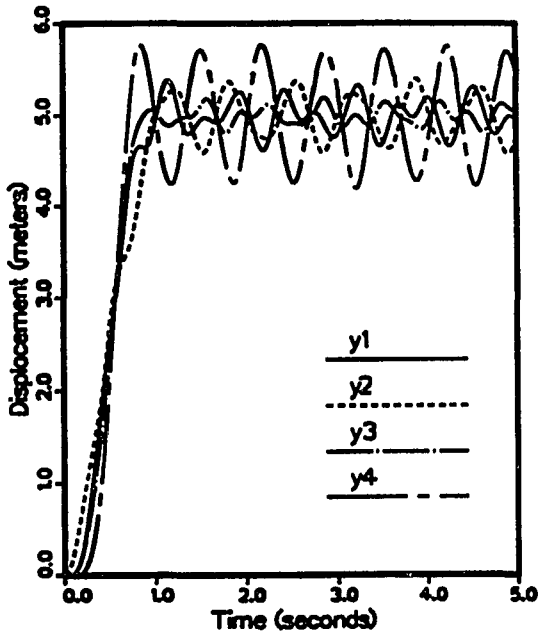

Figure 2.2(a) The Displacement Response When $b_2 = 1$

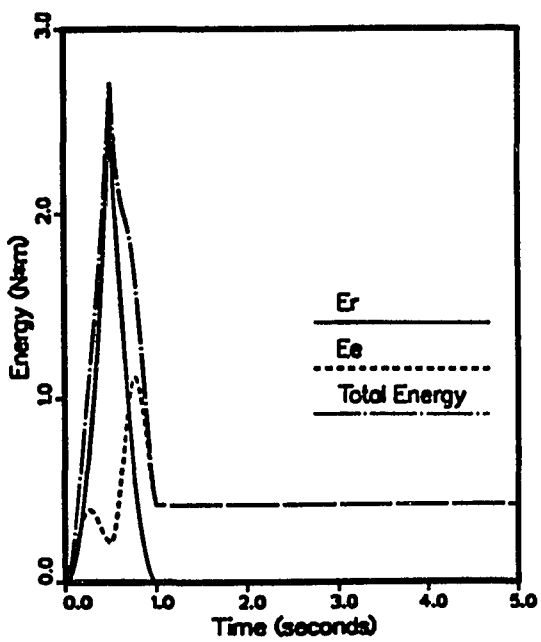

Figure 2.2(b) The Time History of the Energy When $b_2 = 1$

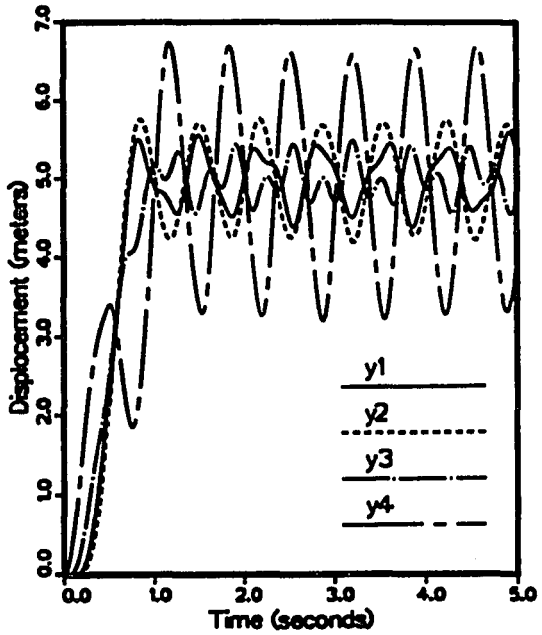

Figure 2.3(a) The Displacement Response When $b_4 = 1$

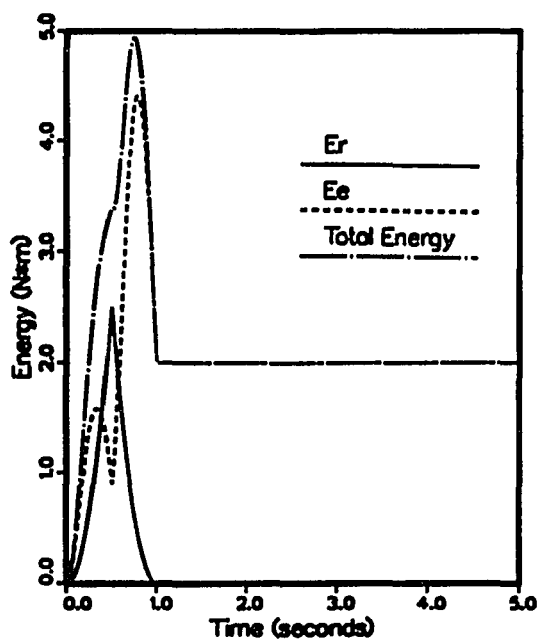

Figure 2.3(b) The Time History of the Energy When $b_4 = 1$

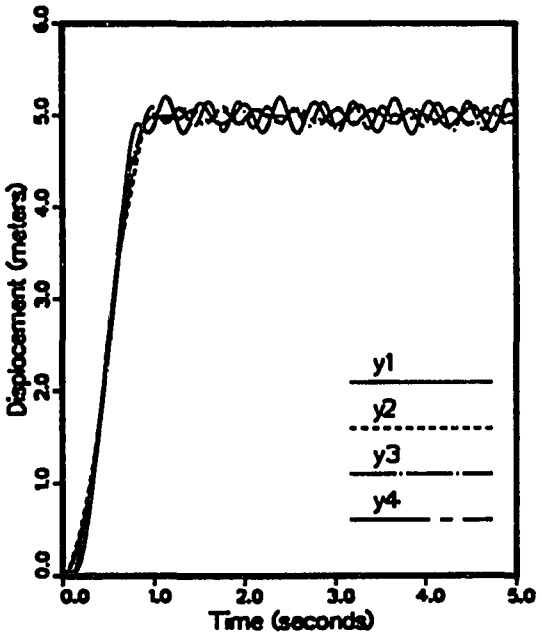

Figure 2.4(a) The Displacement Response When $b_2 = b_4 = 1$

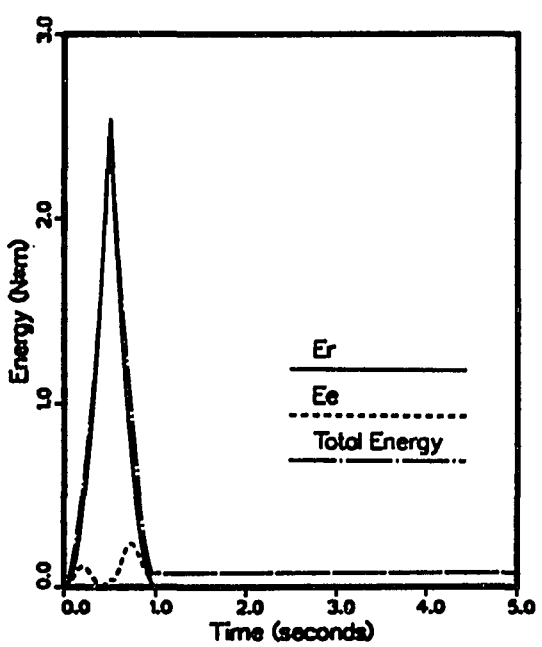

Figure 2.4(b) The Time History of the Energy When $b_2 = b_4 = 1$

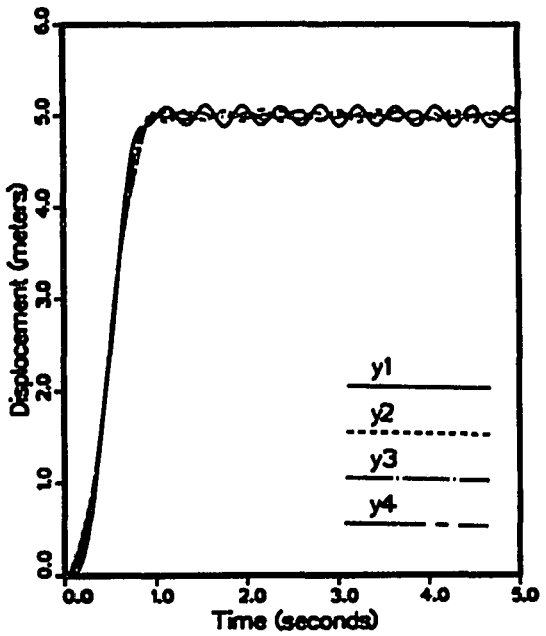

Figure 2.5(a) The Displacement Response When $b_2 = b_3 = b_4 = 1$

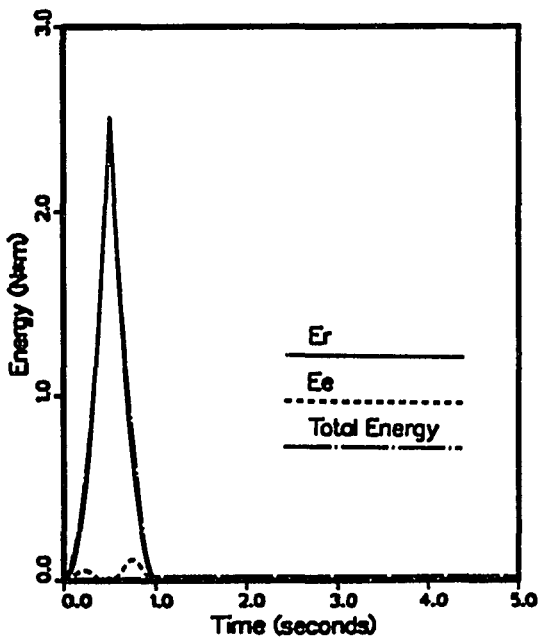

Figure 2.5(b) The Time History of the Energy

When $b_2 = b_3 = b_4 = 1$

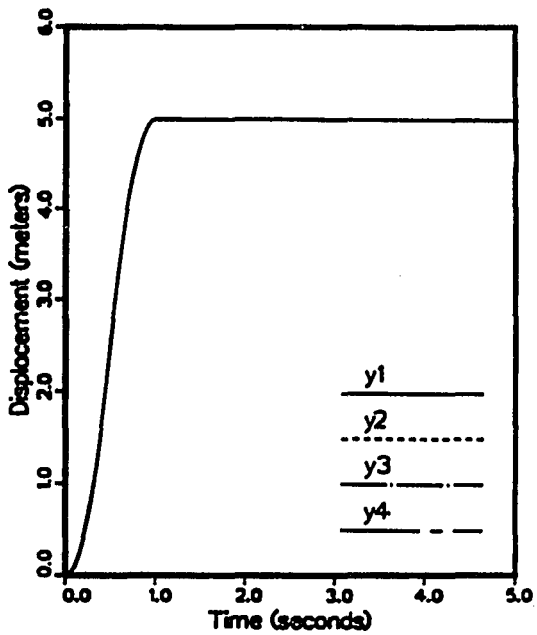

Figure 2.6(a) The Displacement Response

When $b_1 = b_2 = b_3 = b_4 = 1$

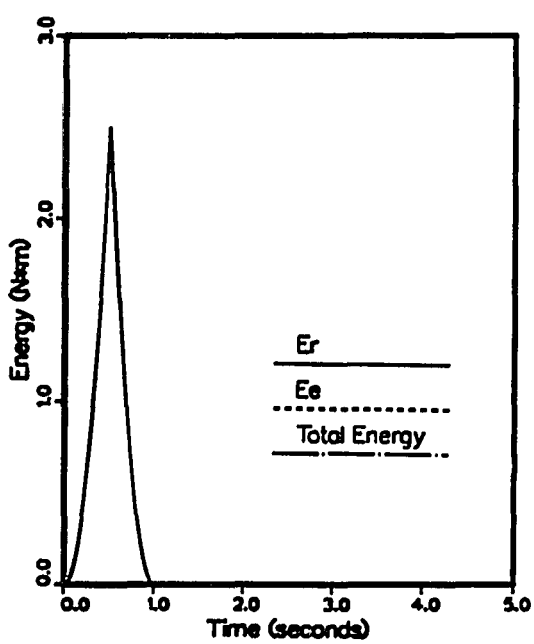

Figure 2.6(b) The Time History of the Energy

When $b_1 = b_2 = b_3 = b_4 = 1$

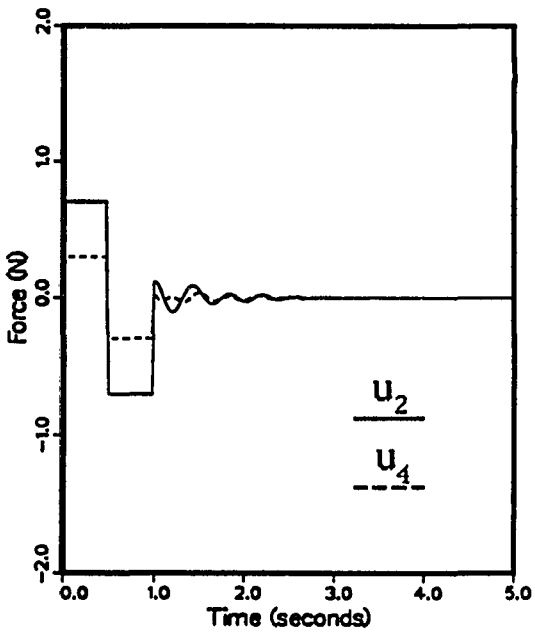

Figure 2.7(a) The Control forces Using Open-loop + Closed-loop Design

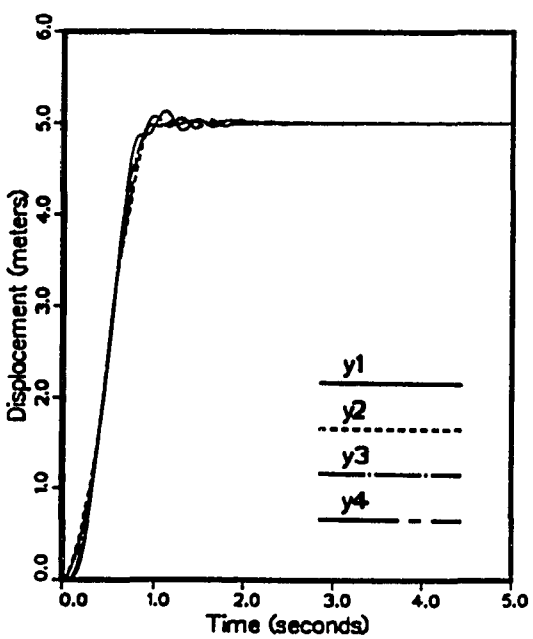

Figure 2.7(b) The Displacement Response Using Open-loop + Closed-loop Design

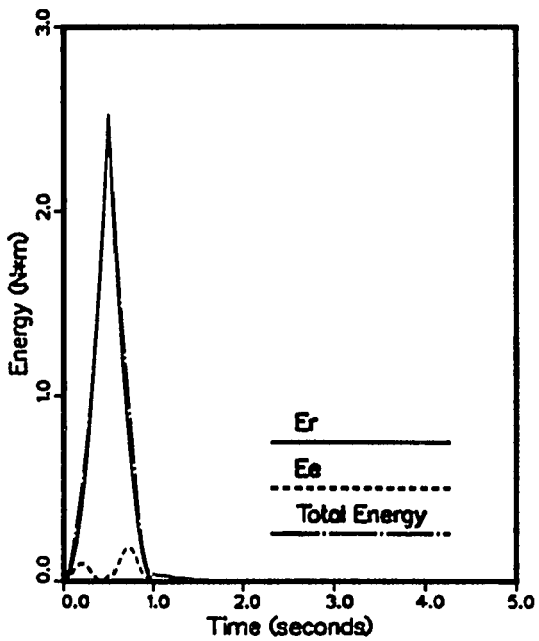

Figure 2.7(c) The Energy Profile Using Open-loop + Closed Design

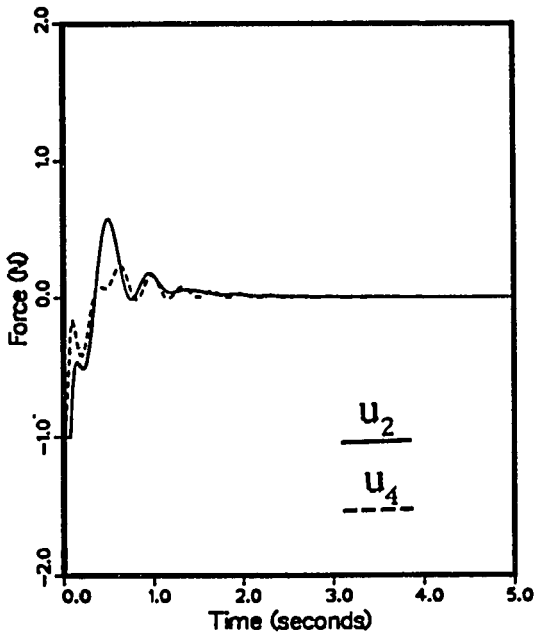

Figure 2.8(a) The Control Forces Using LQ Design

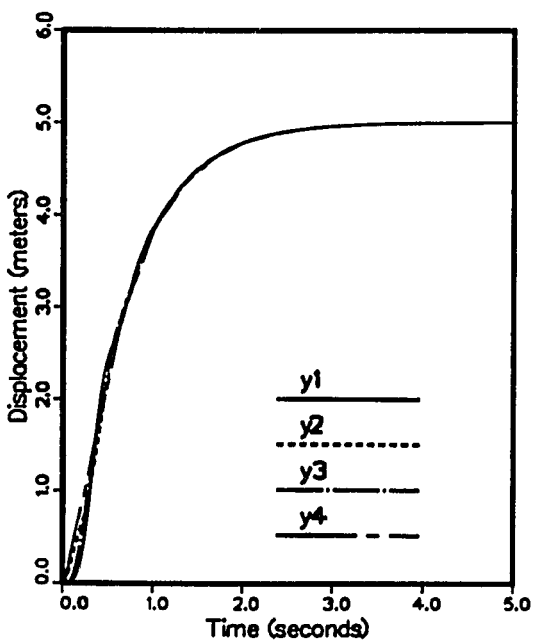

Figure 2.8(b) The Displacement Response Using LQ Design

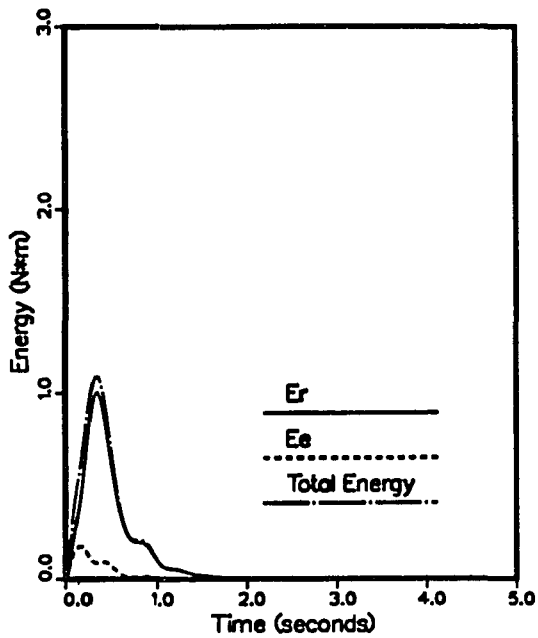

Figure 2.8(c) The Energy Profile Using LQ Design

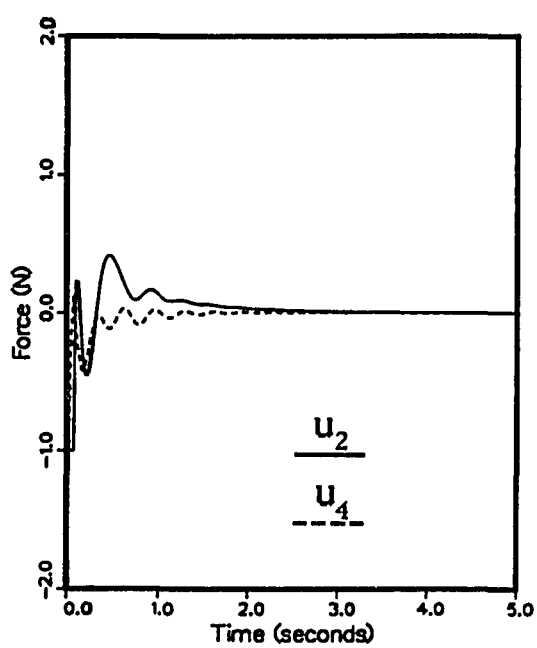

Figure 2.9(a) The Control Forces Using LQ Design (Q = I)

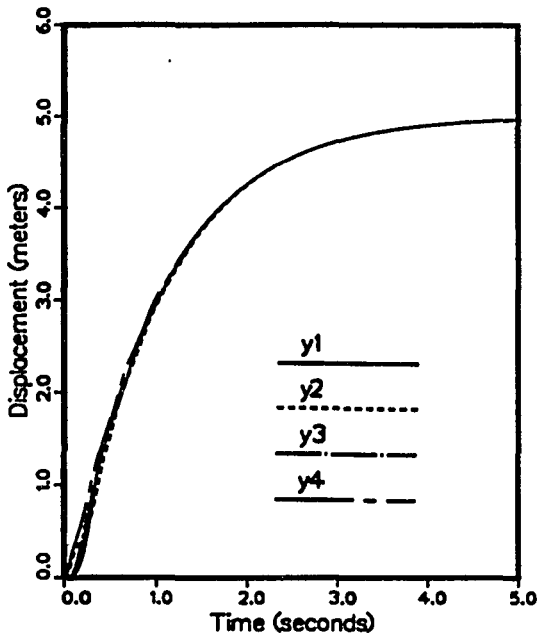

Figure 2.9(b) The Displacement Response Using LQ Design (Q = I)

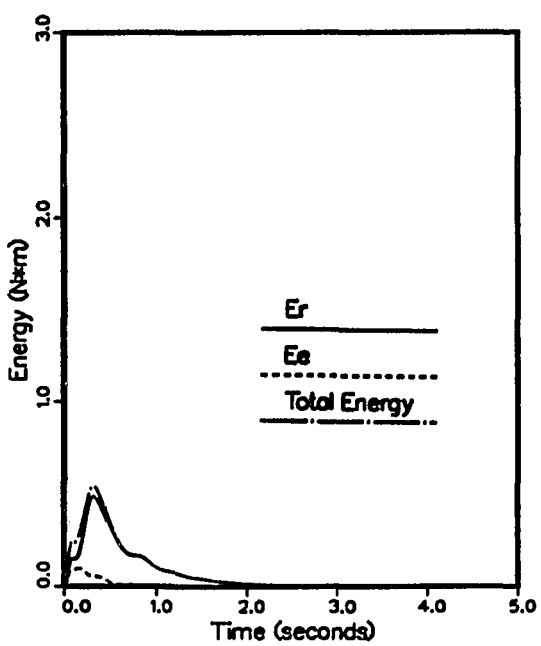

Figure 2.9(c) The Energy Profile Using LQ Design (Q = I)

CHAPTER 3
THEORETICAL DEVELOPMENTS

In this chapter a computational algorithm is presented. It is based on obtaining the optimal location of actuators and command forces in order to minimize energy imparted to the flexible modes. Both mode and energy suppression techniques will be used in the determination of the number, location, and the open-loop control law to be applied to each of the actuators.

3.1. Equations of Motion

Because it is very difficult to derive a closed form solution for a given structure, finite element analysis is used to obtain the stiffness and mass matrices of the structure. Let $\mathbf{q}$ be the total vector of independent coordinates or the degrees of freedom of the structure that includes 3 translations and 3 rotations. The motion of the flexible structure is governed by a set of second-order differential equations of motion that can be written in the following compact matrix form [32, 33]:

$$\mathbf{M}\ddot{\mathbf{q}} + \mathbf{K}\mathbf{q} = \mathbf{u} + \mathbf{v} + \mathbf{w} \tag{3.1}$$

where $\mathbf{M}$ is assumed to be a positive definite mass matrix associated with the independent coordinates, $\mathbf{K}$ is the system stiffness matrix. Both $\mathbf{M}$ and $\mathbf{K}$ may be time varying. The input $\mathbf{u}$ is the vector of generalized external forces associated with the independent coordinates, $\mathbf{v}$ is the quadratic velocity vector that includes the gyroscopic and Coriolis force components, and $\mathbf{w}$ is the closed loop control vector. When the slew motion is very slow, $\mathbf{v}$ is close to zero. The closed-loop control $\mathbf{w}$ will be used to eliminate $\mathbf{v}$ when $\mathbf{v}$ is large (i.e. ideally $\mathbf{v} + \mathbf{w} = \mathbf{0}$). The

following analysis is based on the assumption that $\mathbf{v}$ is close to zero. In order to simplify the procedure, we consider small translation and small rotation such that the mass matrix and stiffness matrix can be regarded as time independent matrices. The closed-loop control system design will be discussed in chapter 6.

The control inputs are the external forces supplied by force and/or torque actuators located on the various locations. The control force, u_i, will have a nonzero or zero value depending on whether actuators are located on node i or not. When $u_i \neq 0$, it implies the existence of an actuator, either force or torque, on node i. The control design process which follows could be used to determine values for the $u_i's$. The actuators are assumed to produce generalized forces which are bounded.

The general form of the matrix for a 6n-degree-of-freedom system is given by equation (3.1), where n is the total number of node points in the model. To uncouple the equations of motion represented by this equation, we start with the linear transformation

$$\mathbf{q} = \mathbf{\Phi z} \tag{3.2}$$

in which $\mathbf{\Phi}$ is the modal matrix. In this matrix, the columns are eigenvectors (mode shapes) and $\mathbf{z}$ is a vector of principal coordinates. Transforming equation (3.1) using (3.2), we obtain [32-35]

$$\mathbf{M\Phi\ddot{z} + K\Phi z = u}. \tag{3.3}$$

Premultiplying by $\mathbf{\Phi^T}$ yields

$$\mathbf{\bar{M}\ddot{z} + \bar{K}z = \Phi^T u}. \tag{3.4}$$

where

$$\mathbf{\bar{M} = \Phi^T M \Phi} \tag{3.5}$$

and

$$\bar{\mathbf{K}} = \mathbf{\Phi}^{\mathbf{T}}\mathbf{K}\mathbf{\Phi}. \tag{3.6}$$

The matrices $\bar{\mathbf{M}}$ and $\bar{\mathbf{K}}$ are diagonal matrices, hence, equation (3.4) is a decoupled system and **z** represents principal coordinates.

3.2. Suppression Methods

To determine the expanded form of the right-hand side of equation (3.4) for the ith mode equation, let us write the modal matrix $\mathbf{\Phi}$ for a 6n-degree-of-freedom system as

$$\mathbf{\Phi} = \begin{bmatrix} \phi_{11} & \phi_{12} & \cdots & \phi_{1m} \\ \phi_{21} & \phi_{22} & \cdots & \phi_{2m} \\ \vdots & \vdots & \ddots & \vdots \\ \phi_{m1} & \phi_{m2} & \cdots & \phi_{mm} \end{bmatrix} \tag{3.7}$$

where m = 6n. The value of the second subscript of $\mathbf{\Phi}$ denotes the column, or mode, number. For example, the first column is the eigenvector (mode shape) for the first mode. Therefore, equation (3.4) can be rewritten as [33]

$$\begin{aligned}
\bar{m}_1\ddot{z}_1 &= \phi_{11}u_1 + \phi_{21}u_2 + \ldots + \phi_{m1}u_m \\
\bar{m}_2\ddot{z}_2 &= \phi_{12}u_1 + \phi_{22}u_2 + \ldots + \phi_{m2}u_m \\
\bar{m}_3\ddot{z}_3 &= \phi_{13}u_1 + \phi_{23}u_2 + \ldots + \phi_{m3}u_m \\
\bar{m}_4\ddot{z}_4 &= \phi_{14}u_1 + \phi_{24}u_2 + \ldots + \phi_{m4}u_m \\
\bar{m}_5\ddot{z}_5 &= \phi_{15}u_1 + \phi_{25}u_2 + \ldots + \phi_{m5}u_m \\
\bar{m}_6\ddot{z}_6 &= \phi_{16}u_1 + \phi_{26}u_2 + \ldots + \phi_{m6}u_m \\
\bar{m}_7\ddot{z}_7 + \bar{k}_7z_7 &= \phi_{17}u_1 + \phi_{27}u_2 + \ldots + \phi_{m7}u_m \\
\bar{m}_8\ddot{z}_8 + \bar{k}_8z_8 &= \phi_{18}u_1 + \phi_{28}u_2 + \ldots + \phi_{m8}u_m \\
&\vdots \\
\bar{m}_m\ddot{z}_m + \bar{k}_mz_m &= \phi_{1m}u_1 + \phi_{2m}u_2 + \ldots + \phi_{mm}u_m
\end{aligned} \tag{3.8}$$

The first six equations in (3.8) correspond to the six rigid body modes and the remaining equations describe the elastic body modes. The number of equations depends on the number of nodes used in the finite element analysis.

Consider an idealized rigid structure of the same configuration with the same dimensions and mass as the flexible one. Displacement and rotation of this structure may be modeled by

$$\begin{aligned} m\ddot{x} &= F_x \\ m\ddot{y} &= F_y \\ m\ddot{z} &= F_z \\ I_x\dot{\omega}_x &= M_x \\ I_y\dot{\omega}_y &= M_y \\ I_z\dot{\omega}_z &= M_z \end{aligned} \tag{3.9}$$

where m is the total mass of the structure, I_x, I_y and I_z are the principal moments of inertia of the structure about the x, y and z axes through the center of mass of the structure and ω_x, ω_y, ω_z are the angular velocities with respect to the x, y, z axes. Here we assumed the gyroscopic and Coriolis forces are zero.

Since the flexible structure is to mimic a rigid one, we use equation (3.9) to determine F_x, F_y, F_z, M_x, M_y and M_z required to produce the desired positioning.

The corresponding control inputs to the actuators must satisfy

$$\begin{aligned} F_x &= \phi_{11}u_1 + \phi_{21}u_2 + \ldots + \phi_{m1}u_m \\ F_y &= \phi_{12}u_1 + \phi_{22}u_2 + \ldots + \phi_{m2}u_m \\ F_z &= \phi_{13}u_1 + \phi_{23}u_2 + \ldots + \phi_{m3}u_m \\ M_x &= \phi_{14}u_1 + \phi_{24}u_2 + \ldots + \phi_{m4}u_m \\ M_y &= \phi_{15}u_1 + \phi_{25}u_2 + \ldots + \phi_{m5}u_m \\ M_z &= \phi_{16}u_1 + \phi_{26}u_2 + \ldots + \phi_{m6}u_m \end{aligned} \tag{3.10}$$

Clearly, we must have six or more actuators. For example, suppose that u_2, u_{11}, u_{25}, u_{32}, u_{38} and u_{42} are selected to be nonzero. Then from equation (3.10) we have

$$\begin{aligned} F_x &= \phi_{21}u_2 + \phi_{11,1}u_{11} + \phi_{25,1}u_{25} + \phi_{32,1}u_{32} + \phi_{38,1}u_{38} + \phi_{42,1}u_{42} \\ F_y &= \phi_{22}u_2 + \phi_{11,2}u_{11} + \phi_{25,2}u_{25} + \phi_{32,2}u_{32} + \phi_{38,2}u_{38} + \phi_{42,2}u_{42} \\ F_z &= \phi_{23}u_2 + \phi_{11,3}u_{11} + \phi_{25,3}u_{25} + \phi_{32,3}u_{32} + \phi_{38,3}u_{38} + \phi_{42,3}u_{42} \\ M_x &= \phi_{24}u_2 + \phi_{11,4}u_{11} + \phi_{25,4}u_{25} + \phi_{32,4}u_{32} + \phi_{38,4}u_{38} + \phi_{42,4}u_{42} \\ M_y &= \phi_{25}u_2 + \phi_{11,5}u_{11} + \phi_{25,5}u_{25} + \phi_{32,5}u_{32} + \phi_{38,5}u_{38} + \phi_{42,5}u_{42} \\ M_z &= \phi_{26}u_2 + \phi_{11,6}u_{11} + \phi_{25,6}u_{25} + \phi_{32,6}u_{32} + \phi_{38,6}u_{38} + \phi_{42,6}u_{42} \end{aligned} \tag{3.11}$$

Provided an inverse exists for the matrix

$$\begin{bmatrix} \phi_{21} & \phi_{11,1} & \phi_{25,1} & \phi_{32,1} & \phi_{38,1} & \phi_{42,1} \\ \phi_{22} & \phi_{11,2} & \phi_{25,2} & \phi_{32,2} & \phi_{38,2} & \phi_{42,2} \\ \phi_{23} & \phi_{11,3} & \phi_{25,3} & \phi_{32,3} & \phi_{38,3} & \phi_{42,3} \\ \phi_{24} & \phi_{11,4} & \phi_{25,4} & \phi_{32,4} & \phi_{38,4} & \phi_{42,4} \\ \phi_{25} & \phi_{11,5} & \phi_{25,5} & \phi_{32,5} & \phi_{38,5} & \phi_{42,5} \\ \phi_{26} & \phi_{11,6} & \phi_{25,6} & \phi_{32,6} & \phi_{38,6} & \phi_{42,6} \end{bmatrix}, \tag{3.12}$$

we are able to solve for $u_2(t)$, $u_{11}(t)$, $u_{25}(t)$, $u_{32}(t)$, $u_{38}(t)$ and $u_{42}(t)$ to produce a motion in the structure. How well this mimics the desired rigid structure motion depends on the degree of flexibility of the actuator structure. Using only six actuators on a flexible structure will produce an m% mimic, with $m < 100$. The

value for m will depend on the location and type of actuators used. Clearly, using only six actuators, m would be maximized by considering all possible locations and actuator types. However, even under optimal actuator placement, additional and usually significant improvement can be obtained by increasing the number of actuators used. With additional actuators, we can either seek to suppress some flexible body modes or seek to minimize the amount of energy that goes into the flexible body modes.

3.2.1 Mode Suppression

Suppose, for example, that seven actuators are available for positioning a flexible structure. These control inputs are $u_2(t)$, $u_{11}(t)$, $u_{25}(t)$, $u_{32}(t)$, $u_{38}(t)$, $u_{42}(t)$, $u_{42}(t)$ and $u_{49}(t)$. We have

$$\begin{aligned}
F_x &= \phi_{21}u_2 + \phi_{11,1}u_{11} + \phi_{25,1}u_{25} + \phi_{32,1}u_{32} + \phi_{38,1}u_{38} + \phi_{42,1}u_{42} + \phi_{49,1}u_{49} \\
F_y &= \phi_{22}u_2 + \phi_{11,2}u_{11} + \phi_{25,2}u_{25} + \phi_{32,2}u_{32} + \phi_{38,2}u_{38} + \phi_{42,2}u_{42} + \phi_{49,2}u_{49} \\
F_z &= \phi_{23}u_2 + \phi_{11,3}u_{11} + \phi_{25,3}u_{25} + \phi_{32,3}u_{32} + \phi_{38,3}u_{38} + \phi_{42,3}u_{42} + \phi_{49,3}u_{49} \\
M_x &= \phi_{24}u_2 + \phi_{11,4}u_{11} + \phi_{25,4}u_{25} + \phi_{32,4}u_{32} + \phi_{38,4}u_{38} + \phi_{42,4}u_{42} + \phi_{49,4}u_{49} \\
M_y &= \phi_{25}u_2 + \phi_{11,5}u_{11} + \phi_{25,5}u_{25} + \phi_{32,5}u_{32} + \phi_{38,5}u_{38} + \phi_{42,5}u_{42} + \phi_{49,5}u_{49} \\
M_z &= \phi_{26}u_2 + \phi_{11,6}u_{11} + \phi_{25,6}u_{25} + \phi_{32,6}u_{32} + \phi_{38,6}u_{38} + \phi_{42,6}u_{42} + \phi_{49,6}u_{49}
\end{aligned} \tag{3.13}$$

Since there are more unknowns (the u_j's) in (3.13) than equations, we must impose additional requirements. In particular, if we wish to suppress all motion in the first flexible mode, we have the condition from (3.8) that is

$$0 = \phi_{27}u_2 + \phi_{11,7}u_{11} + \phi_{25,7}u_{25} + \phi_{32,7}u_{32} + \phi_{38,7}u_{38} + \phi_{42,7}u_{42} + \phi_{49,7}u_{49}. \tag{3.14}$$

Provided that an inverse exists for the matrix

$$\begin{bmatrix} \phi_{21} & \phi_{11,1} & \phi_{25,1} & \phi_{32,1} & \phi_{38,1} & \phi_{42,1} & \phi_{49,1} \\ \phi_{22} & \phi_{11,2} & \phi_{25,2} & \phi_{32,2} & \phi_{38,2} & \phi_{42,2} & \phi_{49,2} \\ \phi_{23} & \phi_{11,3} & \phi_{25,3} & \phi_{32,3} & \phi_{38,3} & \phi_{42,3} & \phi_{49,3} \\ \phi_{24} & \phi_{11,4} & \phi_{25,4} & \phi_{32,4} & \phi_{38,4} & \phi_{42,4} & \phi_{49,4} \\ \phi_{25} & \phi_{11,5} & \phi_{25,5} & \phi_{32,5} & \phi_{38,5} & \phi_{42,5} & \phi_{49,5} \\ \phi_{26} & \phi_{11,6} & \phi_{25,6} & \phi_{32,6} & \phi_{38,6} & \phi_{42,6} & \phi_{49,6} \\ \phi_{26} & \phi_{11,7} & \phi_{25,7} & \phi_{32,7} & \phi_{38,7} & \phi_{42,7} & \phi_{49,7} \end{bmatrix}, \tag{3.15}$$

we will be able to solve for the control inputs to not only produce the rigid body motion in the structure, but to suppress the first flexible mode as well.

A similar procedure may be used for a different number of actuators, actuator locations, and actuator types. For a fixed number of actuators and for the selected suppressed modes, the actuator types and locations can be optimized in order to maximize m.

Depending on design requirements, mode suppression may be a desirable feature. However, the mode suppression technique does not guarantee that m will be maximized subject to a given number of actuators. This is because a given mode suppression configuration may end up dumping energy into unsuppressed modes.

3.2.2 Flexible Energy Suppression

Instead of using a mode suppression technique, we can choose to minimize the energy imparted to the flexible modes of the structure. Before introducing the method of energy suppression, let us calculate the energy expression in terms of forces and spring constants in the flexible modes.

If we replace the right-hand side of the seventh through m equations of (3.8) with inputs f_7, f_8, ..., f_m,we obtain

$$\bar{m}_i\ddot{z}_i + \bar{k}_i z_i = f_i \qquad i = 7, 8, \ldots, m \tag{3.16}$$

where

$$f_i = \phi_{1i}u_1 + \phi_{2i}u_2 + \ldots + \phi_{mi}u_m. \tag{3.17}$$

Under a bang-bang control input f_i is given by

$$f_i = \begin{cases} A_i & \text{if } 0 \leq t \leq T; \\ -A_i & \text{if } T < t \leq 2T, \end{cases} \tag{3.18}$$

where 2T is the time interval of the open-loop phase. The energy after the slew in the ith mode can be calculated [5] by solving

$$E_i = \frac{2A_i^2}{\bar{k}_i}(1 - \cos\omega_i T)^2. \tag{3.19}$$

where ω_i is the undamped natural frequency of the ith mode. Let

$$\tilde{k}_i = \frac{\bar{k}_i}{2(1 - \cos\omega_i T)^2}. \tag{3.20}$$

This $\tilde{k}_i$ is called the modified spring constant.

Let each actuator input be a cosine function at frequency ω, i.e.

$$f_i = A_i \cos\omega t. \tag{3.21}$$

Then, the energy expression is given by [5]

$$E_i = \frac{A_i^2}{2\bar{k}_i[1 - (\frac{\omega}{\omega_i})^2]^2}[(\frac{\omega}{\omega_i}\sin\omega t - \sin\omega_i t)^2 + (\cos\omega_i t - \cos\omega t)^2]. \tag{3.22}$$

In this case, the modified spring constant can be written as

$$\tilde{k}_i = \frac{2\bar{k}_i[1-(\frac{\omega}{\omega_i})^2]^2}{[(\frac{\omega}{\omega_i}\sin\omega t - \sin\omega_i t)^2 + (\cos\omega_i t - \cos\omega t)^2]}. \tag{3.23}$$

Let each actuator input be a sine function at frequency ω, i.e.

$$f_i = A_i \sin\omega t. \tag{3.24}$$

Then, the energy expression is given by [5]

$$E_i = \frac{A_i^2}{2\bar{k}_i[1-(\frac{\omega}{\omega_i})^2]^2}[(\sin\omega t - \frac{\omega}{\omega_i}\sin\omega_i t)^2 + (\frac{\omega}{\omega_i})^2(\cos\omega_i t - \cos\omega t)^2]. \tag{3.25}$$

In this case, the modified spring constant can be written as

$$\tilde{k}_i = \frac{2\bar{k}_i[1-(\frac{\omega}{\omega_i})^2]^2}{[(\sin\omega t - \frac{\omega}{\omega_i}\sin\omega_i t)^2 + (\frac{\omega}{\omega_i})^2(\cos\omega_i t - \cos\omega t)^2]}. \tag{3.26}$$

We will confine our analysis to these three inputs. Under these inputs, it follows that the energy present in a given mode will be proportional to the square of the amplitude, A_i^2, divided by a modified spring constant, $\tilde{k}_i$.

This observation gives us a way of choosing the control inputs for actuators. For example, consider again the situation with seven actuators discussed above and suppose that we wish to minimize the energy going into the first five flexible modes. We can express this as

$$\text{min.} \qquad E = \frac{A_7^2}{\tilde{k}_7} + \frac{A_8^2}{\tilde{k}_8} + \frac{A_9^2}{\tilde{k}_9} + \frac{A_{10}^2}{\tilde{k}_{10}} + \frac{A_{11}^2}{\tilde{k}_{11}}, \tag{3.27}$$

where E is the energy in the first five flexible modes after the slew, subject to the constraints from equation (3.11). If we use a "bar" to denote the maximum amplitude of a constant, bang-bang, sine, or cosine varying function (e.g., F_y =

$\bar{F}_y \sin\omega t$, $u_i = \bar{u}_i \sin\omega t$), we may then write the constraints for minimizing (3.27) by first noting from our definition of f_i that we have

$$A_i = \phi_{1i}\bar{u}_1 + \phi_{2i}\bar{u}_2 + \ldots + \phi_{mi}\bar{u}_m, \qquad i = 7, \ldots, 11 \tag{3.28}$$

and from equation (3.13),

$$\begin{aligned}
\bar{F}_x &= \phi_{21}\bar{u}_2 + \phi_{11,1}\bar{u}_{11} + \phi_{25,1}\bar{u}_{25} + \phi_{32,1}\bar{u}_{32} + \phi_{38,1}\bar{u}_{38} + \phi_{42,1}\bar{u}_{42} + \phi_{49,1}\bar{u}_{49} \\
\bar{F}_y &= \phi_{22}\bar{u}_2 + \phi_{11,2}\bar{u}_{11} + \phi_{25,2}\bar{u}_{25} + \phi_{32,2}\bar{u}_{32} + \phi_{38,2}\bar{u}_{38} + \phi_{42,2}\bar{u}_{42} + \phi_{49,2}\bar{u}_{49} \\
\bar{F}_z &= \phi_{23}\bar{u}_2 + \phi_{11,3}\bar{u}_{11} + \phi_{25,3}\bar{u}_{25} + \phi_{32,3}\bar{u}_{32} + \phi_{38,3}\bar{u}_{38} + \phi_{42,3}\bar{u}_{42} + \phi_{49,3}\bar{u}_{49} \\
\bar{M}_x &= \phi_{24}\bar{u}_2 + \phi_{11,4}\bar{u}_{11} + \phi_{25,4}\bar{u}_{25} + \phi_{32,4}\bar{u}_{32} + \phi_{38,4}\bar{u}_{38} + \phi_{42,4}\bar{u}_{42} + \phi_{49,4}\bar{u}_{49} \\
\bar{M}_y &= \phi_{25}\bar{u}_2 + \phi_{11,5}\bar{u}_{11} + \phi_{25,5}\bar{u}_{25} + \phi_{32,5}\bar{u}_{32} + \phi_{38,5}\bar{u}_{38} + \phi_{42,5}\bar{u}_{42} + \phi_{49,5}\bar{u}_{49} \\
\bar{M}_z &= \phi_{26}\bar{u}_2 + \phi_{11,6}\bar{u}_{11} + \phi_{25,6}\bar{u}_{25} + \phi_{32,6}\bar{u}_{32} + \phi_{38,6}\bar{u}_{38} + \phi_{42,6}\bar{u}_{42} + \phi_{49,6}\bar{u}_{49}
\end{aligned} \tag{3.29}$$

If one chooses the number, type, and location of actuators ahead of time, the control inputs for both mode suppression and energy suppression may be easily calculated as suggested above. If the actuator types and locations are not given, then a selection process must be implemented. Under either mode or energy suppression, a reasonable objective is to minimize the amount of energy which goes into the flexible modes. We will assume the number of actuators is fixed since the energy in the flexible modes could always be made arbitrarily small by making the number of actuators arbitrarily large.

3.3. Optimization Procedure

Since the energy suppression method requires solving a cost function subject to linear constraints, an optimization routine is necessary to make calculations.

We present a method to deal with the case in which only equality constraints are involved, i.e.,

$$\min \quad f(x) = \frac{1}{2}\mathbf{x}^T\mathbf{G}\mathbf{x} + \mathbf{g}^T\mathbf{x} \tag{3.30}$$

subject to

$$\mathbf{H}^T\mathbf{x} = \mathbf{b} \tag{3.31}$$

where $\mathbf{b}$ is an m vector, $\mathbf{H}$ is an $n \times m$ matrix which has rank m, and $m \leq n$. From (3.10), we know that we only deal with equality constraints and (3.27) can be expressed in the form of (3.30) with $\mathbf{g}=\mathbf{0}$.

The computer program to solve (3.30) subject to (3.31) is available in the IMSL math library. The program which was written calls as outside subroutine (QPROG). The subroutine will minimize a function inside given constraints (3.31). The data must be input in matrix form. This means (3.10) can be expressed as (3.30).

3.4. Spring Mass System

In the previous two sections, we have introduced the procedure for selecting actuator locations and the command force associated with each actuator. This section will show how the procedure works on the one dimensional spring-mass system which was discussed in Chapter 2. In this system, there are four masses which can be actuated separately. The masses can be actuated in different combinations (i.e. masses 1 and 3 could be controlled or massed 2, 3, and 4 could be controlled). The object of the procedure is to determine how much force should be delivered to the masses for the different actuations in order to minimize the internal energy in the system after the open-loop phase.

The mass and stiffness matrices are given in Chapter 2. The eigenvectors and eigenvalues associated with this system are

$$\Phi = \begin{bmatrix} 1.0000 & 1.0000 & 1.0000 & 1.0000 \\ -0.2623 & -0.4387 & 0.1397 & 1.0000 \\ 1.0000 & -0.5278 & 0.2982 & -0.2425 \\ -0.4765 & -0.0900 & 1.0000 & -0.3436 \end{bmatrix}, \tag{3.32}$$

$$\begin{aligned} \lambda_1 &= 0 \\ \lambda_2 &= 86.0274 \\ \lambda_3 &= 222.9681 \\ \lambda_4 &= 391.0045 \end{aligned} \tag{3.33}$$

From (3.5) and (3.6) we obtain

$$\bar{M} = \begin{bmatrix} 0.0500 & 0 & 0 & 0 \\ 0 & 0.0147 & 0 & 0 \\ 0 & 0 & 0.0170 & 0 \\ 0 & 0 & 0 & 0.0136 \end{bmatrix}$$

and

$$\bar{K} = \begin{bmatrix} 0 & 0 & 0 & 0 \\ 0 & 1.2674 & 0 & 0 \\ 0 & 0 & 3.8015 & 0 \\ 0 & 0 & 0 & 5.3227 \end{bmatrix}.$$

We may now go through the procedure as mentioned in the previous sections. The resultant forces for all possible combinations of actuator locations are shown in Table 3.1. The optimal location for one actuator is at mass 2. The best location for two actuators is placing one on mass 2 and one on mass 3. For three actuators, the optimal placement of actuators are on masses 2, 3, and 4. It is obvious that there is no internal energy in the flexible modes if four actuators are used.

3.5. Discussion

Two criteria to determine the actuators' location have been introduced; one is mode suppression, the other one is energy suppresion. Energy suppression is a

better criteria to calculate the location of actuators when we consider the undamped system only. If there is passive damping in the system, for example 2% in each mode, then we should consider using lower frequency mode suppression instead of energy suppression since high frequency modes will damp out internal energy faster than lower ones.

The spring-mass example illustrates some of the principles which are applicable to the design of a control system for a flexible structure. Through the use of extra actuators, the amount of energy in the flexible modes at the end of the positioning maneuver can be greatly reduced using either a mode suppression or an energy suppression technique. While illustrated by this example, these techniques may also be used to determine effective actuator location and to evaluate the relative advantage of adding additional actuators. Furthermore, additional actuators can also provide backup in case of actuator failure.

Table 3.1 Spring-Mass System Simulation Results

Number of Actuators	u_1 (Newton)	u_2 (Newton)	u_3 (Newton)	u_4 (Newton)	E (N·m)
1	1.0000	—	—	—	0.6531
1	—	1.0000	—	—	0.4184
1	—	—	1.0000	—	1.4032
1	—	—	—	1.0000	1.9943
2	0.3522	0.6478	—	—	0.3275
2	0.6151	—	0.3849	—	0.1408
2	0.7096	—	—	0.2904	0.3616
2	—	0.7094	0.2906	—	0.2198
2	—	0.7033	—	0.2967	0.0777
2	—	—	0.5769	0.4231	0.7148
3	0.4058	0.2818	0.3124	—	0.1001
3	0.0904	0.6288	—	0.2808	0.0720
3	0.5237	—	0.3214	0.1549	0.0764
3	—	0.5882	0.1661	0.2457	0.0222
4	0.2000	0.4000	0.2000	0.2000	0.0000

CHAPTER 4

CONTROLLING A FLEXIBLE PLATE TO MIMIC A RIGID ONE

Selection of optimal actuator locations and command forces are discussed in Chapter 2. It has been shown that the procedure works well on one (physical) dimensional systems. In this Chapter, the procedure is applied to a three dimensional structure that is a thin plate. Also included are modeling the thin plate and calculating energy from the displacement sensor output.

4.1. Theoretical Considerations

According to theory, the continuous dynamic system representation of a plate is given by [28, 30]

$$m(p,q)\frac{\partial^2 y(p,q,t)}{\partial^2 t} + \frac{Eh^3}{12(1-\nu)}\nabla^4 y(p,q,t) = f(p,q,t) \tag{4.1}$$

where y is displacement perpendicular to the coordinate axes p and q. The p and q axes are in the plane of the undeflected plate with p in the direction of the width, and q in the direction of the height. Time is denoted by t, h is plate thickness, E is the elastic modulus, ν is Poisson's ratio, and ∇^4 is the differential operator defined by

$$\nabla^4 = \frac{\partial^4}{\partial^4 p} + 2\frac{\partial^4}{\partial^2 p \partial^2 q} + \frac{\partial^4}{\partial^4 q}.$$

The first term of (4.1) represents inertial forces, the second term represents elastic stiffness, and the term on the right-hand side represents external forces, including control actions. In general, the closed-form solutions to continuous formulation are not available for complex loading and boundary conditions.

A continuous structure with infinite degrees of freedom is represented by finite degrees of freedom in various ways. When the motion of the plate is defined in terms of a finite number of elements in the structure, the formulation is known as a finite element method. This method discretizes the plate into a finite number of smaller elements and expresses the displacement at any point of the continuous structure in terms of a finite number of displacements at the boundaries of the element,

$$\bar{w}(p,q,t) = \sum_{i=1}^{3n} N_i(p,q)\bar{v}_i(t), \tag{4.2}$$

where $\bar{w}(p, q, t)$ is the displacement at a point in an element, $\bar{v}_i(t)$ are the generalized displacements at the nodes, and $N_i(p, q)$ are shape functions. For a rectangular bending plate element, we consider only one translational and two rotational degrees of freedom for each node. There are 12 degrees of freedom for each element. Substituting Equation (4.2) into the kinetic and potential energy expressions, we obtain the following forms:

$$T(t) = \frac{1}{2}\sum_{i=1}^{3n}\sum_{j=1}^{3n} m_{ij}\dot{\bar{v}}_i\dot{\bar{v}}_j \tag{4.3}$$

and

$$V(t) = \frac{1}{2}\sum_{i=1}^{3n}\sum_{j=1}^{3n} k_{ij}\bar{v}_i\bar{v}_j \tag{4.4}$$

where n is the number of nodes. Substituting Equations (4.3) and (4.4) into Lagrange's equation, we have

$$\mathbf{M}\ddot{\mathbf{Y}} + \mathbf{K}\mathbf{Y} = \mathbf{U}, \tag{4.5}$$

where **M** and **K** are mass and stiffness matrices, respectively, **U** is a vector of generalized nodal forces, and

$$\mathbf{Y} = \begin{bmatrix} y_1 \\ \vdots \\ y_n \\ \theta_1 \\ \vdots \\ \theta_n \\ \sigma_1 \\ \vdots \\ \sigma_n \end{bmatrix} \tag{4.6}$$

where y_i is the displacement at each node point i, θ_i is the rotation about the p axis at each node point i, and σ_i is the rotation about the q axis at each node point i.

The shape functions for the plate element of width a and height b are given as follows [30] (transverse deflection and rotation are the degrees of freedom at each node):

$$\begin{aligned}
N_1 &= (1+2p)(1-p)^2(1+2q)(1-q)^2 & N_7 &= -(3-2p)p^2(1-q)q^2b \\
N_2 &= (3-2p)p^2(1+2q)(1-q)^2 & N_8 &= -(1+2p)(1-p)^2(1-q)q^2b \\
N_3 &= (3-2p)p^2(3-2q)q^2 & N_9 &= -p(1-p)^2(1+2q)(1-q)^2a \\
N_4 &= (1+2p)(1-p)^2(3-2q)q^2 & N_{10} &= -p(1-p)^2(1+2q)(1-q)^2a \\
N_5 &= (1+2p)(1-p)^2q(1-q)^2b & N_{11} &= (1-p)p^2(3-2q)q^2a \\
N_6 &= (3-2p)p^2q(1-q)^2b & N_{12} &= -p(1-p)^2(3-2q)q^2a
\end{aligned} \tag{4.7}$$

The stiffness and mass matrices are given in Table 4.1 and Table 4.2.

4.2. Finite Element Model of a Free-Free Plate

Consider the uniform flexible plate illustrated in Figure 4.1. It is assumed that there are no forces acting on the plate other than those that will be imposed

by means of actuators. The area of the plate is 1 meter square, with a thickness of 0.635×10^{-3}m, a density distribution of $\rho = 2637.9$ kg/m^3, Young's modulus of 6.82×10^{10} N/m^2, and Poisson's ratio $\mu = 0.33$. Henceforth, this particular plate will be referred to as the UA plate.

Our objective is to design a controller for the flexible plate so that it will mimic a rigid one. It is assumed that there are no forces acting on the plate other than those that will be imposed by force actuators. We want to have the UA plate oscillate at a frequency of 4.6 Hz in a direction perpendicular to the plane using only force actuators. The amplitude of oscillation is to be 0.140 mm.

Using a finite element analysis, one may obtain the matrices **M**, **K**, and **Φ** [28-30] so that the plate may be modeled as an equation of the form of (4.5). For the 16-element and 25-node plate illustrated in Figure 4.1, we obtain the stiffness and mass matrices as given in Table 4.1 and Table 4.2 for each element and then assemble them to be a global mass and stiffness matrices of the form of (4.5). Since we only consider 3 degrees of freedom for each node, equation (3.8) can be rewritten as

$$\begin{aligned}
\bar{m}_1\ddot{z}_1 &= \phi_{11}u_1 + \phi_{21}u_2 + \ldots + \phi_{m1}u_m \\
\bar{m}_2\ddot{z}_2 &= \phi_{12}u_1 + \phi_{22}u_2 + \ldots + \phi_{m2}u_m \\
\bar{m}_3\ddot{z}_3 &= \phi_{13}u_1 + \phi_{23}u_2 + \ldots + \phi_{m3}u_m \\
\bar{m}_4\ddot{z}_4 + \bar{k}_4 z_4 &= \phi_{14}u_1 + \phi_{24}u_2 + \ldots + \phi_{m4}u_m \quad , \qquad (4.8) \\
\bar{m}_5\ddot{z}_5 + \bar{k}_5 z_5 &= \phi_{15}u_1 + \phi_{25}u_2 + \ldots + \phi_{m5}u_m \\
&\vdots \\
\bar{m}_m\ddot{z}_m + \bar{k}_m z_m &= \phi_{1m}u_1 + \phi_{2m}u_2 + \ldots + \phi_{mm}u_m
\end{aligned}$$

where m = 75. The first three equations in (4.8) correspond to the three rigid body modes and the remaining equations describe the elastic body modes. The number of equations depends on the number of nodes used in the finite element analysis. Then equation (3.9) can be expressed as

$$\begin{aligned} m\ddot{y} &= F_y \\ I_{pp}\dot{\omega}_{pp} &= M_{pp} \\ I_{qq}\dot{\omega}_{qq} &= M_{qq} \end{aligned} \tag{4.9}$$

where m is the total mass of the structure, I_{pp} and I_{qq} are the principal moments of inertia of the structure about the pp and qq axes through the center of mass of the structure, and ω_{pp}, ω_{qq} are the angular velocities with respect to the pp, qq axes. The generalized displacements, forces, and masses are related to (4.9) as follows:

$$\begin{aligned} m &= \bar{m}_1 \qquad y = z_1 \\ I_{pp} &= \bar{m}_2 \qquad \theta = z_2 \\ I_{qq} &= \bar{m}_3 \qquad \sigma = z_3 \end{aligned} \tag{4.10}$$

and

$$\begin{aligned} F_y &= \phi_{11}u_1 + \phi_{21}u_2 + \ldots + \phi_{m1}u_m \\ M_{pp} &= \phi_{12}u_1 + \phi_{22}u_2 + \ldots + \phi_{m2}u_m \,. \\ M_{qq} &= \phi_{13}u_1 + \phi_{23}u_2 + \ldots + \phi_{m3}u_m \end{aligned} \tag{4.11}$$

The eigenvalues and eigenvectors can be obtained by solving $|M\lambda - K| = 0$ The first 10 modal frequencies in hertz according to the finite element analysis are given by

$$\begin{aligned} \lambda_1 &= 0.002 \qquad \lambda_6 = 3.845 \\ \lambda_2 &= 0.002 \qquad \lambda_7 = 5.631 \\ \lambda_3 &= 0.002 \qquad \lambda_8 = 5.631 \,. \\ \lambda_4 &= 2.201 \qquad \lambda_9 = 9.657 \\ \lambda_5 &= 3.030 \qquad \lambda_{10} = 9.657 \end{aligned} \tag{4.12}$$

These compare favorably with experimental results for frequencies in hertz [48]

$$\begin{aligned} \lambda_1 &= 0.000 & \lambda_6 &= 3.842 \\ \lambda_2 &= 0.000 & \lambda_7 &= 5.507 \\ \lambda_3 &= 0.000 & \lambda_8 &= 5.507. \\ \lambda_4 &= 2.122 & \lambda_9 &= 9.676 \\ \lambda_5 &= 3.112 & \lambda_{10} &= 9.676 \end{aligned} \tag{4.13}$$

Using (4.12) along with the **M** and **K** matrices, we can obtain the modal matrix. The 75 × 75 transformation matrix Φ is defined by

$$\Phi = [\,\xi_1 \quad \cdots \quad \xi_{75}\,],$$

where ξ_i is the eigenvector associated with the i-th frequency. Due to the size of this matrix, it is not reproduced here. Indeed, it is not necessary as it is far more useful to examine a number of 5 × 5 matrices formed from Φ^T. The first three rows of Φ^T relate the actuator inputs to the first three rigid body modes. The remaining 72 rows of Φ^T relate the actuator inputs to the flexible body modes. Since our example involves only force inputs, we are concerned with only the first 25 elements of each row. The 1st element is asociated with the force actuator at the 1st node, and the 2nd element is associated with the force actuator at the 2nd node, etc. Thus, if we form a 5 × 5 force effectiveness matrix of the form

$$\mathbf{F_j} = \begin{bmatrix} \phi^T_{j,1} & \phi^T_{j,2} & \phi^T_{j,3} & \phi^T_{j,4} & \phi^T_{j,5} \\ \phi^T_{j,6} & \phi^T_{j,7} & \cdots & \cdots & \phi^T_{j,10} \\ \phi^T_{j,11} & \phi^T_{j,12} & \cdots & \cdots & \phi^T_{j,15} \\ \phi^T_{j,16} & \phi^T_{j,17} & \cdots & \cdots & \phi^T_{j,20} \\ \phi^T_{j,21} & \phi^T_{j,22} & \cdots & \cdots & \phi^T_{j,25} \end{bmatrix} \tag{4.14}$$

where $\phi^T_{j,k}$ is the j^{th} row and k^{th} column element of the Φ^T matrix, we have a convenient representation of how a force actuator at a particular node interacts

with that mode. For example, a force actuator at node 13 (see Figure 4.1) will enter the j^{th} mode through $\phi^T_{j,13}$. Table 4.3 lists $\mathbf{F_j}$ for j = 1, ..., 10. From Table 4.3 we know mode 2, 3, 4, 5, 7, 8, 9, 10 are not controllable if we place a force actuator at node 13 because the entries of $\mathbf{F_j}$ are zero.

Each of the modes listed in Table 4.3 will have a characteristic mode shape. These are illustrated in Figures 4.1-4.11. A 64-element analysis was used to generate Figures 4.4-4.11 in order to more accurately portray the shapes obtained. Figures 4.1-4.3 illustrate the rigid body modes and Figures 4.4-4.11 illustrate the first eight flexible modes.

The zero displacement curves for the first eight flexible mode shapes are denoted by the solid lines of Figures 4.12-4.19. Figures 4.12-4.19 are in agreement with the experimental results [48].

4.3. Plate Dynamics

In order to illustrate the techniques of mode and energy suppression, we will examine positioning of the plate with one, two, and three force actuators at specified node points. Since the objective is to displace the plate normal to itself, only a single actuator is needed for this rigid requirement. We will examine the single-actuator case first. This will allow us to illustrate some of the computations used for the other cases, as well as providing a standard for comparison.

If we place a single actuator at node 13, we see from Table 4.3 that this actuator will affect only the 1^{st} and 6^{th} modes (of the 10 listed). The equivalent

mass of the UA plate is 1.675 kg. The design requirement is that the displacement of the UA plate oscillate according to

$$y = (0.140\text{mm})\cos[1 - 2\pi(4.6)t]. \tag{4.15}$$

From the first equation of (4.11), we obtain

$$F_y = (0.196\text{N})\cos 2\pi(4.6)t. \tag{4.16}$$

Thus, from conditions of the form of (4.11), we find $u_{13}(t)$. In particular, we have

$$F_y = u_{13} \tag{4.17}$$

with $M_{pp} = 0$ and $M_{qq} = 0$. Applying this control to the flexible plate as modeled by (4.5), we obtain its dynamic response. We will characterize this reponse here in terms of the Fast Fourier Transform (FFT) spectrum of the displacement obtained at nodes 7, 11, 13, 21 and 23, as illustrated in Figures 4.20a-4.20e. As predicted, the 1^{st} mode at 0 Hz and the 6^{th} mode at 3.845 Hz, along with the driving frequency at 4.6 Hz, dominate the dynamics. It is of interest to compare the average energy in the plate with the average energy in each of the excited modes. This may be easily done during the computer simulation run, provided the run is long enough to provide a good average. The total energy in the plate is given by

$$E_T = \frac{1}{T}\int_0^T \frac{1}{2}(\dot{\mathbf{Y}}\mathbf{M}\dot{\mathbf{Y}} + \mathbf{YKY})dt, \tag{4.18}$$

where $\mathbf{Y}$ as defined by (4.6) is the vector of generalized displacements and $\mathbf{M}$ and $\mathbf{K}$ are defined previously. The total average energy in each mode is given by

$$E_i = \frac{1}{T}\int_0^T \frac{1}{2}(\bar{m}_i\dot{z}_i^2 + \bar{k}_i z_i^2)dt, \tag{4.19}$$

where z_i are the decoupled generalized displacements defined by (3.2) and $\bar{m}_i$ and $\bar{k}_i$ are the mass and stiffness associated with each mode.

For this one-actuator case, we obtain the energies as summarized in Table 4.4. Clearly, most of the elastic energy is in the 6^{th} mode. We see that 99.1% of the total energy has gone into the elastic modes, so we have only a 0.9% mimic with the single-actuator case.

In an experimental setting, the energy in a given elastic mode would have to be determined from measurements. For example, if displacement sensors are placed at nodes 7, 11, 13, 21, and 23, then an FFT of these data would produce results similar to Figures 4.20a-4.20e. The displacement at a given node j will be a sum of the modal contributions,

$$y_j = R_j + \sum_{i=4}^{75} \phi_{ji} z_i, \tag{4.20}$$

where R_j is the rigid body contribution that will be at the driving frequency. The solution to (4.8) with $f_i = A_i \cos\omega t$ is given by

$$z_i = \frac{A_i/\bar{k}_i}{\left[1 - (\frac{\omega}{\omega_i})^2\right]}(\cos\omega t - \cos\omega_i t). \tag{4.21}$$

Thus,

$$y_j = R_j + \sum_{i=4}^{75} \frac{\phi_{ji} A_i/\bar{k}_i}{\left[1 - (\frac{\omega}{\omega_i})^2\right]} \cos\omega t - \sum_{i=4}^{75} \frac{\phi_{ji} A_i/\bar{k}_i}{\left[1 - (\frac{\omega}{\omega_i})^2\right]} \cos\omega_i t. \tag{4.22}$$

This may be compared with the representation obtained from the FFT (no damping in the actual system is assumed)

$$y_j = D_j \sin(\omega t + \alpha) - \sum_{i=4}^{75} D_{ji} \cos\omega_i t, \tag{4.23}$$

where D_j is the j-node Fourier coefficient corresponding to the driving frequency and D_{ji} is the j^{th}-node Fourier coefficient corresponding to the i-th mode. Comparing (4.22) and (4.23), it follows that

$$D_{ji} = \frac{\phi_{ji} A_i / \bar{k}_i}{\left[1 - (\frac{\omega}{\omega_i})^2\right]}. \tag{4.24}$$

Thus,

$$\frac{A_j^2 / \bar{k}_i}{\left[1 - (\frac{\omega}{\omega_i})^2\right]^2} = [\frac{D_{ji}}{\phi_{ji}}]^2 \bar{k}_i. \tag{4.25}$$

It then follows from (3.22) that

$$E_i = \frac{\bar{k}_i}{4}[3 + (\frac{\omega}{\omega_i})^2][\frac{D_{ji}}{\phi_{ji}}]^2. \tag{4.26}$$

Note that the elastic energy in any given mode may be calculated at any node provided that the mode is significantly represented. For example, the 6^{th} mode is well represented at node 21 and node 13. From these FFT spectrums, we obtain

$$D_{21,6} = 0.2129 \times 10^{-2} \quad \text{and} \quad D_{13,6} = 0.1270 \times 10^{-2}. \tag{4.27}$$

Correspondingly, we obtain from Table 4.3

$$\phi_{21,6} = \phi^T_{6,21} = 0.42944 \quad \text{and} \quad \phi_{13,6} = \phi^T_{6,13} = -0.25548. \tag{4.28}$$

For the 6^{th} mode, $\bar{k}_6 = 21.5291$ and $\omega_6 = 3.8448$. From (4.26), we obtain

$$E_6 = 5.862 \times 10^{-4} \quad \text{and} \quad E_6 = 5.894 \times 10^{-4}, \tag{4.29}$$

which is in quantitative agreement with the direct calculation given in Table 4.4.

The method used to calculate energy in the elastic modes only requires sensor output. This method will give us a good estimate of the energy in each

mode when we do not have all information to calculate the energy. When we consider reducing the energy in a specific mode we can apply the mode suppression technique to eliminate the internal energy.

From the result obtained above we know we have a 0.9% mimic with the single actuator case. With a single actuator, most energy is in the 6^{th} mode. Therefore we can use the mode suppression technique to suppress energy in this particular mode. But when we apply the mode suppression technique we may dump energy into other modes. So we might consider using the energy suppression technique such that the energy in the elastic modes will be minimized.

4.4. Mode Suppression

With two actuators, a form of mode suppression may be employed. From equations (3.15) and (4.11) we know that four actuators are required to apply the mode suppression technique because equation (4.11) has to be satisfied which means $M_{pp} = 0$ and $M_{qq} = 0$. If we place the two actuators at nodes 11 and 15 or 12 and 14, then the constraints are satisfied. But equation (3.15) is not satisfied because

$$-0.1477u_{11} - 0.1477u_{15} \neq 0$$

where -0.1477 is from Table 4.3. Here, we will show how having one more actuator will alter the energy in the structure.

We see from Table 4.3 that, if we place the actuators at node 11 and 15, these actuators will affect only the 1^{st}, 5^{th}, and 6^{th} modes, provided that the actuators produce exactly the same force. (The forces will then cancel on modes 2, 3, 7, 8, 9, and 10, with no effect on the 4^{th} mode.) We will take this as our

objective, that is, to prevent energy going into any of the first 10 modes except for the 1^{st}, 5^{th}, and 6^{th}. The force F_y is still determined from (4.11) so that we can find u_{11} and u_{15} simply from

$$\begin{aligned} 0.196 &= \bar{u}_{11} + \bar{u}_{15} \\ 0 &= \bar{u}_{11} - \bar{u}_{15}. \end{aligned} \tag{4.30}$$

Since smaller forces are used (the amplitude of each force input is 0.098 N), we expect less energy to go into the two elastic modes. Figures 4.21a-4.21e illustrate the FFT spectrum of the displacement obtained at node 7, 11, 13, 21, and 23. It is evident from Figures 4.21a-4.21e that the expected modes are excited. In every figure, the first mode (0 Hz) and the driving frequency (4.6 Hz) are evident. However, the other two excited modes are not equally represented in every figure. For example, only the 6^{th} mode (3.8 Hz) appears at node 21, whereas the 5^{th} mode (3.0 Hz) is dominate at node 11. This is not unexpected, as the contribution of each mode to the total displacement y_j as given by (4.20) depends on ϕ_{ji}. From Table 4.3, we have

$$\begin{aligned} \phi_{21,5} &= \phi^{T}_{5,11} = 0 \\ \phi_{21,6} &= \phi^{T}_{6,11} = 0.42944, \end{aligned} \tag{4.31}$$

which explains the absence of the 5^{th} mode at node 21. Furthermore,

$$\begin{aligned} \phi_{11,5} &= \phi^{T}_{5,11} = 0.30207 \\ \phi_{11,6} &= \phi^{T}_{6,11} = 0.06159, \end{aligned} \tag{4.32}$$

which explains the results obtained at node 11.

A summary of the average energies for this case are given in Table 4.4. The majority of elastic energy went into the 5^{th} mode. In this case, 98.2% of the total energy is in the elastic modes, making the two-actuator case a 1.8% mimic. This factor-of-two improvement over the single-actuator case is consistent with the fact

that the maximum force produced by each actuator was one-half of that used in the single actuator case.

Thinking of Figures 4.20a-4.20e as experimental data, we can estimate the energies in the two elastic modes. We obtain $D_{21,6} = 0.5165 \times 10^{-3}$ from Figure 4.21d and $D_{11,5} = 0.1305 \times 10^{-2}$ from Figure 4.21d. Correspondingly, from Table 4.3, $\phi_{21,6} = \phi^{T}_{6,21} = 0.42944$ and $\phi_{11,5} = \phi^{T}_{5,11} = 0.30207$. For the 5^{th} mode, $\bar{k}_5$=10.2131 and ω_5=0.0302. From (4.26), we obtain $E_5 = 2.528 \times 10^{-4}$ and (using previously given values for $\bar{k}_6$ and ω_6) $E_6 = 0.3450 \times 10^{-4}$, which is again in qualitative agreement with Table 4.4.

With three actuators, some additional mode suppression may take place. We see from Table 4.3 that if we place the actuators at node 11, 13, and 15, and if the actuators at nodes 11 and 15 again produce equal forces ($u_{11} = u_{15}$), there will be no input into modes 2, 3, 4, 7, 8, 9, 10. Because of the requirement that $u_{11} = u_{15}$ and the fact that $\phi^{T}_{5,13} = 0$, the 5^{th} mode cannot be suppressed (which would require $u_{11} = -u_{15}$). However, the additional actuator may be used to suppress the 6^{th} by choosing the controls to satisfy

$$\begin{aligned} 0.196 &= \bar{u}_{11} + \bar{u}_{13} + \bar{u}_{15} \\ 0 &= \bar{u}_{11} - \bar{u}_{15} \\ 0 &= 0.0616\bar{u}_{11} - 0.2555\bar{u}_{13} + 0.0616\bar{u}_{15}. \end{aligned} \tag{4.33}$$

These equations yield force amplitudes of 0.079N, 0.038N, and 0.079N for $\bar{u}_{11}$, $\bar{u}_{13}$, and $\bar{u}_{15}$, respectively. Figures 4.22a-4.22e illustrate the FFT spectrum of the displacement at nodes 7, 11, 13, 21, 23. The driving frequency is again at 4.6 Hz. These figures show the complete suppression of the 6^{th} (3.8 Hz) mode.

Note that the impact of the 5^{th} mode varies from node to node. While the 6^{th} mode was suppressed, significant energy still went into the 5^{th} (3 Hz) mode (see Table 4.3). In this case, 96.9% of the total energy is in the elastic modes, making this three-actuator case a 3.1% mimic.

4.5. Energy Suppression

For those situations where minimizing the total flexible energy is important, the energy suppression technique offers an alternative control strategy. Suppose that we have two actuators at our disposal. We may make a direct comparison with mode suppression. Our objective is to minimize the energy going into the first 8 flexible modes,

$$E = \sum_{i=4}^{11} \frac{A_i^2}{\tilde{k}_i}, \tag{4.34}$$

where $\tilde{k}_4 = 52.7168$, $\tilde{k}_5 = 13.1044$, $\tilde{k}_6 = 3.6172$, $\tilde{k}_7 = 1.4262$, $\tilde{k}_8 = 1.4262$, $\tilde{k}_9 = 15.3261$, $\tilde{k}_{10} = 15.3261$, and $\tilde{k}_{11} = 34.1228$. The function E is to be minimized subject to the constraints (4.11).

From Table 4.5 we know that the optimal placement of two actuators (at node 7, 19 or 9, 17) will provide a 19.7% mimic for the UA plate under the conditions described above. This was determined by systematically examining all feasible actuator locations and determining the corresponding energy in the first 8 flexible modes. Different design requirements from those specified above will, in general, result in different optimal locations.

For the three-actuator case we know the third one did not increase the percentage of mimic. A similar procedure with more actuators can be used to provide additional mode or energy suppression. Introducing a 4th actuator allows

for a considerable improvement in performance. Note that with four actuators, we can produce a 54.3% mimic using energy suppression.

4.6. Discussion

Sensor and actuator placement has been discussed from a controllability and observability point of view and from an overall performance point of view. The energy suppression idea presented here can also be used to evaluate actuator location. These two examples (spring-mass and plate) show that the procedure works well. The procedure is different from traditional control system design [6-19, 60, 61]. We do not need to feedback all state variables to position and stablize the structure.

The optimal solution depends on the model obtained by the finite element analysis. For example, there are several bending elements [30]. Some of them are overstiff and some are understiff compared with the experimental results. Choosing one close to the real structure is not easy. But if we can obtain the mode shapes and natural frequencies from the experimental measurement then we can go through the procedure to get the optimal solution for a given number, type of actuators. In the next chapter, we have set up an experiment to prove the theory can be applied in the real structure.

Table 4.1 Stiffness Elements Matrix ($k = Eh^2/[12(1-\mu^2)ab]$)

$\frac{156}{35}(\beta^2+\beta^2)$ $+\frac{72}{25}$											
$-\frac{156}{35}\beta^2+\frac{54}{35}\beta^2$ $-\frac{72}{25}$	$\frac{156}{35}(\beta^2+\beta^2)$ $+\frac{72}{25}$										
$-\frac{54}{35}(\beta^2+\beta^2)$ $+\frac{72}{25}$	$\frac{54}{35}\beta^2-\frac{156}{35}\beta^2$ $-\frac{72}{25}$	$\frac{156}{35}(\beta^2+\beta^2)$ $+\frac{72}{25}$									
$\frac{54}{35}\beta^2-\frac{156}{35}\beta^2$ $-\frac{72}{25}$	$-\frac{54}{35}(\beta^2+\beta^2)$ $+\frac{72}{25}$	$-\frac{156}{35}\beta^2+\frac{54}{35}\beta^2$ $-\frac{72}{25}$	$\frac{156}{35}(\beta^2+\beta^2)$ $+\frac{72}{25}$					$\beta=\frac{b}{a}$			
$\left[\frac{22}{35}\beta^2+\frac{78}{35}\beta^2\right.$ $\left.+\frac{6}{25}(1+5\nu)\right]b$	$\left[-\frac{22}{35}\beta^2+\frac{27}{35}\beta^2\right.$ $\left.-\frac{6}{25}(1+5\nu)\right]b$	$\left(-\frac{13}{35}\beta^2-\frac{27}{35}\beta^2\right.$ $\left.+\frac{6}{25}\right)b$	$\left(\frac{13}{35}\beta^2-\frac{78}{35}\beta^2\right.$ $\left.-\frac{6}{25}\right)b$	$\left(\frac{4}{35}\beta^2+\frac{52}{35}\beta^2\right.$ $\left.+\frac{8}{25}\right)b^2$							
$\left[-\frac{22}{35}\beta^2+\frac{27}{35}\beta^2\right.$ $\left.-\frac{6}{25}(1+5\nu)\right]b$	$\left[\frac{22}{35}\beta^2+\frac{78}{35}\beta^2\right.$ $\left.+\frac{6}{25}(1+5\nu)\right]b$	$\left(\frac{13}{35}\beta^2-\frac{78}{35}\beta^2\right.$ $\left.-\frac{6}{25}\right)b$	$\left(-\frac{13}{35}\beta^2-\frac{27}{35}\beta^2\right.$ $\left.+\frac{6}{25}\right)b$	$\left(-\frac{4}{35}\beta^2+\frac{18}{35}\beta^2\right.$ $\left.-\frac{8}{25}\right)b^2$	$\left(\frac{4}{35}\beta^2+\frac{52}{35}\beta^2\right.$ $\left.+\frac{8}{25}\right)b^2$						
$\left(\frac{13}{35}\beta^2+\frac{27}{35}\beta^2\right.$ $\left.-\frac{6}{25}\right)b$	$\left(-\frac{13}{35}\beta^2+\frac{78}{35}\beta^2\right.$ $\left.+\frac{6}{25}\right)b$	$-\left[\frac{22}{35}\beta^2+\frac{78}{35}\beta^2\right.$ $\left.+\frac{6}{25}(1+5\nu)\right]b$	$\left[\frac{22}{35}\beta^2-\frac{27}{35}\beta^2\right.$ $\left.+\frac{6}{25}(1+5\nu)\right]b$	$\left(\frac{3}{35}\beta^2+\frac{9}{35}\beta^2\right.$ $\left.+\frac{2}{25}\right)b^2$	$\left(-\frac{3}{35}\beta^2+\frac{26}{35}\beta^2\right.$ $\left.-\frac{2}{25}\right)b^2$	$\left(\frac{4}{35}\beta^2+\frac{52}{35}\beta^2\right.$ $\left.+\frac{8}{25}\right)b^2$					
$\left(-\frac{13}{35}\beta^2+\frac{78}{35}\beta^2\right.$ $\left.+\frac{6}{25}\right)b$	$\left(\frac{13}{35}\beta^2+\frac{27}{35}\beta^2\right.$ $\left.-\frac{6}{25}\right)b$	$\left[\frac{22}{35}\beta^2-\frac{27}{35}\beta^2\right.$ $\left.+\frac{6}{25}(1+5\nu)\right]b$	$-\left[\frac{22}{35}\beta^2-\frac{78}{35}\beta^2\right.$ $\left.+\frac{6}{25}(1+5\nu)\right]b$	$\left(-\frac{3}{35}\beta^2+\frac{26}{35}\beta^2\right.$ $\left.-\frac{2}{25}\right)b^2$	$\left(\frac{3}{35}\beta^2+\frac{9}{35}\beta^2\right.$ $\left.+\frac{2}{25}\right)b^2$	$\left(-\frac{4}{35}\beta^2+\frac{18}{35}\beta^2\right.$ $\left.-\frac{8}{25}\right)b^2$	$\left(\frac{4}{35}\beta^2+\frac{52}{35}\beta^2\right.$ $\left.+\frac{8}{25}\right)b^2$				
$-\left[\frac{78}{35}\beta^2+\frac{22}{35}\beta^2\right.$ $\left.+\frac{6}{25}(1+5\nu)\right]a$	$\left(\frac{78}{35}\beta^2-\frac{13}{35}\beta^2\right.$ $\left.+\frac{6}{25}\right)a$	$\left(\frac{27}{35}\beta^2+\frac{13}{35}\beta^2\right.$ $\left.-\frac{6}{25}\right)a$	$\left(-\frac{27}{35}\beta^2+\frac{22}{35}\beta^2\right.$ $\left.+\frac{6}{25}(1+5\nu)\right]a$	$-\left[\frac{11}{35}(\beta^2+\beta^2)\right.$ $\left.+\frac{1}{50}(1+60\nu)\right]ab$	$\left[\frac{11}{35}\beta^2-\frac{13}{70}\beta^2\right.$ $\left.+\frac{1}{50}(1+5\nu)\right]ab$	$\left[-\frac{13}{70}(\beta^2+\beta^2)\right.$ $\left.+\frac{1}{50}\right]ab$	$\left[\frac{13}{70}\beta^2-\frac{11}{35}\beta^2\right.$ $\left.-\frac{1}{50}(1+5\nu)\right]ab$	$\left(\frac{52}{35}\beta^2+\frac{4}{35}\beta^2\right.$ $\left.+\frac{8}{25}\right)a^2$		
$\left[-\frac{78}{35}\beta^2+\frac{13}{35}\beta^2\right.$ $\left.-\frac{6}{25}\right]a$	$\left[\frac{78}{35}\beta^2+\frac{22}{35}\beta^2\right.$ $\left.+\frac{6}{25}(1+5\nu)\right]a$	$\left[\frac{27}{35}\beta^2-\frac{22}{35}\beta^2\right.$ $\left.-\frac{6}{25}(1+5\nu)\right]a$	$\left(-\frac{27}{35}\beta^2-\frac{13}{35}\beta^2\right.$ $\left.+\frac{6}{25}\right)a$	$\left[-\frac{11}{35}\beta^2+\frac{13}{70}\beta^2\right.$ $\left.-\frac{1}{50}(1+5\nu)\right]ab$	$\left[\frac{11}{35}(\beta^2+\beta^2)\right.$ $\left.+\frac{1}{50}(1+60\nu)\right]ab$	$\left[-\frac{13}{70}\beta^2+\frac{11}{35}\beta^2\right.$ $\left.+\frac{1}{50}(1+5\nu)\right]ab$	$\left[\frac{13}{70}(\beta^2+\beta^2)\right.$ $\left.-\frac{1}{50}\right]ab$	$\left(\frac{26}{35}\beta^2-\frac{3}{35}\beta^2\right.$ $\left.-\frac{2}{25}\right)a^2$	$\left(\frac{52}{35}\beta^2+\frac{4}{35}\beta^2\right.$ $\left.+\frac{8}{25}\right)a^2$	
$\left[-\frac{27}{35}\beta^2-\frac{13}{35}\beta^2\right.$ $\left.+\frac{6}{25}\right]a$	$\left[\frac{27}{35}\beta^2-\frac{22}{35}\beta^2\right.$ $\left.-\frac{6}{25}(1+5\nu)\right]a$	$\left[\frac{78}{35}\beta^2+\frac{22}{35}\beta^2\right.$ $\left.+\frac{6}{25}(1+5\nu)\right]a$	$\left(-\frac{78}{35}\beta^2+\frac{13}{35}\beta^2\right.$ $\left.-\frac{6}{25}\right]a$	$\left[-\frac{13}{70}(\beta^2+\beta^2)\right.$ $\left.+\frac{1}{50}\right]ab$	$\left[\frac{13}{70}\beta^2-\frac{11}{35}\beta^2\right.$ $\left.-\frac{1}{50}(1+5\nu)\right]ab$	$-\left[\frac{11}{35}(\beta^2+\beta^2)\right.$ $\left.+\frac{1}{50}(1+60\nu)\right]ab$	$\left[\frac{11}{35}\beta^2-\frac{13}{70}\beta^2\right.$ $\left.+\frac{1}{50}(1+5\nu)\right]ab$	$\left(\frac{9}{35}\beta^2+\frac{3}{35}\beta^2\right.$ $\left.+\frac{2}{25}\right)a^2$	$\left(\frac{18}{35}\beta^2-\frac{4}{35}\beta^2\right.$ $\left.-\frac{8}{25}\right)a^2$	$\left(\frac{52}{35}\beta^2+\frac{4}{35}\beta^2\right.$ $\left.+\frac{8}{25}\right)a^2$	
$\left[-\frac{27}{35}\beta^2+\frac{22}{35}\beta^2\right.$ $\left.+\frac{6}{25}(1+5\nu)\right]a$	$\left(\frac{27}{35}\beta^2+\frac{13}{35}\beta^2\right.$ $\left.-\frac{6}{25}\right)a$	$\left(\frac{78}{35}\beta^2-\frac{13}{35}\beta^2\right.$ $\left.+\frac{6}{25}\right)a$	$-\left[\frac{78}{35}\beta^2+\frac{22}{35}\beta^2\right.$ $\left.+\frac{6}{25}(1+5\nu)\right]a$	$\left[-\frac{13}{70}\beta^2+\frac{11}{35}\beta^2\right.$ $\left.+\frac{1}{50}(1+5\nu)\right]ab$	$\left[\frac{13}{70}(\beta^2+\beta^2)\right.$ $\left.-\frac{1}{50}\right]ab$	$\left[-\frac{11}{35}\beta^2+\frac{13}{70}\beta^2\right.$ $\left.-\frac{1}{50}(1+5\nu)\right]ab$	$\left[\frac{11}{35}(\beta^2+\beta^2)\right.$ $\left.+\frac{1}{50}(1+60\nu)\right]ab$	$\left(\frac{18}{35}\beta^2-\frac{4}{35}\beta^2\right.$ $\left.-\frac{8}{25}\right)a^2$	$\left(\frac{9}{35}\beta^2+\frac{3}{35}\beta^2\right.$ $\left.+\frac{2}{25}\right)a^2$	$\left(\frac{26}{35}\beta^2-\frac{3}{35}\beta^2\right.$ $\left.-\frac{2}{25}\right)a^2$	$\left(\frac{52}{35}\beta^2+\frac{4}{35}\beta^2\right.$ $\left.+\frac{8}{25}\right)a^2$

Table 4.2 Consistent Mass Elements Matrix (m = ρhab/176400)

1	24336											
2	8424	24336										
3	2916	8424	24336									
4	8424	2916	8424	24336								
5	3432b	1188b	702b	2028b	$624b^2$							
6	1188b	3432b	2028b	702b	$216b^2$	$624b^2$						
7	-702b	-2028b	-3432b	-1188b	$-162b^2$	$-468b^2$	$624b^2$					
8	-2028b	- 702b	-1188b	-3432b	$-468b^2$	$-162b^2$	$216b^2$	$624b^2$				
9	-3432a	-2028a	- 702a	-1188a	-484ab	-286ab	169ab	286ab	$624a^2$			
10	2028a	3432a	1188a	702a	286ab	484ab	-286ab	-169ab	$-468a^2$	$624a^2$		
11	702a	1188a	3432a	2028a	169ab	286ab	-484ab	-286ab	$-162a^2$	$216a^2$	$624a^2$	
12	-1188a	- 702a	-2028a	-3432a	-286ab	-169ab	286ab	484ab	$216a^2$	$-162a^2$	$-468a^2$	$624a^2$
	1	2	3	4	5	6	7	8	9	10	11	12

Table 4.3 The F_j Matrics for the First 10 Modes

1st Mode (Rigid Body in y)					6th Mode (3rd Flexible)				
1.0000	1.0000	1.0000	1.0000	1.0000	0.4294	0.1839	0.0616	0.1839	0.429
1.0000	1.0000	1.0000	1.0000	1.0000	0.1839	-0.0376	-0.1477	-0.0376	0.1839
1.0000	1.0000	1.0000	1.0000	1.0000	0.0616	-0.1477	-0.2555	-0.1477	0.0616
1.0000	1.0000	1.0000	1.0000	1.0000	0.1839	-0.0376	-0.1477	-0.0376	0.1839
1.0000	1.0000	1.0000	1.0000	1.0000	0.4294	0.1839	0.0616	0.1839	0.4294
2nd Mode (Rigid Body in θ)					7th Mode (4th Flexible)				
-0.5984	-0.3484	-0.0984	0.1516	0.4016	0.1859	-0.0550	-0.1693	-0.0198	0.2357
-0.5492	-0.2992	-0.0492	0.2008	0.4508	0.1538	-0.0031	-0.0774	-0.0039	0.1450
-0.5000	-0.2500	0.0000	0.2500	0.5000	0.0200	0.0091	0.0000	-0.0091	-0.0200
-0.4508	-0.2008	0.0492	0.2992	0.5492	-0.1450	0.0039	0.0774	0.0031	-0.1538
-0.4016	-0.1516	0.0984	0.3484	0.5984	-0.2357	0.0198	0.1693	0.0550	-0.1859
3rd Mode (Rigid Body in θ)					8th Mode (5th Flexible)				
0.4016	0.4508	0.5000	0.5492	0.5984	0.2357	0.1450	-0.0200	-0.1538	-0.1859
0.1516	0.2008	0.2500	0.2992	0.3484	-0.0198	-0.0039	-0.0091	0.0031	0.0550
-0.0984	-0.0492	0.0000	0.0492	0.0984	-0.1693	-0.0774	0.0000	0.0774	0.1693
-0.3484	-0.2992	-0.2500	-0.2008	-0.1516	-0.0550	-0.0031	0.0091	0.0039	0.0198
-0.5984	-0.5492	-0.5000	-0.4508	-0.4016	0.1859	0.1538	0.0200	-0.1450	-0.2357
4th Mode (1st Flexible)					9th Mode (6th Flexible)				
-0.4437	-0.2495	0.0000	0.2495	0.4437	-0.1434	0.0642	-0.0063	-0.0800	0.1253
-0.2495	-0.1333	0.0000	0.1333	0.2495	-0.1132	0.0702	0.0051	-0.0613	0.1229
0.0000	0.0000	0.0000	0.0000	0.0000	-0.0940	0.0763	0.0000	-0.0763	0.0940
0.2495	0.1333	0.0000	-0.1333	-0.2495	-0.1229	0.0613	-0.0051	-0.0702	0.1132
0.4437	0.2495	0.0000	-0.2495	-0.4437	-0.1253	0.0800	0.0063	-0.0642	0.1434
5th Mode (2nd Flexible)					10th Mode (7th Flexible)				
0.0000	0.2086	0.3021	0.2086	0.0000	0.1253	0.1229	0.0940	0.1132	0.1434
-0.2086	0.0000	0.0889	0.0000	-0.2086	-0.0800	-0.0613	-0.0763	-0.0702	-0.0642
-0.3021	-0.0889	0.0000	-0.0889	-0.3021	-0.0063	0.0051	0.0000	-0.0051	0.0063
-0.2086	0.0000	0.0889	0.0000	-0.2086	0.0642	0.0702	0.0763	0.0613	0.0800
0.0000	0.2086	0.3021	0.2086	0.0000	-0.1434	-0.1132	-0.0940	-0.1229	-0.1253

Table 4.4 Average Energy (Newton-meters) Components for the Three Cases

Case	E_T Total Average Energy	Modes				
		E_1 1st Rigid	E_4 1st Elastic	E_5 2nd Elastic	E_8 3rd Elastic	$\sum_{i=4}^{75} E_i$ All Elastic
1 actuator	7.5995×10^{-4}	0.0687×10^{-4}	0.0	0.0	7.2198×10^{-4}	7.5308×10^{-4}
2 actuators	3.8925×10^{-4}	0.0687×10^{-4}	0.0	2.8752×10^{-4}	0.4815×10^{-4}	3.8238×10^{-4}
3 actuators (mode suppression)	2.2281×10^{-4}	0.0687×10^{-4}	0.0	1.8684×10^{-4}	0.0	2.1595×10^{-4}

Table 4.5 Optimal Solutions for Free-Free Plate

Number of Actuators	Node Number	E (Newton·meters)	m
1	13	0.760×10^{-4}	0.90
2	7, 19	0.280×10^{-4}	19.70
3	7, 13, 19	0.280×10^{-4}	19.70
4	7, 10, 16, 19	0.058×10^{-4}	54.30

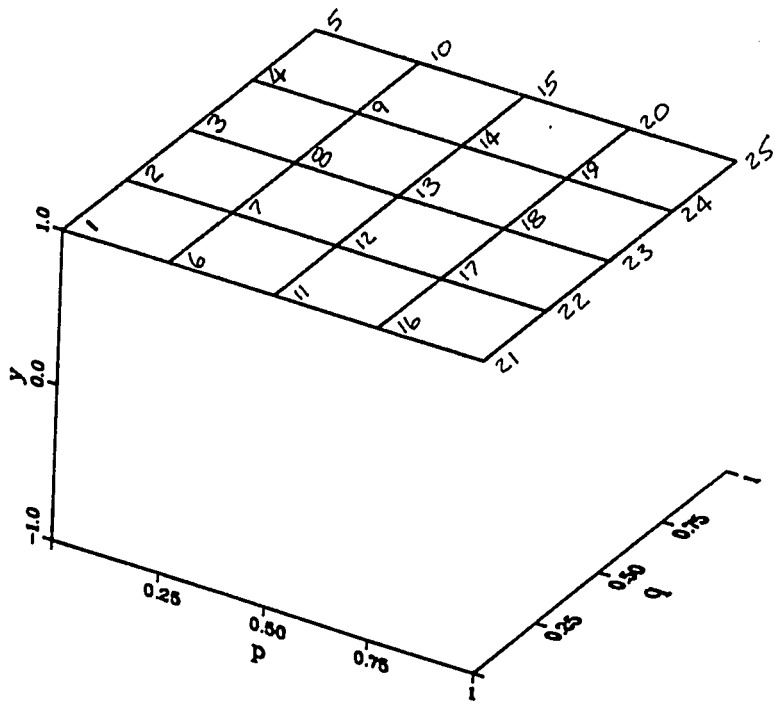

Figure 4.1 First Rigid Body Mode

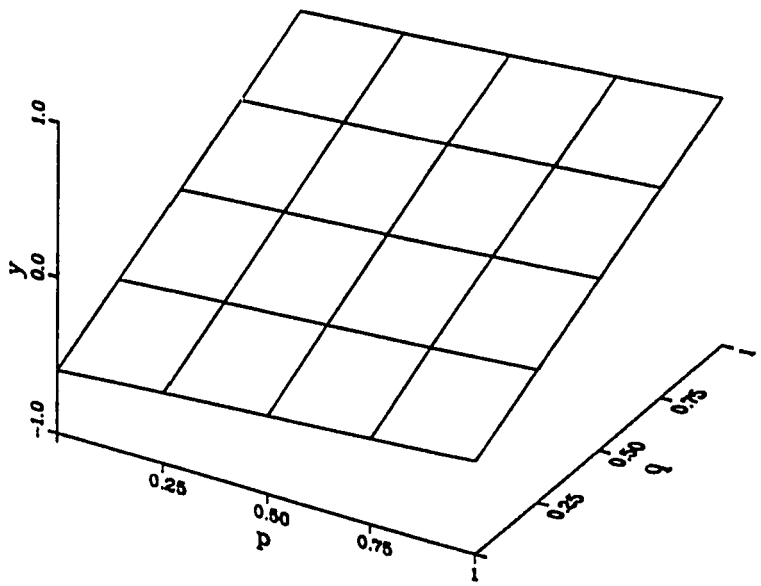

Figure 4.2 Second Rigid Body Mode

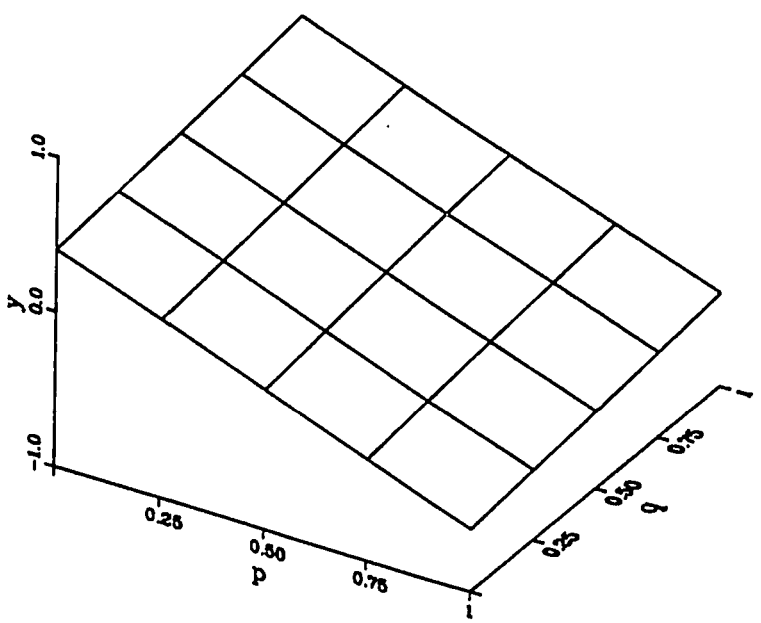

Figure 4.3 Third Rigid Body Mode

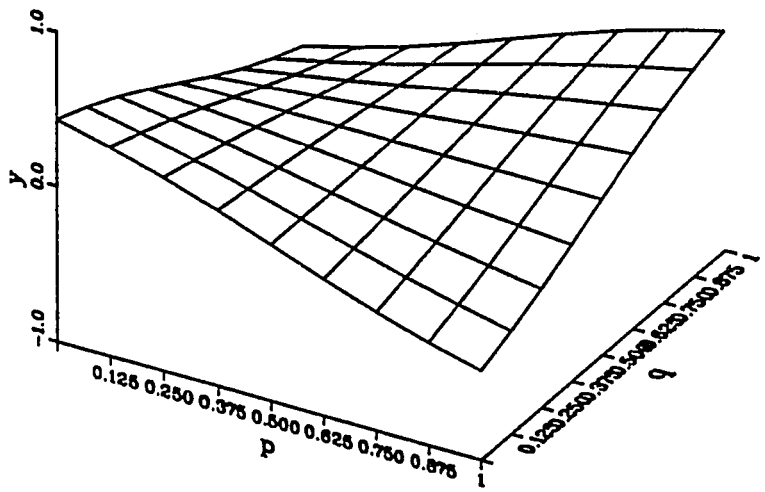

Figure 4.4 First Flexible Body Mode

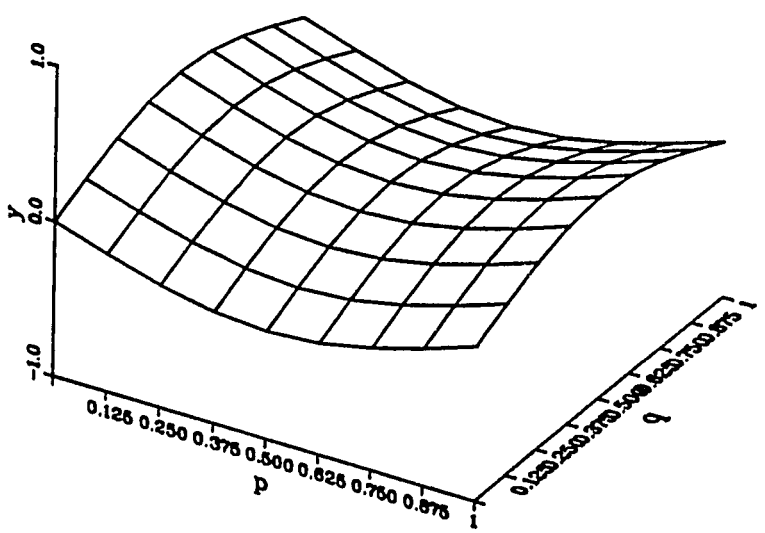

Figure 4.5 Second Flexible Body Mode

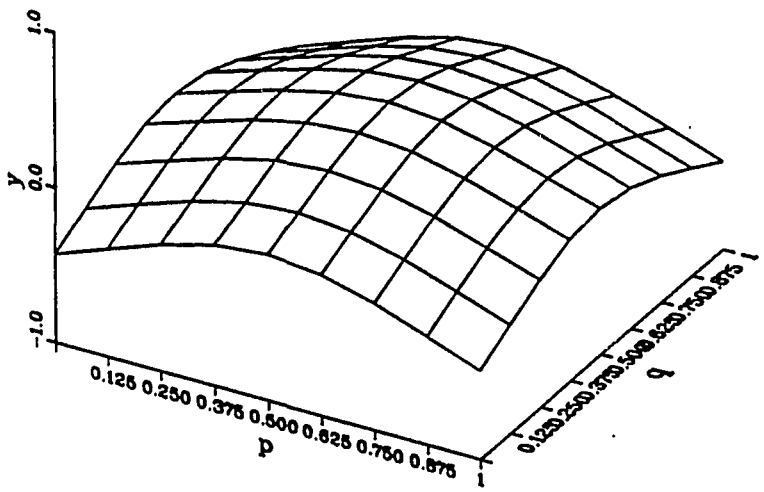

Figure 4.6 Third Flexible Body Mode

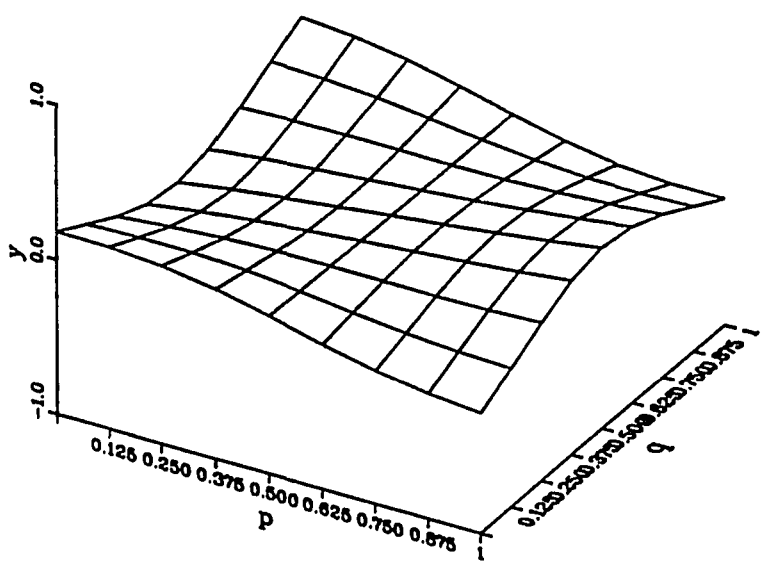

Figure 4.7 Fourth Flexible Body Mode

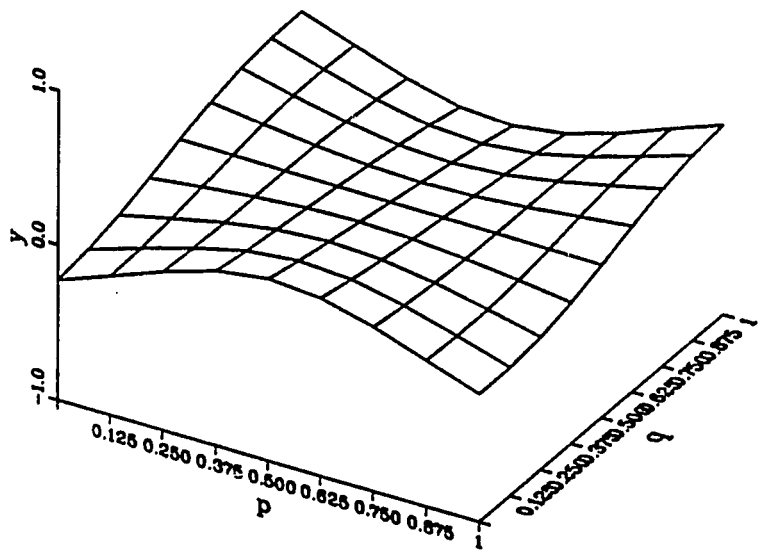

Figure 4.8 Fifth Flexible Body Mode

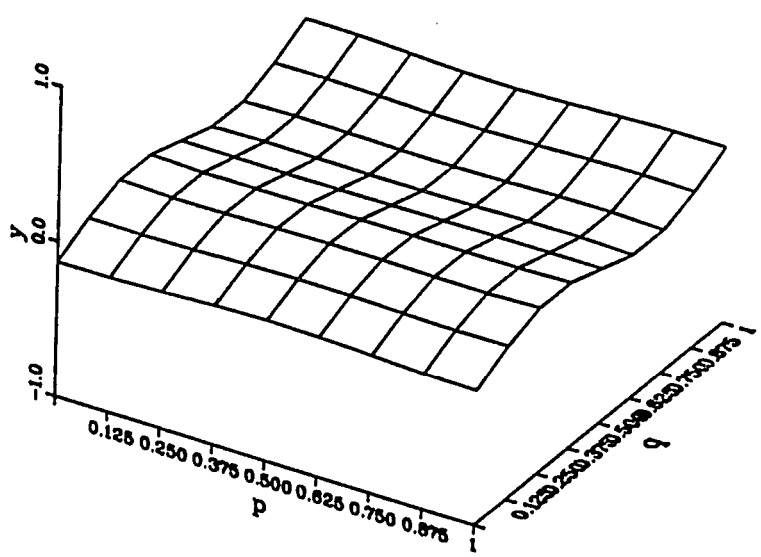

Figure 4.9 Sixth Flexible Body Mode

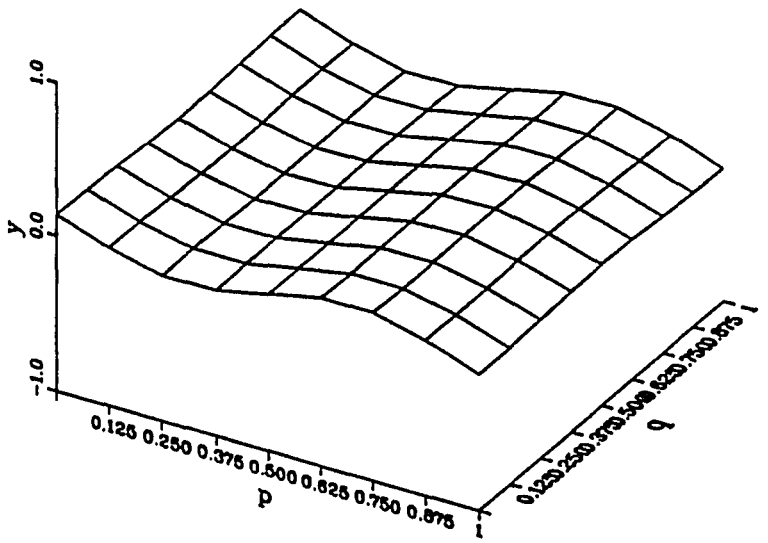

Figure 4.10 Seventh Flexible Body Mode

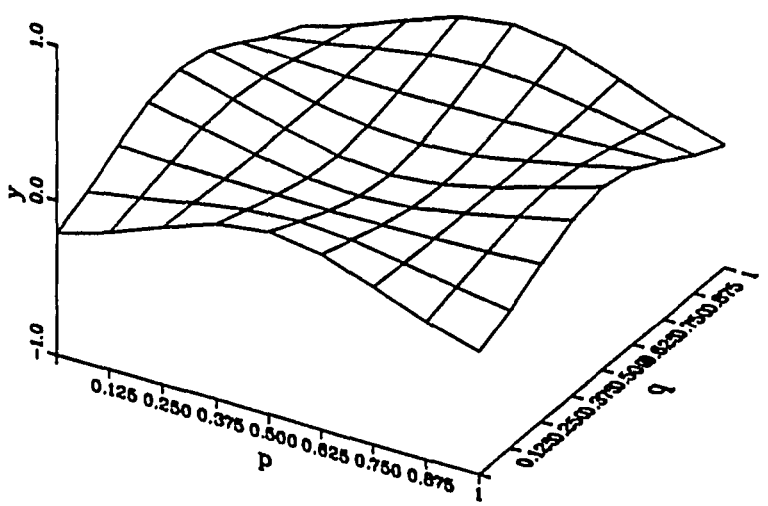

Figure 4.11 Eighth Flexible Body Mode

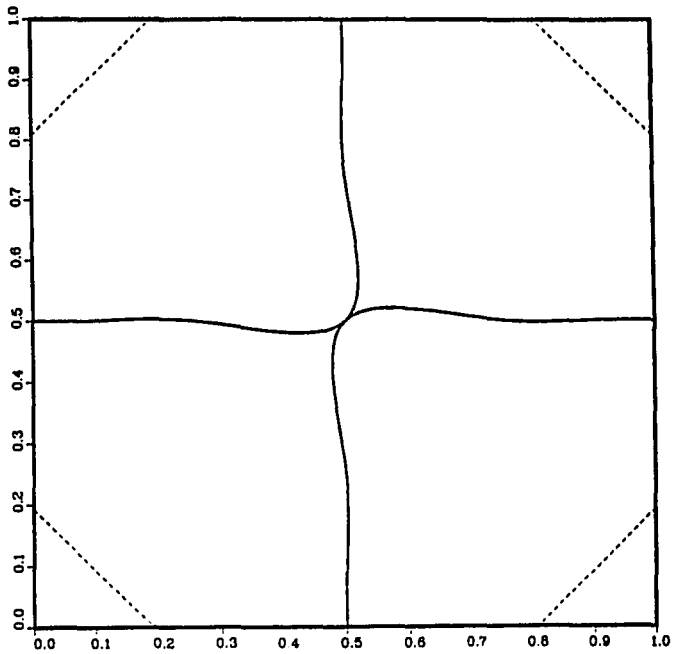

Figure 4.12 Zero Displacement Curve for the First Flexible Mode

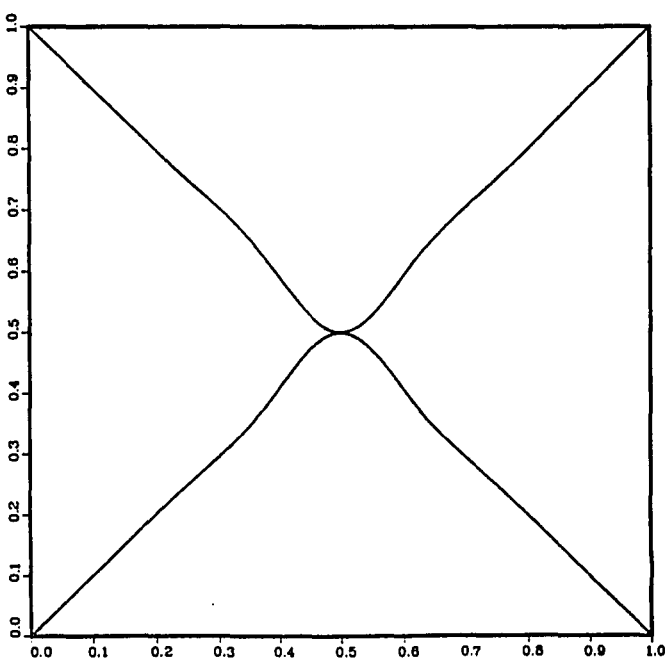

Figure 4.13 Zero Displacement Curve for the Second Flexible Mode

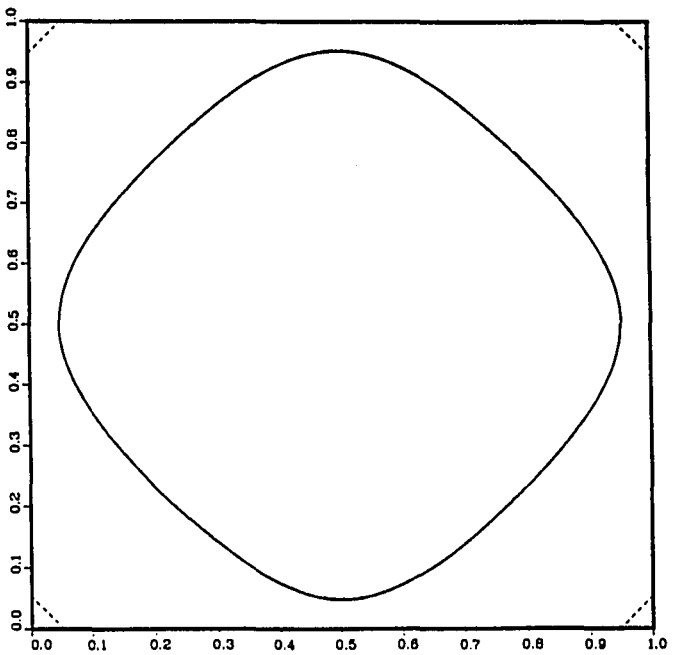

Figure 4.14 Zero Displacement Curve for the Third Flexible Mode

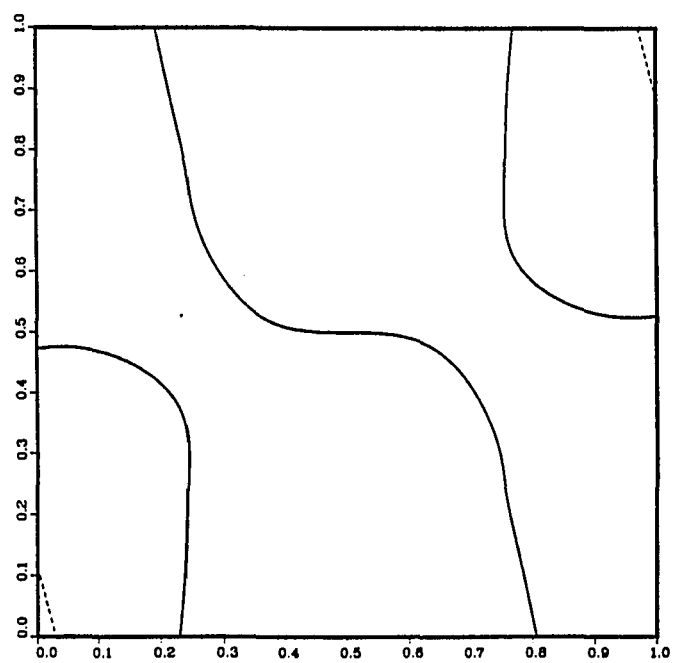

Figure 4.15 Zero Displacement Curve for the Fourth Flexible Mode

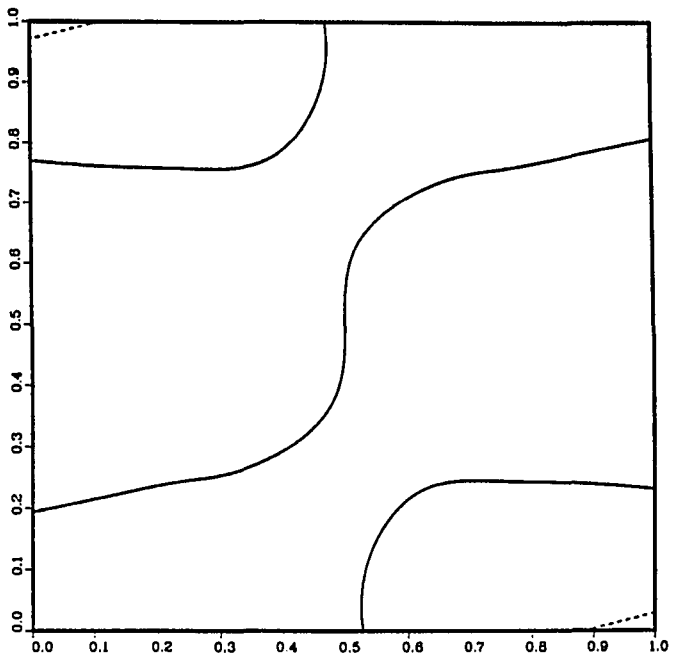

Figure 4.16 Zero Displacement Curve for the Fifth Flexible Mode

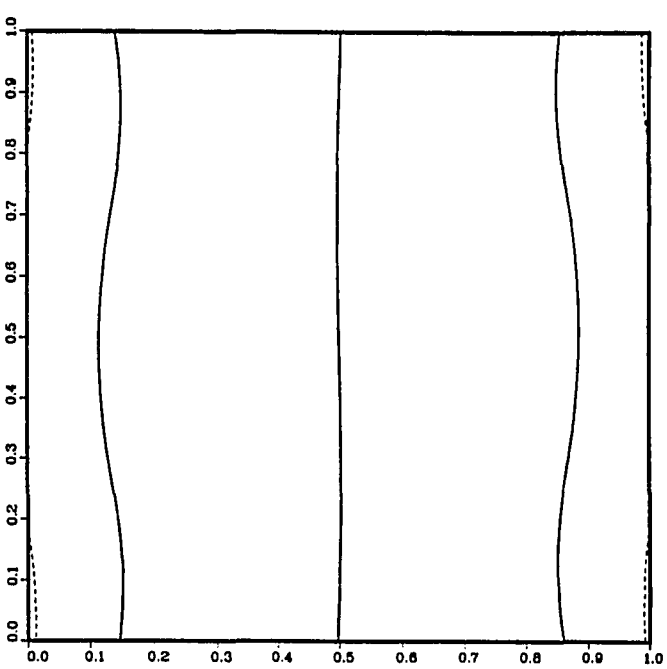

Figure 4.17 Zero Displacement Curve for the Sixth Flexible Mode

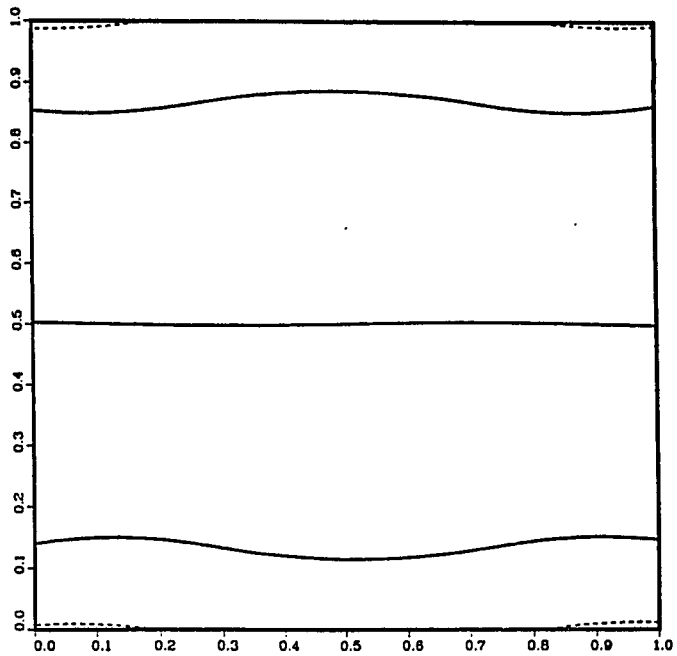

Figure 4.18 Zero Displacement Curve for the Seventh Flexible Mode

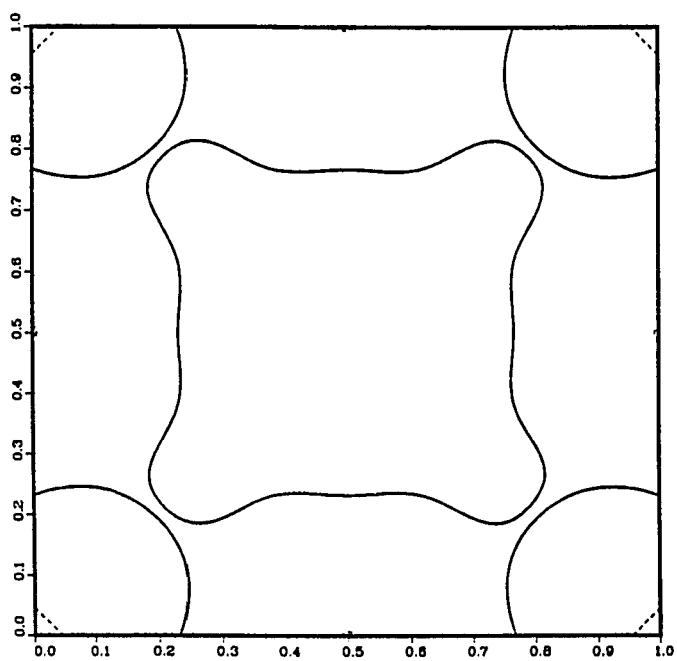

Figure 4.19 Zero Displacement Curve for the Eighth Flexible Mode

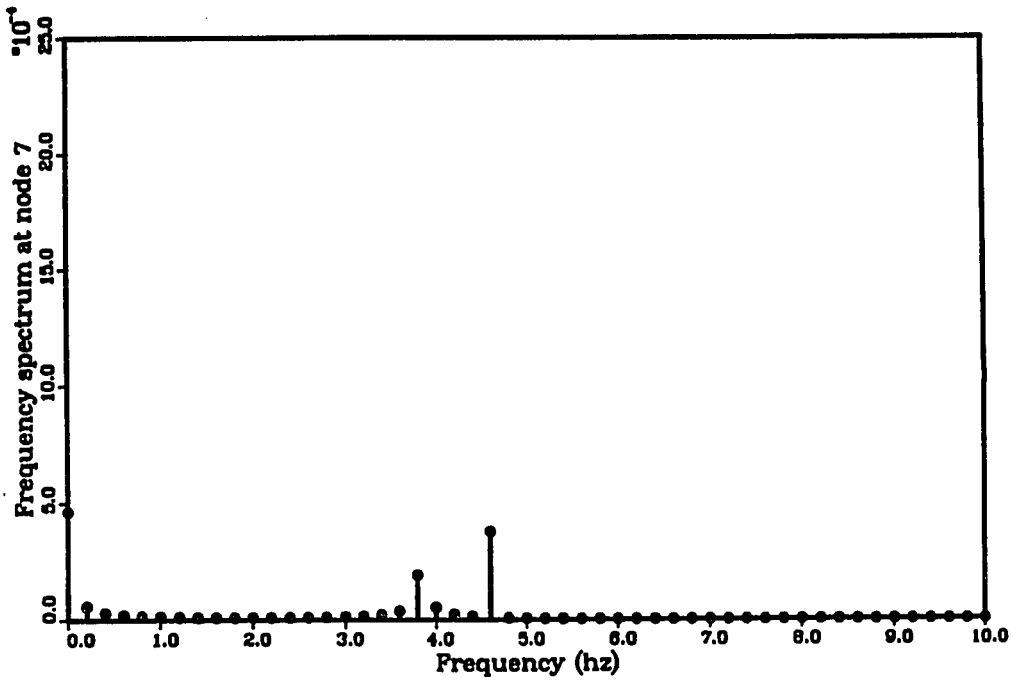

Figure 4.20(a) FFT (at Node 7) Obtained Using a Single Actuator

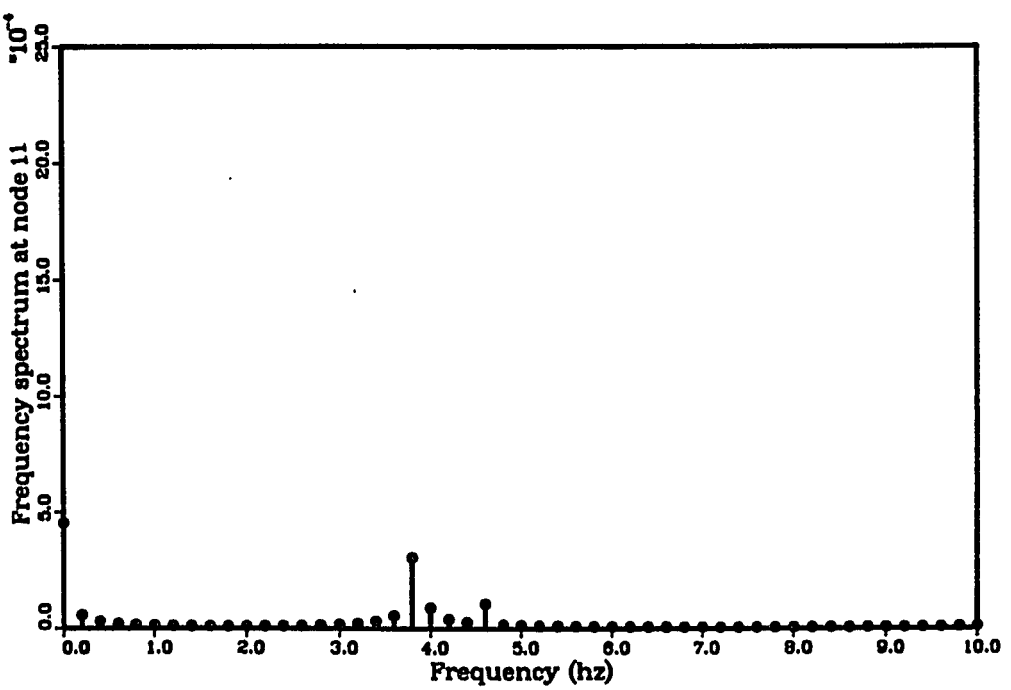

Figure 4.20(b) FFT (at Node 11) Obtained Using a Single Actuator

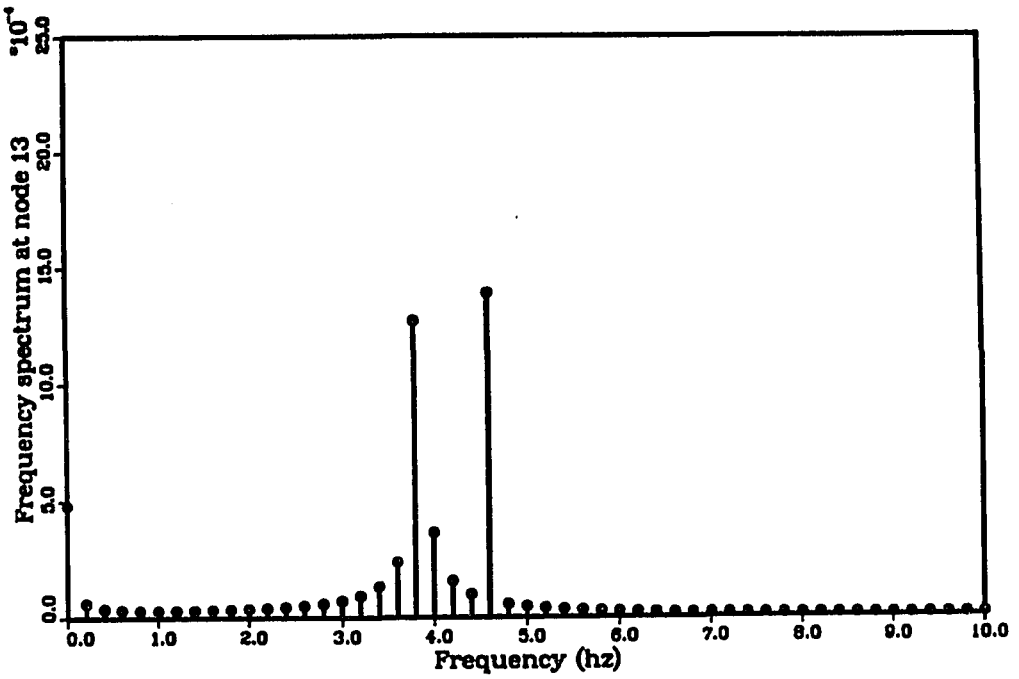

Figure 4.20(c) FFT (at Node 13) Obtained Using a Single Actuator

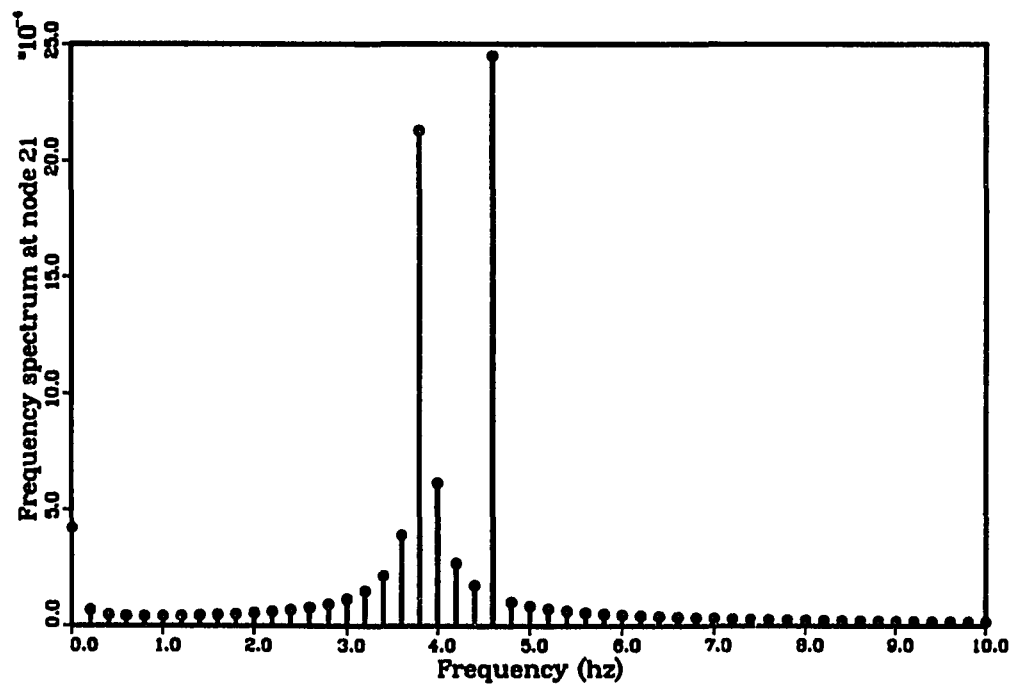

Figure 4.20(d) FFT (at Node 21) Obtained Using a Single Actuator

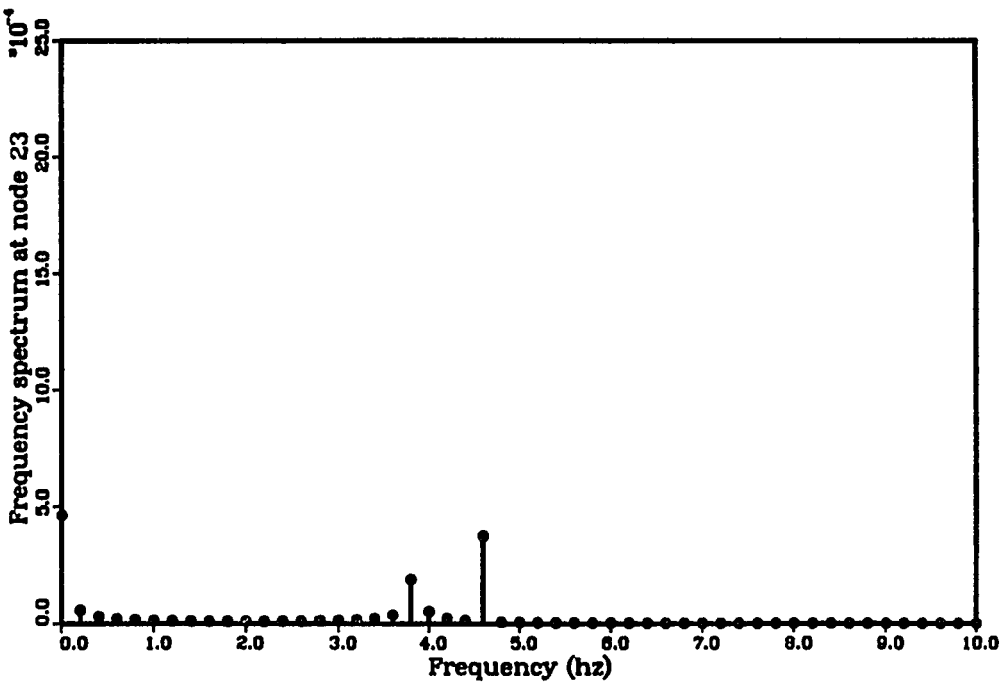

Figure 4.20(e) FFT (at Node 23) Obtained Using a Single Actuator

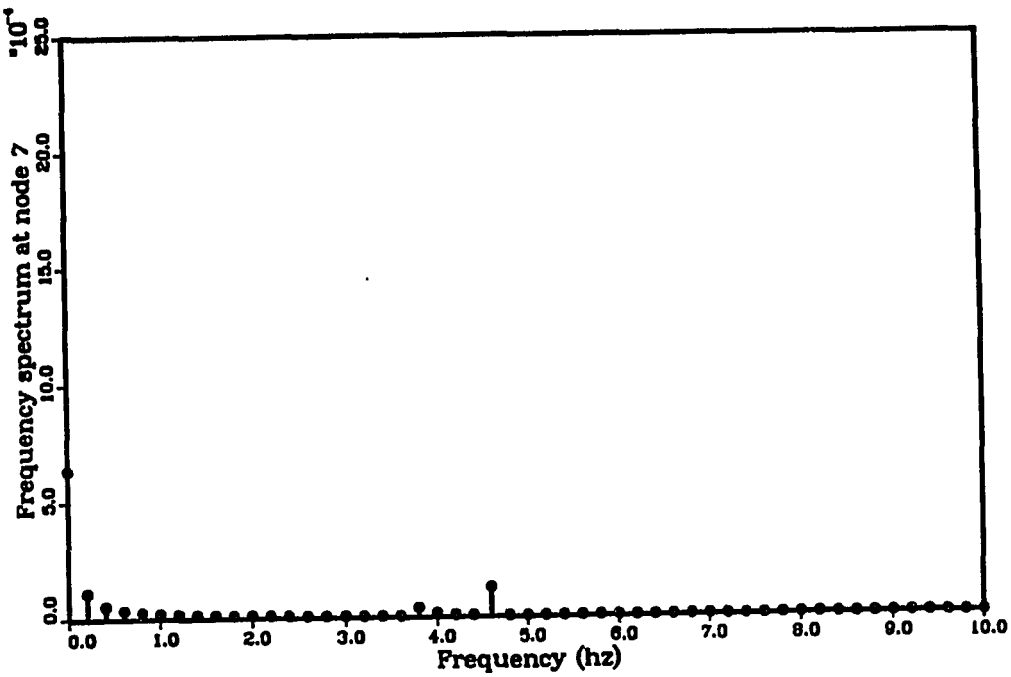

Figure 4.21(a) FFT (at Node 7) Obtained Using Two Actuators

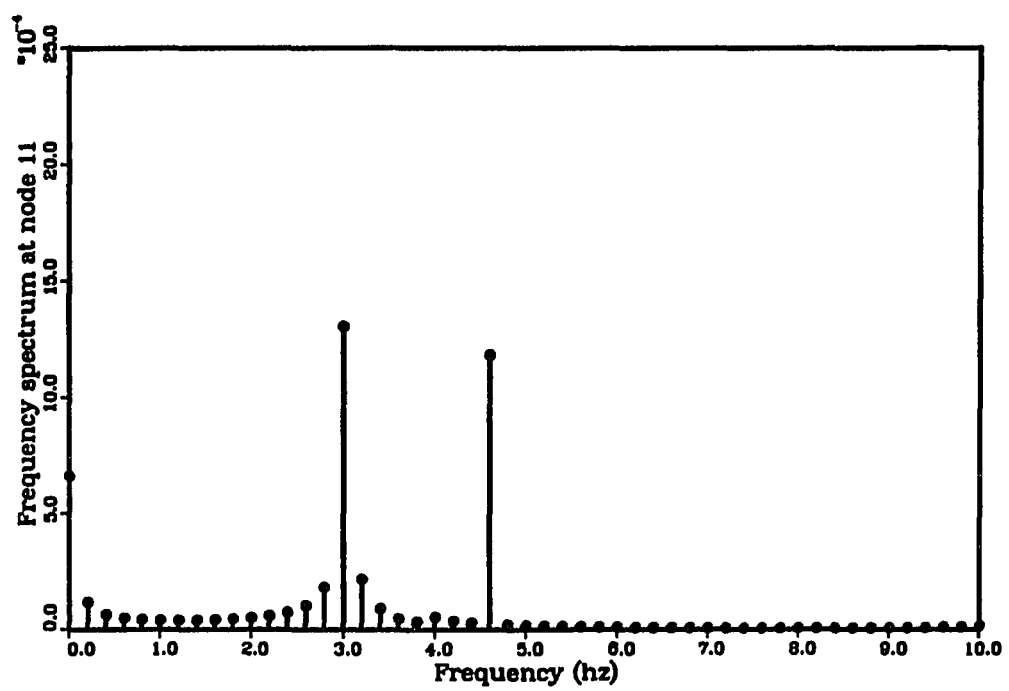

Figure 4.21(b) FFT (at Node 11) Obtained Using Two Actuators

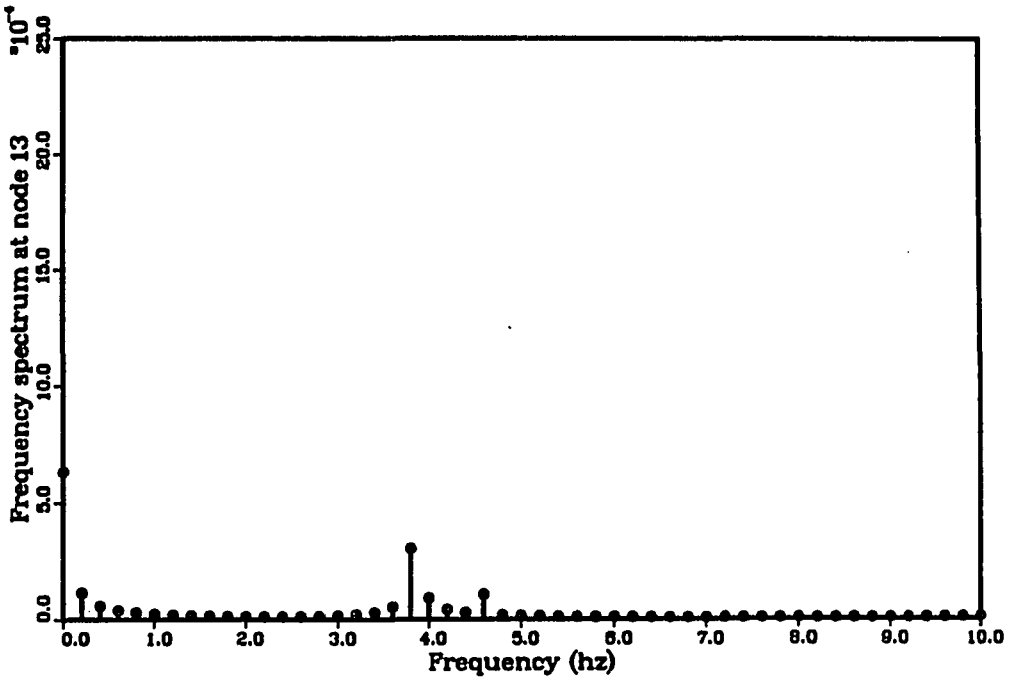

Figure 4.21(c) FFT (at Node 13) Obtained Using Two Actuators

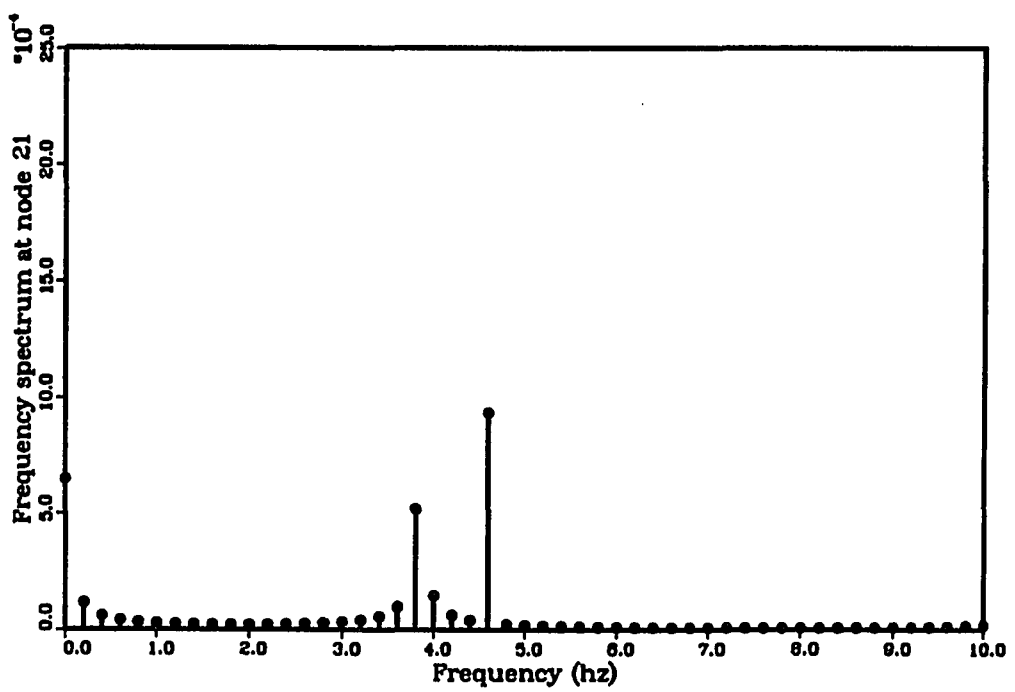

Figure 4.21(d) FFT (at Node 21) Obtained Using Two Actuators

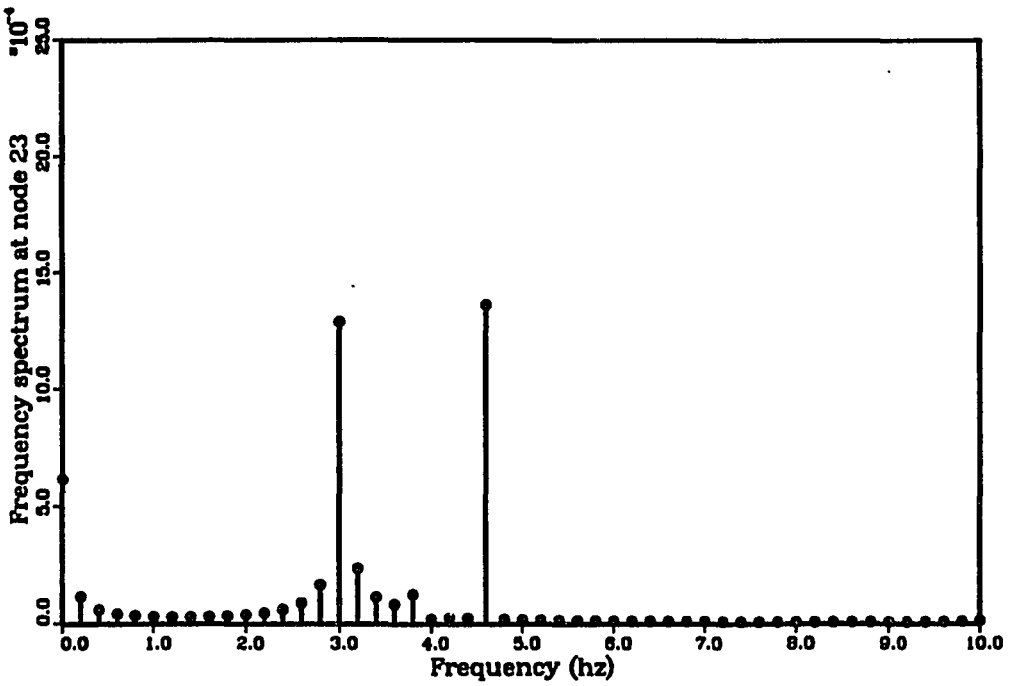

Figure 4.21(e) FFT (at Node 23) Obtained Using Two Actuators

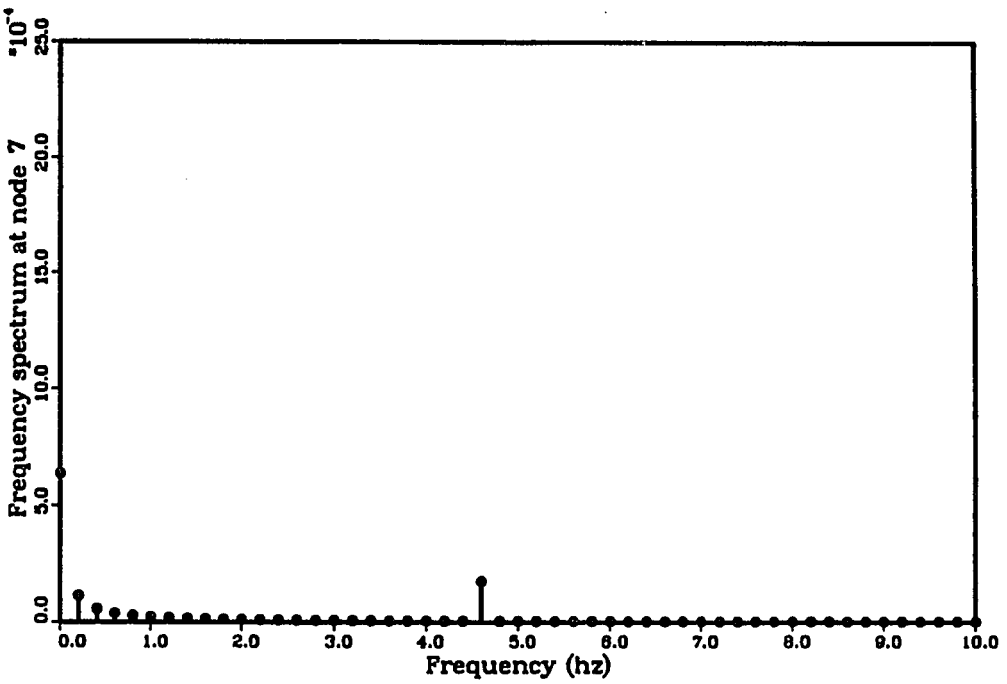

Figure 4.22(a) FFT (at Node 7) Obtained Using Three Actuators

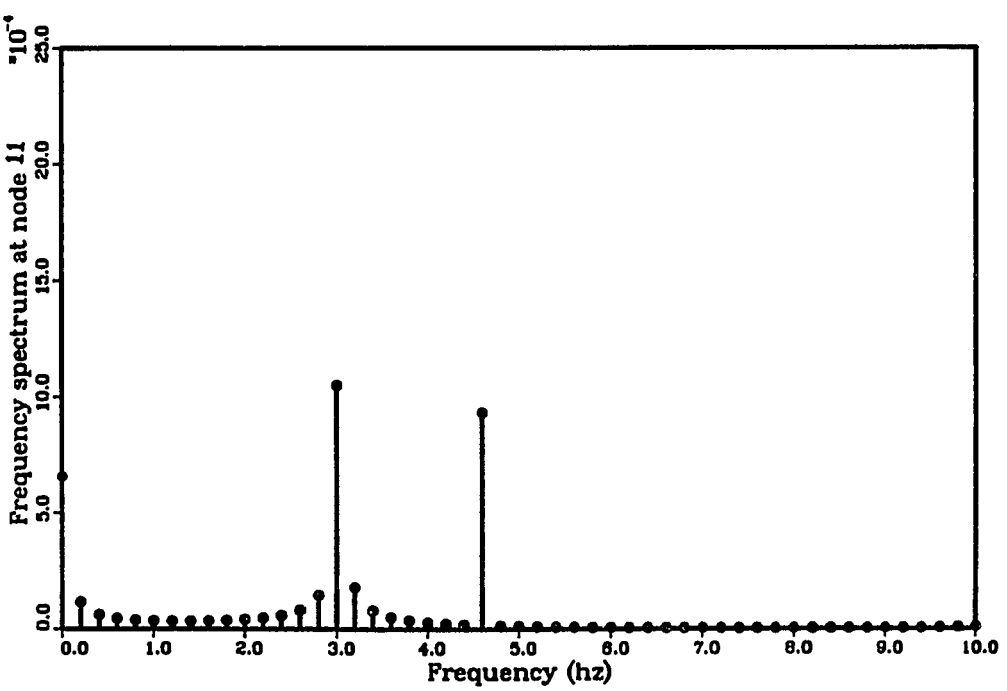

Figure 4.22(b) FFT (at Node 11) Obtained Using Three Actuators

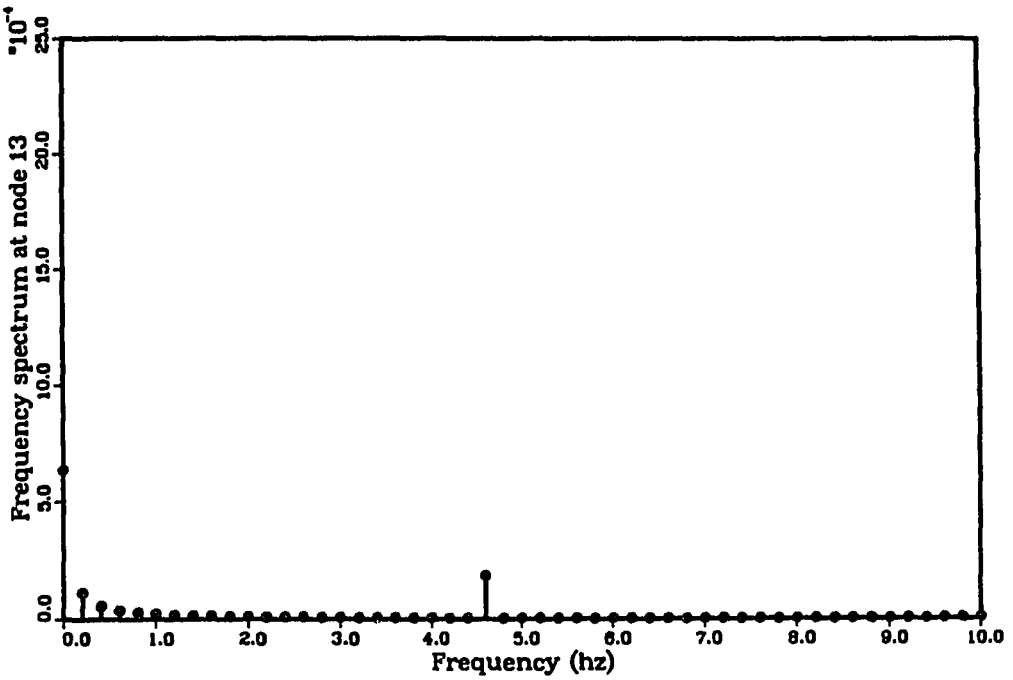

Figure 4.22(c) FFT (at Node 13) Obtained Using Three Actuators

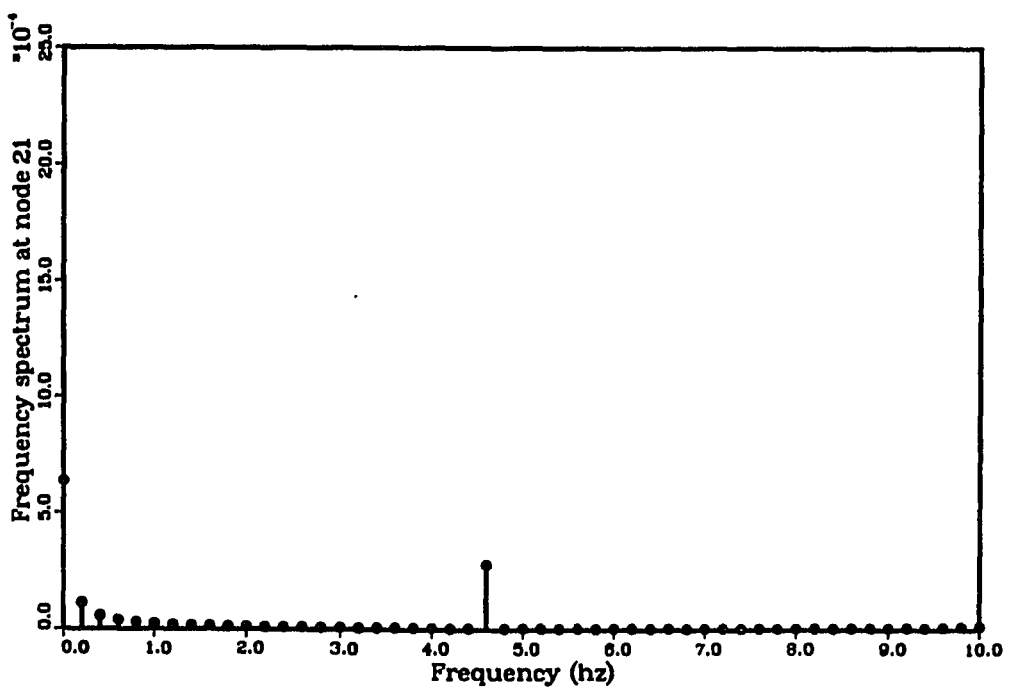

Figure 4.22(d) FFT (at Node 21) Obtained Using Three Actuator

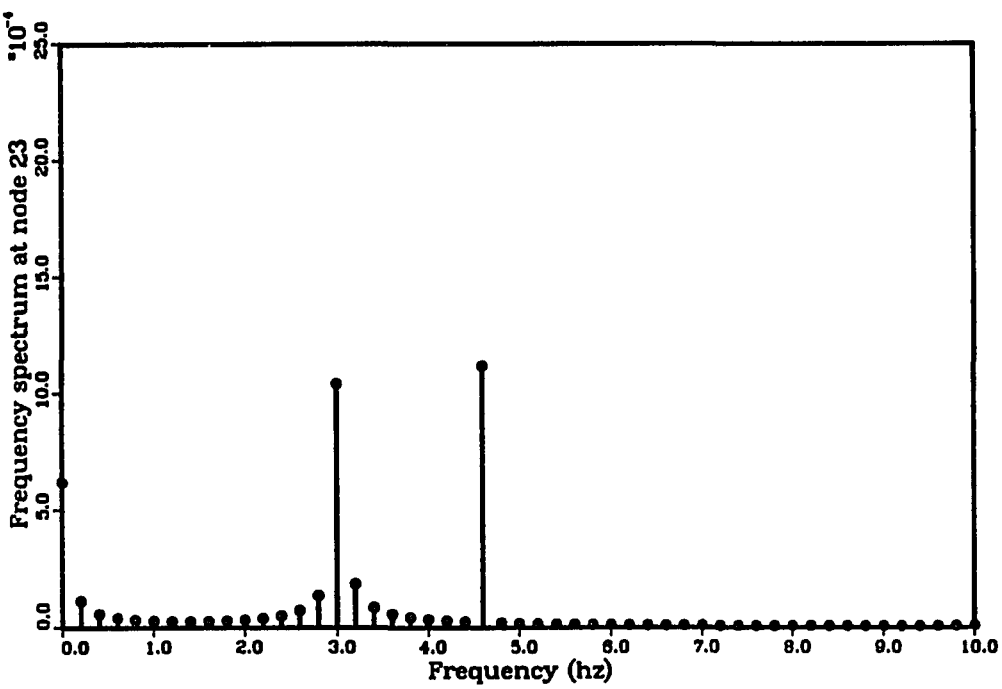

Figure 4.22(d) FFT (at Node 23) Obtained Using Three Actuators

CHAPTER 5
EXPERIMENT VERIFICATION

Experiments were conducted to test the accuracy of the theoretical predictions against laboratory measurements [36-50] of the open-loop control system performance. Both of the control schemes (mode and energy suppression) described in the previous chapters were tested on the structure using identical control hardware. Displacement response was measured at three positions distributed on the plate and compared with computer simulations for the same locations.

The main experimental objectives were: (1) verify system model, (2) verify applicability of control methods. The experiment is set up at the University of Arizona control laboratory. The structure is a one meter square, 0.635 mm thick, vertically suspended aluminum plate. Figure 5.1 illustrates the overall apparatus. Figure 5.2 indicates the finite element mesh, where locations on the plate refer to finite element model node numbers.

5.1. System Identification

Finite element mode shape analysis is useful prior to an experimental modal analysis. Most engineers have used the FEA mode shape data to determine optimum test strategies and compare experimental results. For example, one can use FEA mode shapes to determine excitation and response locations to extract the modes of interest.

There are three common ways of determining the natural frequencies and mode shapes. One is to utilize multiple shakers and the sinusoidal excitation

method. This type of test excites one mode of vibration at a time. When the shaker amplitudes and phase are tuned to excite a single resonance, the overall structural response could be used as an estimate of the mode shape of interest. This kind of test could be performed with analog instrumentation, using an oscilloscope display to observe the motion of the structure.

The second method is Fast Fourier Transform (FFT) analysis. Once the FFT analyzer has been developed, modal testing is accomplished in an entirely different manner. This type of test allows the simultaneous excitation of many modes at a time, using a variety of different sine, random, and transient excitation signals. This method can examine all the natural frequencies within a wide bandwidth of interest. The accuracy of test results depends on the sampling interval.

The third method is called driving point residues (DPRs) diagram [51]. Driving point residues are equivalent to modal participation factors, and are a measure of how much each mode is excited, or participates in the overall response, at the driving point. This method involves choosing the proper locations for mounting force transducers and shakers to the structure, such that one can obtain the certain mode shapes of interest. For example, suppose we want to excite the third vibration mode of a flat plate (in Chapter 4) and not excite the first and second modes. Then the best location to mount the actuator is node 13, because the DPRs is zero at node 13 for the first and second vibration modes and is the largest number in the third vibration mode (see Table 4.3).

Here, we combine the first and the third methods to examine experimentally the natural frequencies and mode shapes. We excite one mode at a time by choosing the point at which DPRs is as large as possible. Then we attach the actuators

(perhaps one or two of them) to the plate. The shaking signals will be sent by the power amplifier to the actuator.

5.1.1 Experiment Setup

The basic experimental equipment consists of linear voice coil actuators (BEI MOTION SYSTEM COMPANY, LA11-27-003A), noncontacting displacement sensors(KAMAN, KD-2300-8c), data translation (A/D, D/A) boards (DATA TRANSLATION, 2801A), a power amplifier, and an oscilloscope (Hi-Technique, IQ200).

The voice coil actuator is designed to provide large stroke and good low frequency response. The actuator, as shown in Figure 5.3, employs a magnetically driven reaction mass to provide the control force. Application of a current to a force actuator coil produces a proportional control force. Since the actuator is attached to the plate, a bearing is used to allow relative translation between the reaction mass and the actuator base. To avoid adding rigidity into the structure, a piano wire is used to connect the actuator to the plate. Since the actuator is attached to the plate by a double side tape, we are not able to drive the actuator higher than 6 Hz.

Each noncontacting displacement sensor consists of a small structure-borne coil that moves within an annular magnetic field generated by an externally supported magnetic field assembly. Movement of a displacement sensing coil through the magnetic field produces a voltage proportional to the displacement. The valid distance between the sensors and the structure of interest is 0.635 cm.

The data translation board is designed to transfer digital signals to analog signals, or vice versa. A program is required to collect or send data for the translation board. For example, the control signals generated by a PC are sent to the translation board, which sends the analog signals that will be translated to the amplifier. For this particular board (2801-A), only two channels are available to send the data and no more than two different signals may be generated. Also, when we collect the data from the sensors, the range of acceptable sampling frequencies are between 12.21 Hz to 4×10^5 for eight channels.

The power amplifier is used to supply desired currents to the voice coil actuator to drive the plate. The power amplifier was designed to eliminate the back EMF from the actuator so that a force command remains proportional to the voltage. The range of currents is 20 mA to 100 mA.

A digital oscilloscope is used to observe the structure's motion and display the output collected by the sensors. From the amplitudes and phases of the outputs we are able to estimate the natural frequencies and mode shapes. Since only two channels are available, two outputs will be displayed on the screen.

5.1.2 Natural Frequencies and Mode Shapes

A program has been developed in the UA control laboratory to calculate the natural frequencies and mode shapes. The results (natural frequencies and mode shapes) are verified by ANSYS. The difference between the results obtained in chapter 4 and the results obtained by using ANSYS is less than 0.1%. The model developed in Chapter 4 does not include the cables that hang the plate. The natural frequencies of this system including the cables are recalculated by ANSYS. The

results are shown in Table 5.1. We assume that the damping force is significantly less than the inertial or stiffness force and was not included in the model.

A finite element model of the experimental 1 meter by 1 meter aluminum plate was made. The resulting eigenvalues are compared with the actual structure in the UA control laboratory. The model is composed of 64 bending plate elements, with three degrees of freedom at each node, translation in the Z direction, and rotations about the X and Y axes. There are 25 master node points, as shown in Figure 5.2. The first three modes are rigid body modes and are not used in the analysis. The first 5 flexible modes were examined experimentally. Natural frequencies higher than 6 Hz were not tested.

Selecting the driving point is referred to Table 4.3. We used both one and two actuators to drive the plate. The comparison of the finite element model and the experimental measure is shown in Table 5.1. Good agreement was obtained for the first 4 flexible modes. From the modal frequencies, the finite element model is a little stiffer than the plate.

To obtain the first flexible mode we place two actuators on the plate; one is on node 8 and one is on node 18. When the driving frequency is close to the first natural frequency, the whole plate responds as Figure 5.4. The frequency is 2.05 Hz.

Then the driving frequency is increased gradually. The plate shows the mode shape in Figure 5.5 when the driving frequency is 2.90 Hz. This frequency is very close to the analytical result which is 3.03 Hz.

In order to obtain the third flexible mode, we place only one actuator at node 13 because the driving point residue is the greatest at that node. When the experimental mode shape is as shown in Figure 5.6, the natural frequency is 3.53 Hz. The finite element analysis result is 3.82 Hz.

We continue increasing the driving frequency by using two actuators placed at nodes 8 and 18, and obtain the fourth and the fifth vibration modes, which are anti-symmetric. These two modes are shown in Figures 5.7 and 5.8. The natural frequencies measured are 5.70 Hz and the finite element result is 5.40 Hz.

Table 5.1 Comparison of analytical and experimental results for the flat plate.

Mode	Analytical Frequency (hz)	Experimental Frequency (Hz)	Difference
1	2.07	2.05	0.02
2	3.03	2.90	0.13
3	3.82	3.53	0.29
4	5.40	5.70	-0.30

5.2. Examining Open-loop Control

The computer model is verified in the previous section. The mode shapes and natural frequencies agree with each other. This section involves the verification of the open-loop control designs that result from the computer simulations. The experimental data will be analyzed and compared to the numerical predictions to establish the fidelity of simulations.

Figure 5.9 shows a schematic diagram of the structure and open-loop control system. The open-loop control involves 4 steps. Step 1: the command signals are sent by a PC. A program [Appendix A] is used to generate the desired voltage. Then the data translation board transfers digital signals to analog signals. Step 2: the amplifier receives the analog signals and converts voltages to currents. Here, one voltage is converted to 10 mA. The actuators will be driven by these currents. Step 3: Sensors will provide the displacement information to the data translation board and will be transfered to digital signals via A/D board. A program [Appendix B] is used to specify the sampling time, channels, and data points. Here, the sampling frequency is 102.4 Hz. There are 512 data points collected for each channel. Step 4: Another PC was used to analyze the digital signals and do a FFT on the data.

The experimental data agree with the computer simulations, although not 100%. Let us consider the one-actuator case. Figure 5.10(a) shows the analytical time response at node 24. From Table 4.3 we know that only one mode which is the third flexible mode will be excited when one actuator is placed at node 13. The applied force is 0.142 $\cos\omega t$ Newton and ω = 4.6 Hz. Because the DPRs of node 24 are not zero associated with mode 4, 5, 6, 7, and 8, the output at node 24 can be used to predict energy in those modes. Figure 5.10(b) illustrates that

there is energy in mode 6 because the spectrum magnitude associated with 3.82 Hz is not zero. Due to the resolution of FFT we can not obtain one peak at 3.82 Hz. Therefore the exact energy can not be calculated. But energy is proportional to the spectrum magnitude. Note the driving frequency is 4.6 Hz.

Figure 5.11(a) shows experimental test data at node 24. The profile of the time reponse is similar to the simulation (See Figure 5.10(a)). Figure 5.11(b) represents the FFT at node 24. The result shows that there is only one mode excited, at 3.53 Hz. The driving frequency is 4.6 Hz.

Since the plate is hung by cables, there is no optimal location for the two-actuator case. The pendulum motion will affect the rigid modes such that equation (4.3) cannot be satisfied. The optimal location for the plate was not tested. For two-actuator case, we place actuators at node 8 and node 18. The magnitude of the command force for each actuator is 0.071 Newton. Figure 5.12(a) is the analytical time response at node 24 and Figure 5.12(b) is the FFT of the data. From Table 4.3, we know energy in mode 6 will decrease and energy will be dumped into mode 5, which is associated with 3.03 Hz. The spectrum magnitude at mode 6 in Figure 5.12(b) is much less than in Figure 5.10(b). The spectrum is not zero at frequency 3.03 Hz.

Figure 5.13(a) shows experimental test data at node 24 with two actuators attached to the plate. The transient response disappears shortly after 1 second because the rigidity from the actuators is larger than for the one-actuator case. The spectrum magnitude at frequencies 2.90 Hz and 3.53 Hz as shown in Figure 5.13(b) are not zero, and are obviously less than the simulation because the damping

has become larger. The pendulum motion becomes clear because of the spectrum near 0 Hz.

For the three-actuator case, we place actuators at nodes 8, 13 and 18. Our objective was to suppress the energy in the sixth mode. The magnitudes of command forces of the actuators are 0.1683, -0.1946 and 0.1683 Newtons, respectively. Figure 5.14(a) is the simulation time response at node 24. Figure 5.14(b) shows the energy in the sixth mode is eliminated, but energy is dumped into the fifth mode. Figure 5.15(a) illustrates the experimental data for this same case. The transient response is not clear because the three actuators attached to the plate add rigidity to the plate; the plate behaves almost as a rigid plate. Figure 5.15(b) represents the spectrum analysis of the data. In Figure 5.15(b), the magnitude in the fifth mode is smaller than the computer simulation, as shown in Figure 5.14(b).

The spectrum magnitude and the time history differ between the experiment and the simulation because the plate becomes more rigid when more actuators are attached. In the control laboratory we are not able to procure a very thin, flat plate. The shape of the plate looks like a dome, which is similar to the sixth mode's shape. This means there exists some strain energy in that particular mode. Additionally, when we hang the plate rotated 90 degrees about the z axis, as shown in Figure 5.2, we are not able to obtain the desired frequencies and mode shapes. The error between the experimental results and the simulation can not be avoided.

5.3. Discussion

To compare the experimental data with analytical results is not easy. There are many uncertainties such as aerodynamic, actuator dynamic, and equipment

dynamic. Those unknowns cause errors and make the comparison difficult. The test data represent a significant effort in providing a ground-based test facility to prove the open-loop control of a thin plate.

The plate example illustrates some of the principles that are applicable to the design of a control system for the space experimental article. Through the use of extra actuators, the amount of energy in the flexible modes at the end of the positioning maneuver can be reduced using either a mode or an energy suppression technique. While not entirely illustrated by these test results, the proposed techniques may also be used to determine effective actuator location and to evaluate the relative advantage of adding additional actuators.

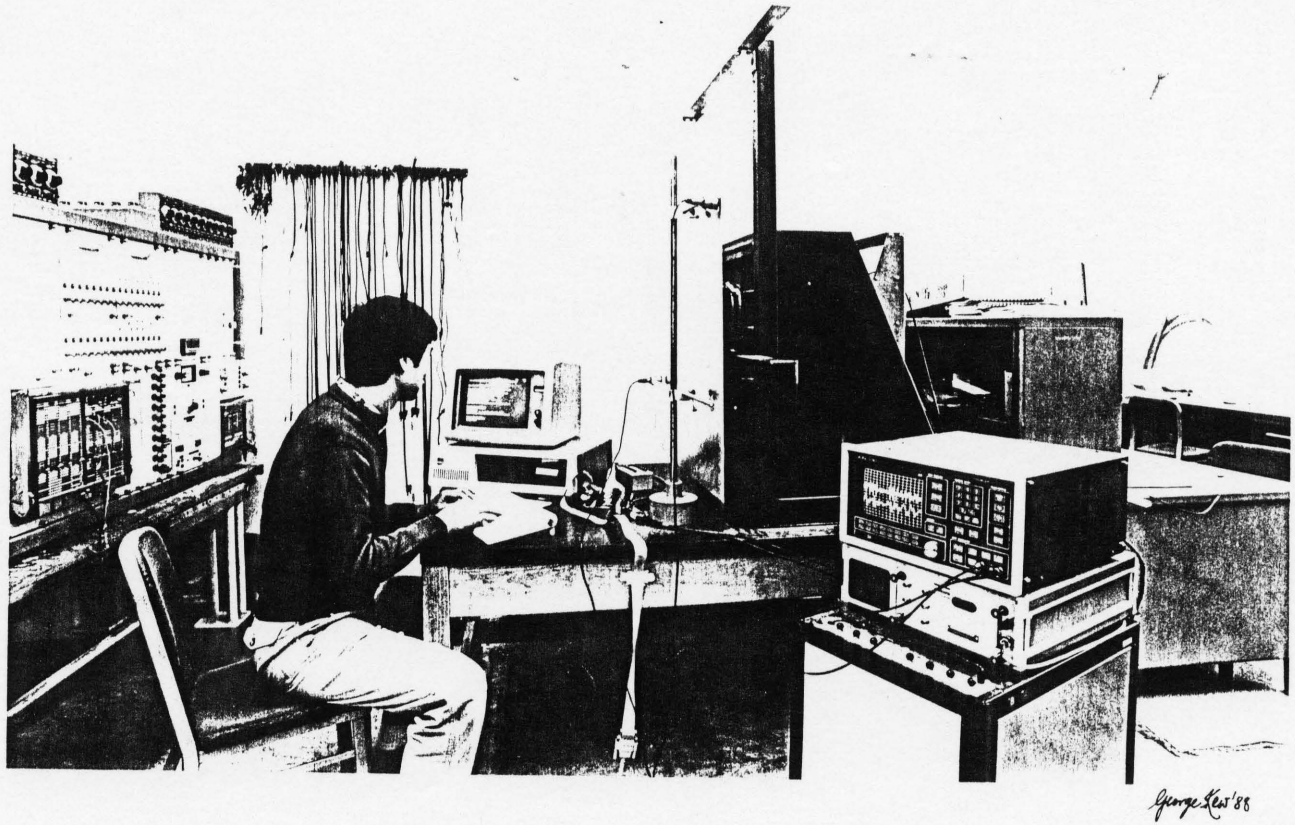

Figure 5.1 The Overall Apparatus of Experiment Set Up

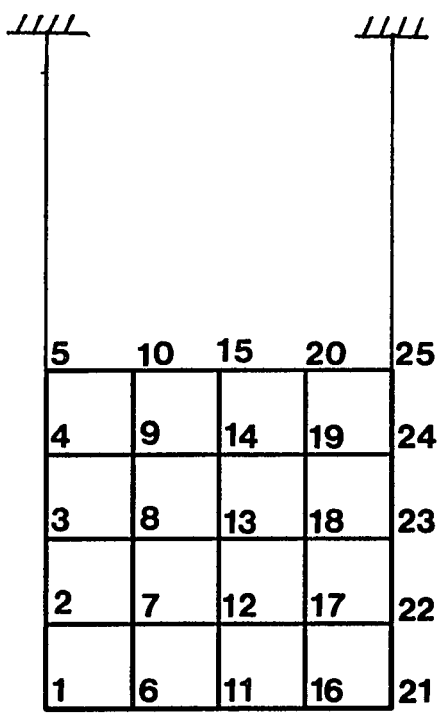

Figure 5.2 Plate Experiment Actuators and Sensors Configuration

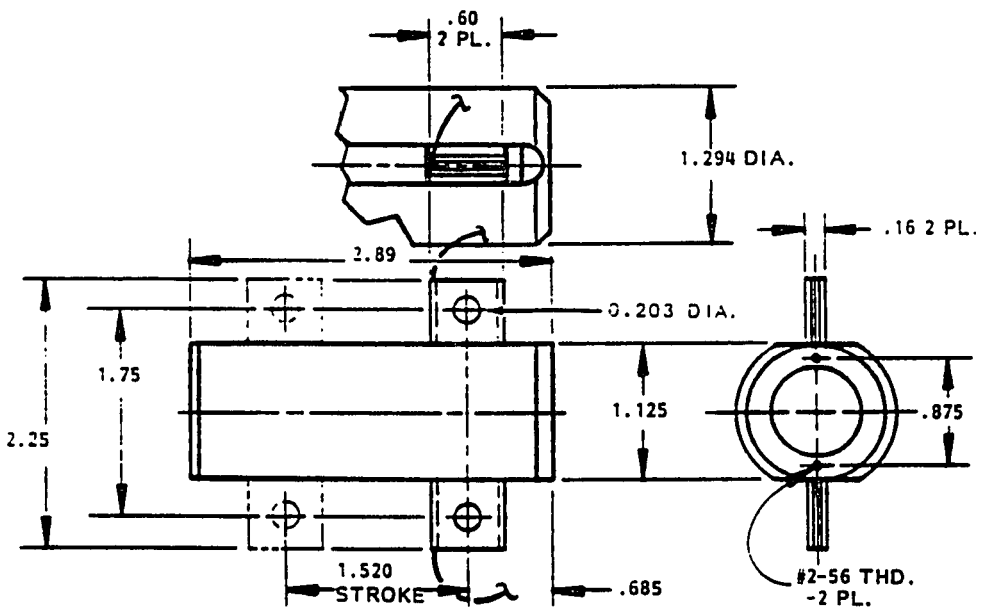

Figure 5.3 Voice Coil Actuator

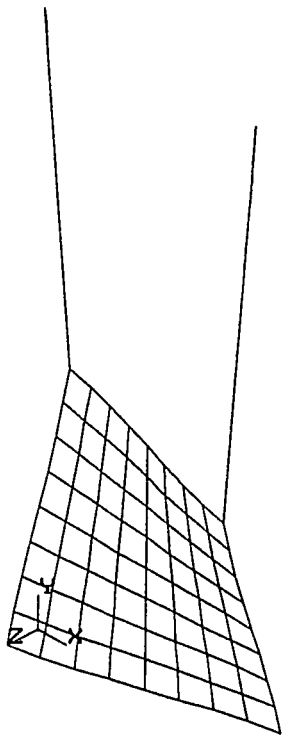

Figure 5.4 The First Flexible Mode

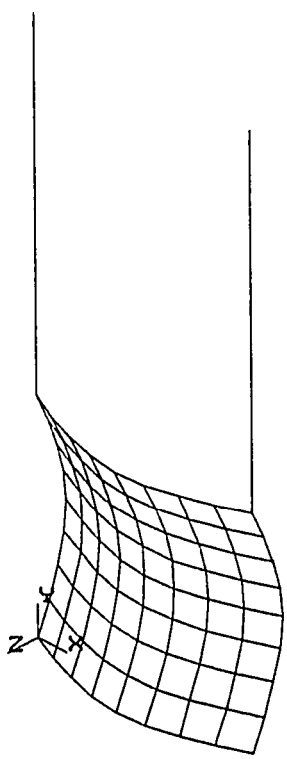

Figure 5.5 The Second Flexible Mode

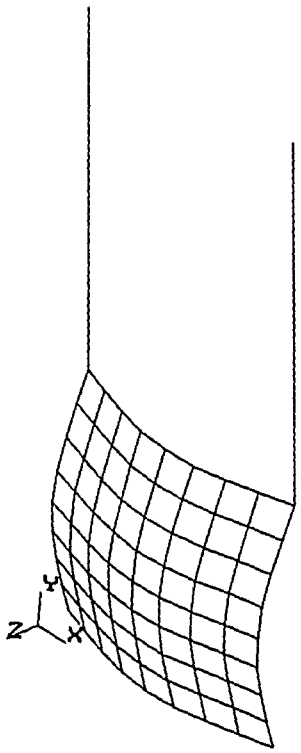

Figure 5.6 The Third Flexible Mode

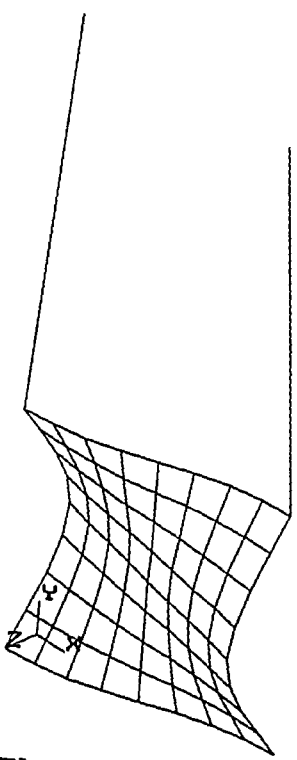

Figure 5.7 The Fourth Flexible Mode

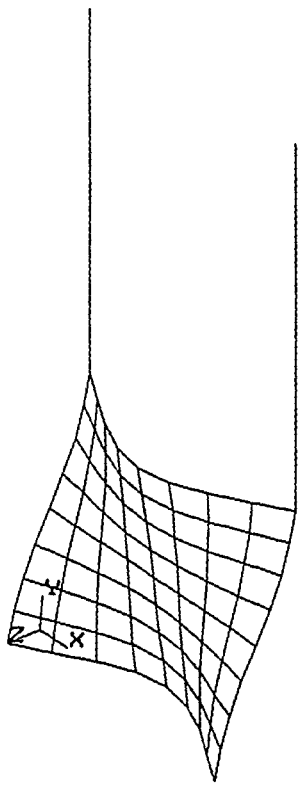

Figure 5.8 The Fifth Flexible Mode

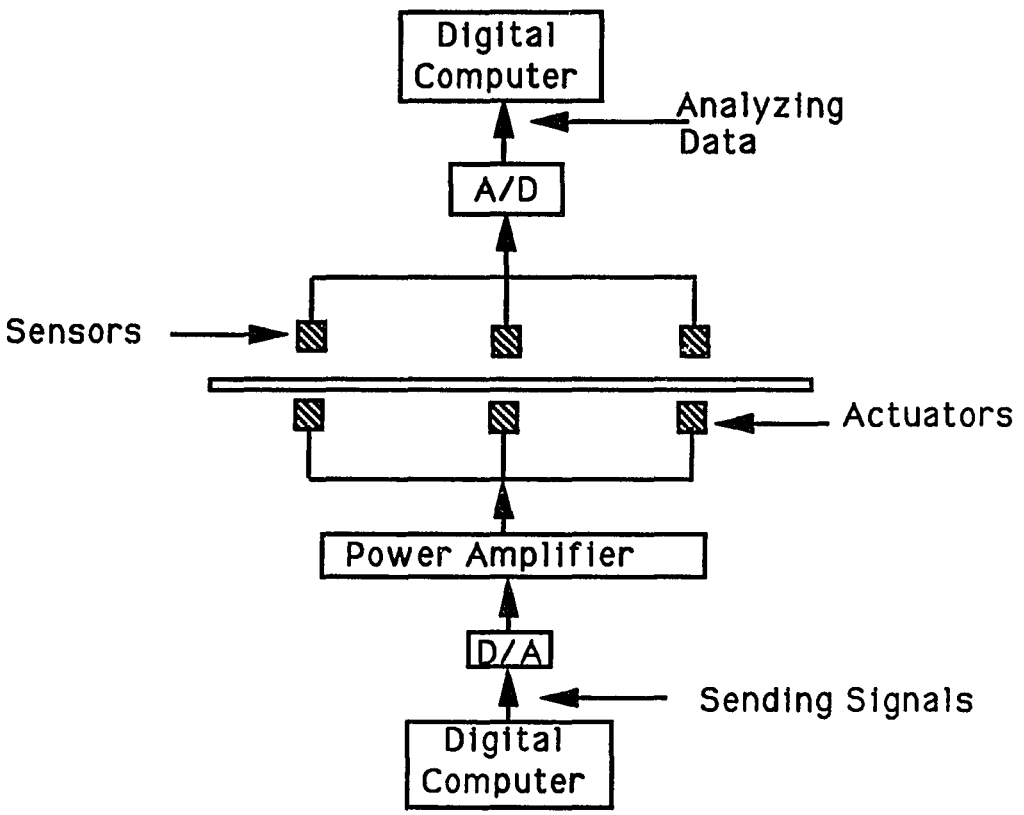

Figure 5.9 Schematic Diagram of the Control System

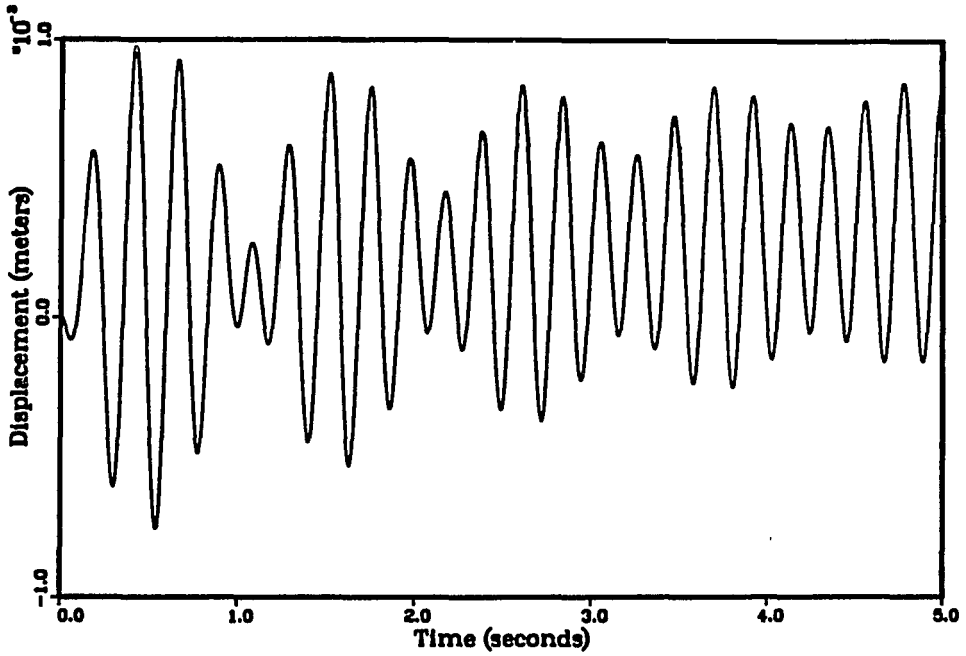

Figure 5.10(a) The Numerical Time Response at Node 24 Using a Single Actuator

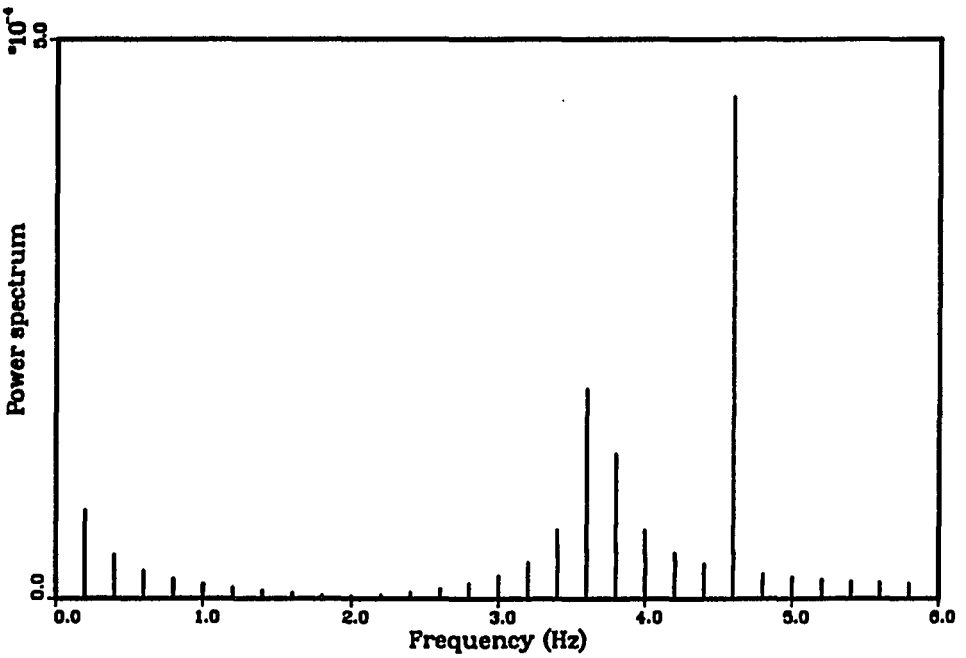

Figure 5.10(b) FFT of the Numerical Data at Node 24 Using a Single Actuator

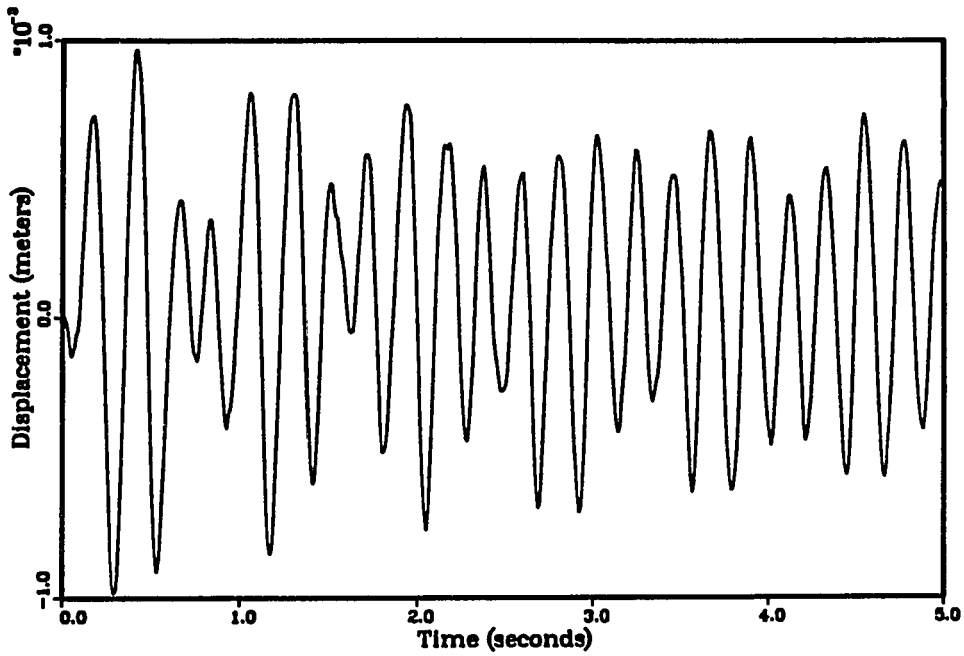

Figure 5.11(a) The Test Data at Node 24 Using a Single Actuator

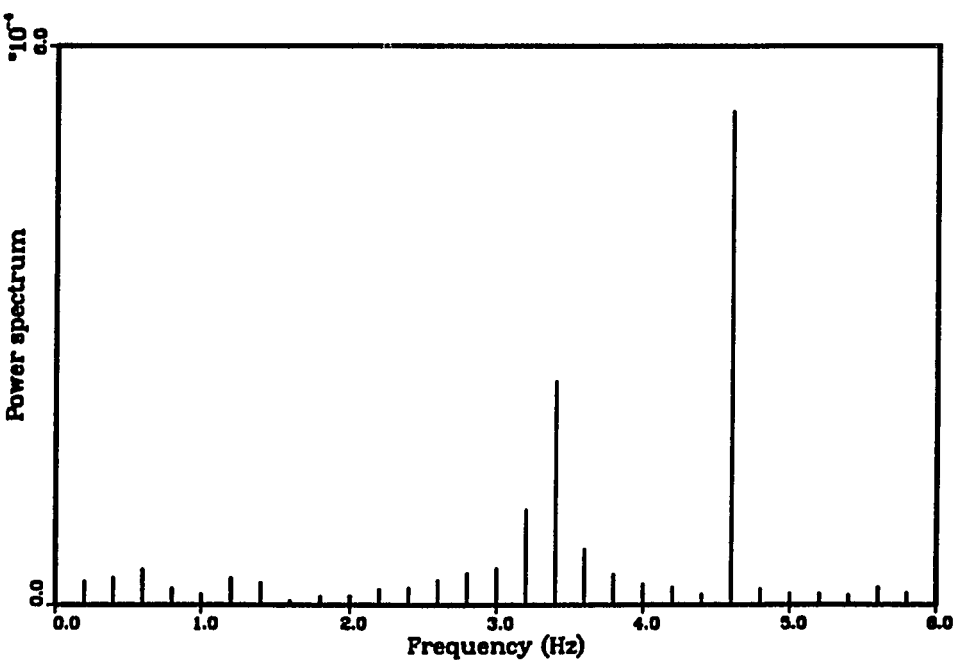

Figure 5.11(b) FFT of the Experimental Data at Node 24 Using a Single Actuator

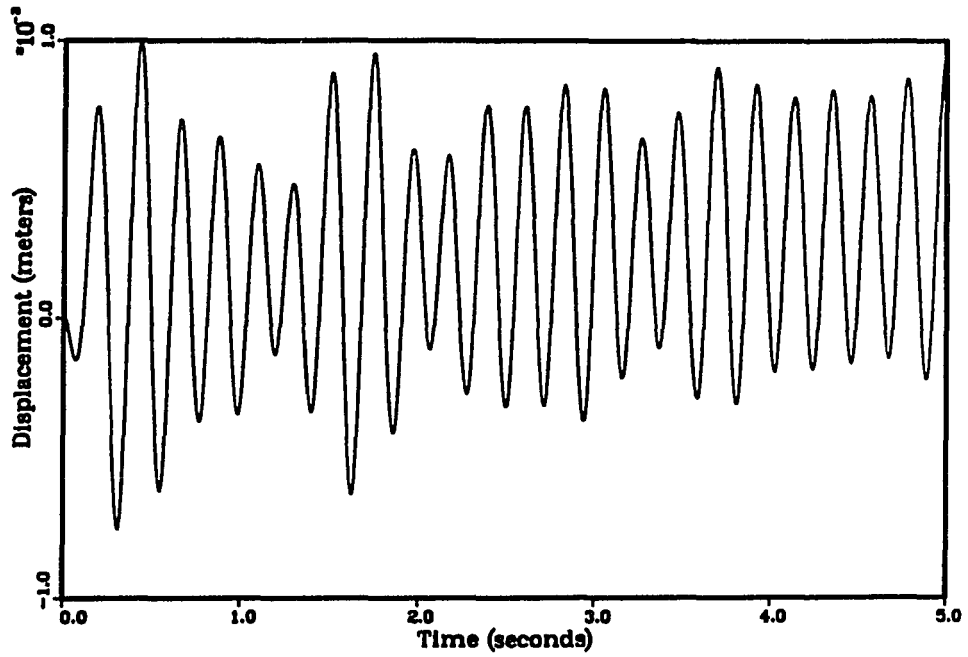

Figure 5.12(a) The Numerical Time Response at Node 24 Using Two Actuators

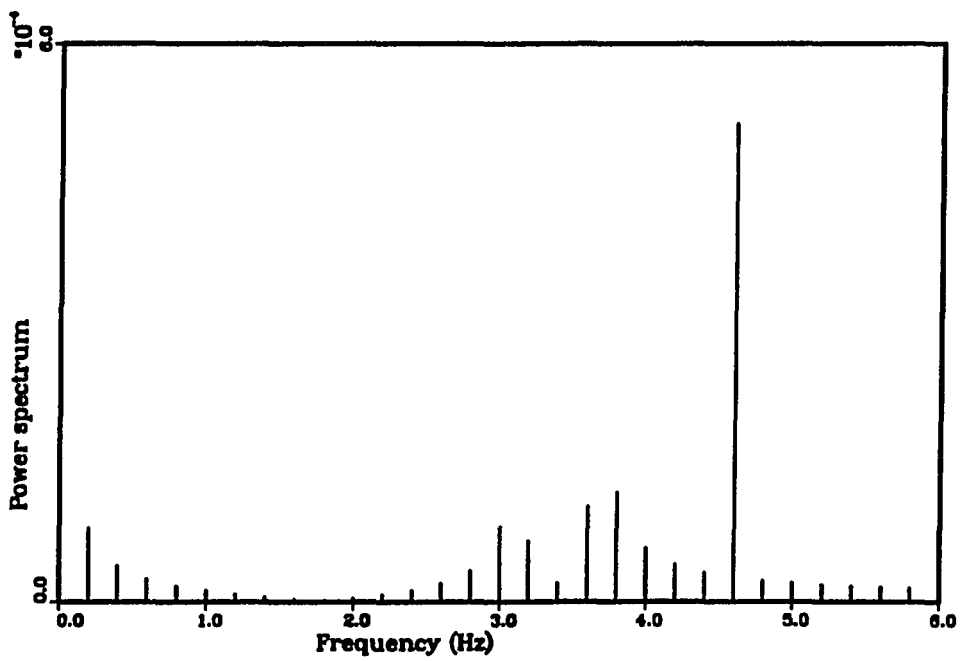

Figure 5.12(b) FFT of the Numerical Data at Node 24 Using Two Actuators

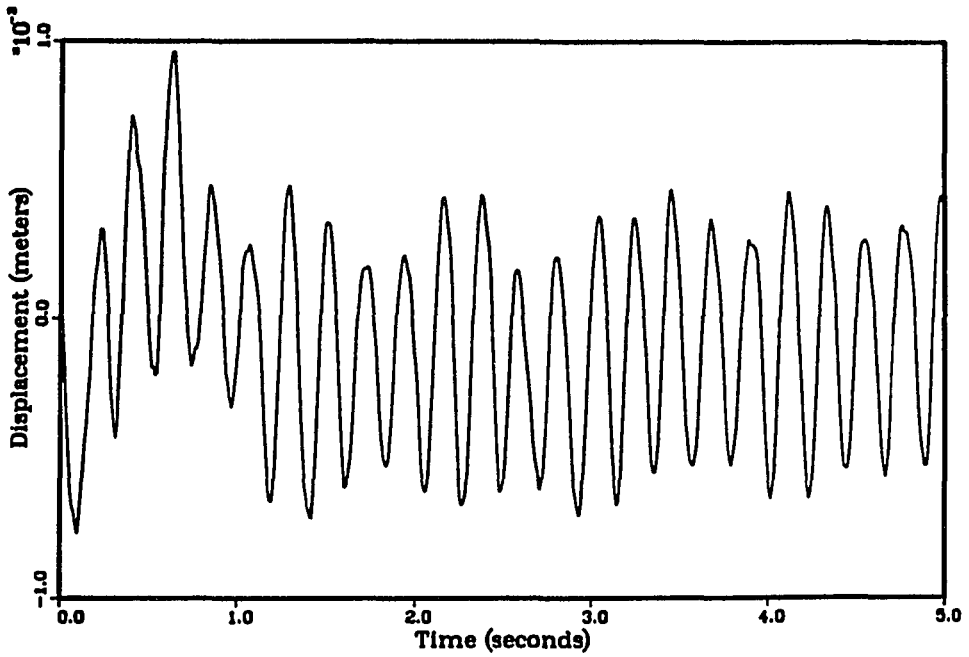

Figure 5.13(a) The Test Data at Node 24 Using Two Actuators

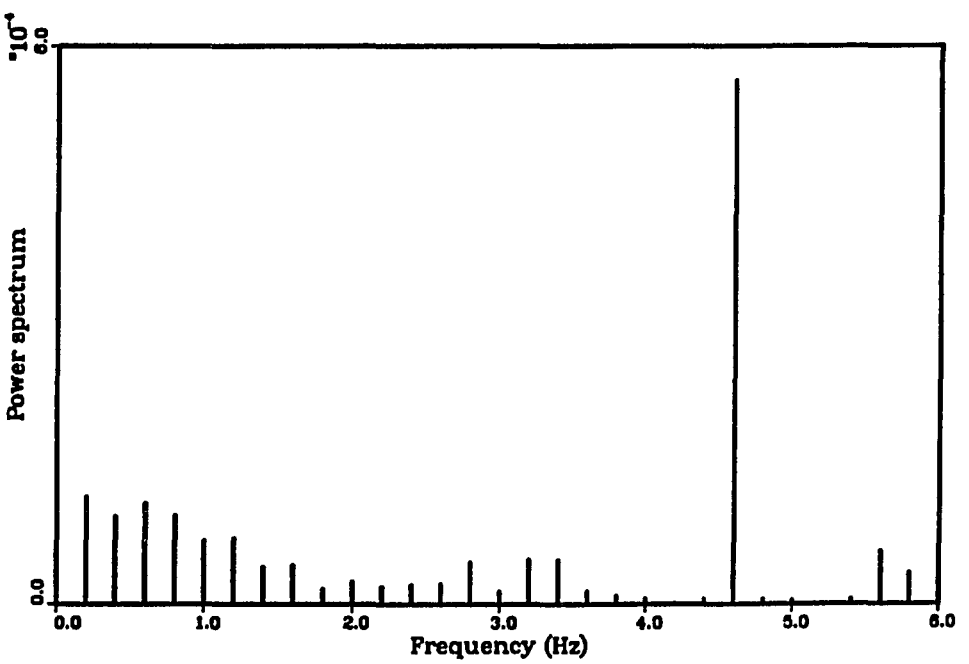

Figure 5.13(b) FFT of the Experimental Data at Node 24 Using Two Actuators

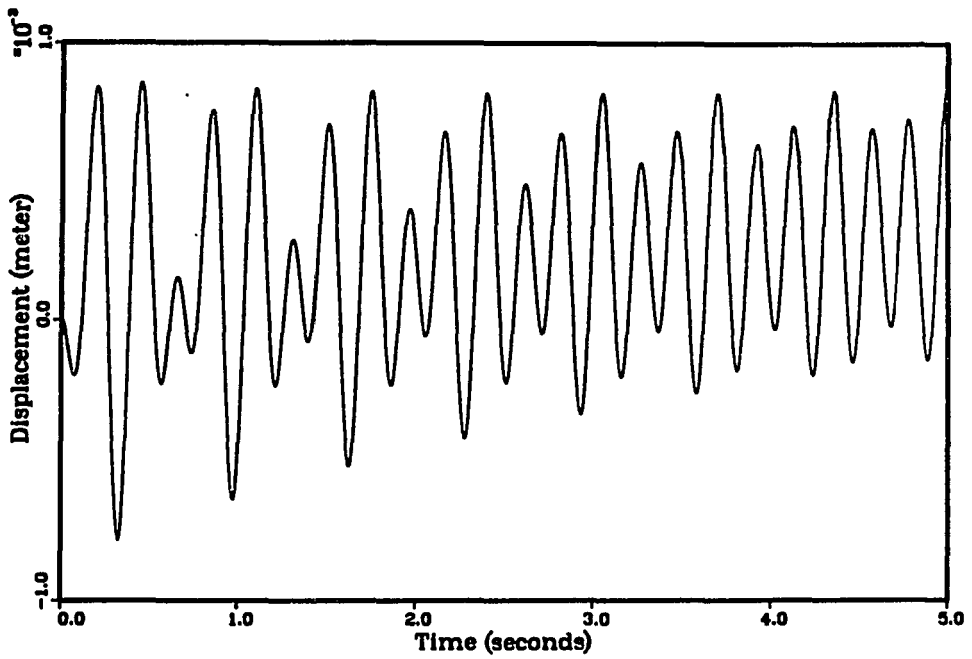

Figure 5.14(a) The Numerical Time Response at Node 24 Using Three Actuators

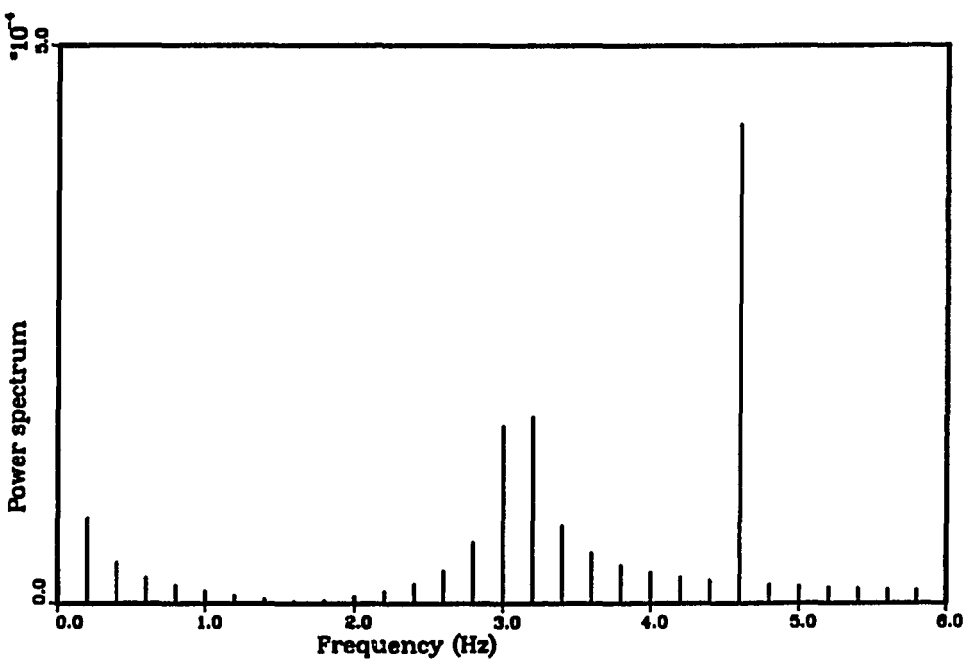

Figure 5.14(b) FFT of the Numerical Data at Node 24 Using Two Actuators

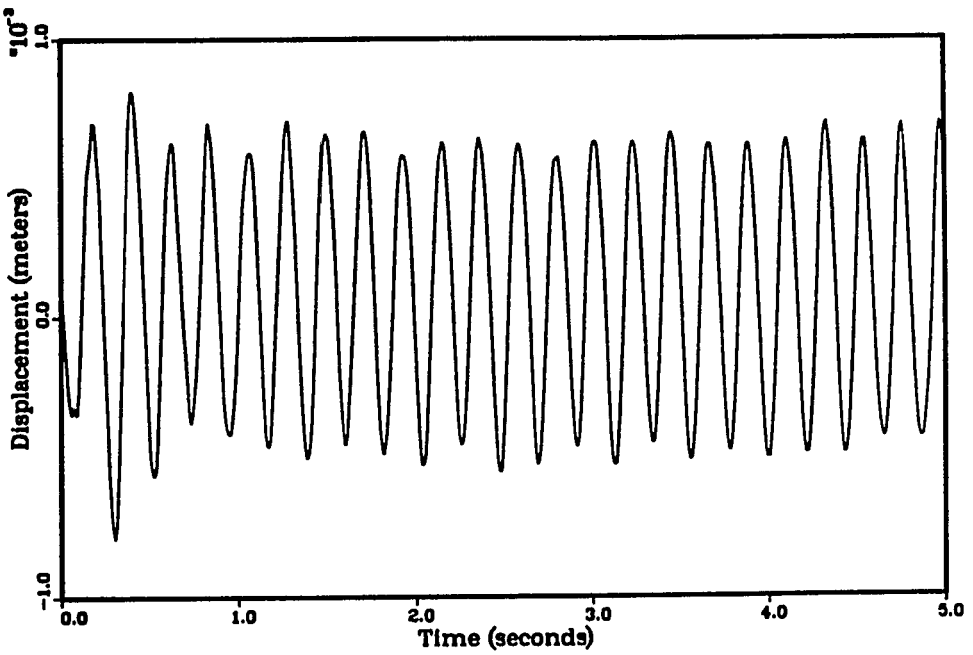

Figure 5.15(a) The Test Data at Node 24 Using Three Actuators

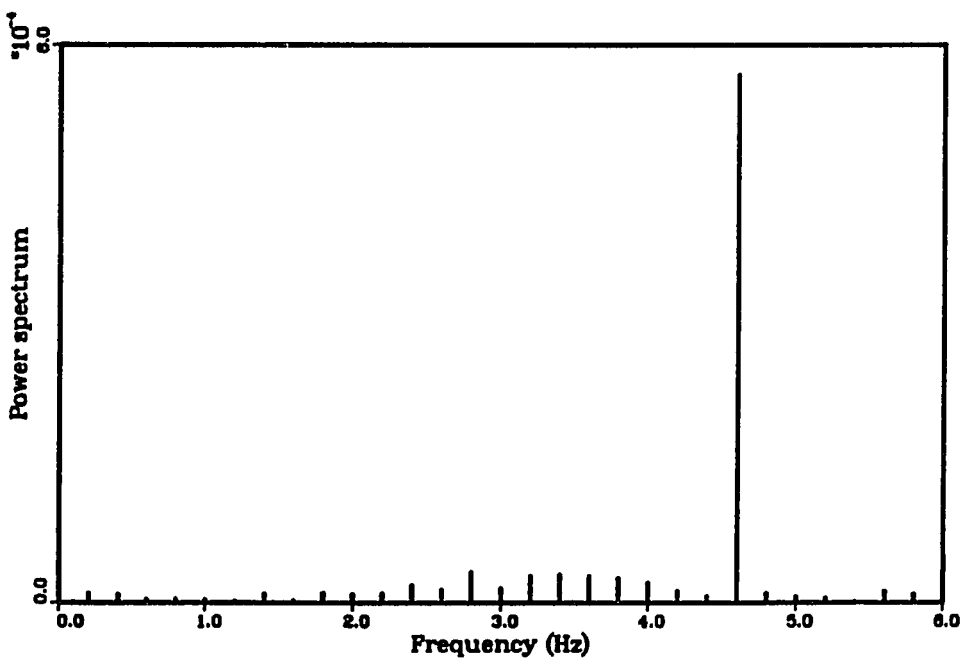

Figure 5.15(b) FFT of the Experimental Data at Node 24 Using Three Actuators

CHAPTER 6
METHODS FOR UNCERTAINTIES

Chapter 3 discussed the open-loop control system design. This chapter presents the closed-loop control law, which eliminates the uncertainties. There are a number of promising research methods that can deal with uncertainties. We will consider four approaches to handle the nonlinear effect.

In the first two sections, the methods used to control uncertainties will be introduced [52-58]. An example will be presented for comparing different approaches. Then a new approach will be provided that eliminates the nonlinear effect such that the system will follow a desired trajectory.

6.1. Introduction

Consider a two dimensional system of the form

$$\begin{aligned} \dot{x}_1 &= f_1(x_1, x_2, w, v) \\ \dot{x}_2 &= f_2(x_1, x_2, w, v) \end{aligned} \tag{6.1}$$

where f_1 and f_2 are C^1 functions of the state x_1, x_2, control w, and uncertain input v. The dot denotes differentiation with respect to time. The control is assumed to be bounded according to

$$|w| \leq w_m \tag{6.2}$$

and the uncertain input is assumed to be bounded by

$$|v| \leq v_m \tag{6.3}$$

where w_m and v_m are both positive numbers and $v_m < w_m$. Furthermore, assume that when $w = v = 0$, the system has a single unstable equilibrium point at the origin. Because of this instability and because of the limited control available, the controllable set (under $v = 0$) will be a subset of the state space. Our design objective here is to determine a state feedback control law for w such that the system will be driven to within the closest possible neighborhood of the origin from the largest possible subset of the controllable set. This is to be accomplished in spite of all possible control action by the uncertain input v to the contrary.

If a given stabilizing feedback control law $w(x_1, x_2)$ satisfies (6.2), then (6.1) may be rewritten as

$$\begin{aligned} \dot{x}_1 &= g_1(x_1, x_2, v) \\ \dot{x}_2 &= g_2(x_1, x_2, v) \end{aligned} \tag{6.4}$$

where now with $v = 0$, this system should be a stable system to the origin throughout some subset of the controllable set which can be considered the domain of attraction for $w(x_1, x_2)$. Consider now the set of points reachable by all possible control actions by v satisfying (6.3) for the system (6.4). We have previously called this reachable set the v-reachable set (Gayek and Vincent, 1985).

For two dimensional systems, the v-reachable set can readily be determined using methods of qualitative control theory. For example, in (6.4) the boundary of the v-reachable set may be found by satisfying the necessary conditions for a control that will drive the system along the boundary of the v-reachable set (Gramham and Vincent, 1975). In particular, along the boundary of the v-reachable set the input v must maximize the function

$$H = \lambda_1 g_1(x_1, x_2, v) + \lambda_2 g_2(x_1, x_2, v) \tag{6.5}$$

such that the maximum value is zero. The $\lambda's$ are adjoint to the system perturbation equations. For those situations where the v-reachable set boundary control is bang-bang, the adjoint equations may be dispensed with, since a switching curve for determining the control may be determined from the conditions

$$\begin{aligned} H &= 0 \\ \partial H/\partial v &= 0. \end{aligned} \tag{6.6}$$

Hopefully, the v-reachable set will be a small subset of the domain of attraction under w. It represents the extent that the uncertainty can destabilize the system while the system is operating under the given control law for w.

The domain of attraction under a given control law for w, subject to the uncertainty v, is like a donut with an inner hole defined by the v-reachable set. The shape and size of both the v-reachable set and the outer boundary depend on the control law for w. While there have been several methods proposed for dealing with system uncertainty, few studies calculate the v-reachable set or the domain of attraction and compare the efficiency of a given method with respect to others based on this information.

6.2. Methods for Uncertain Systems

Classical control theory has always been concerned with uncertain systems. However, this concern has generally been implicit rather than explicit. The idea of "turning up the gain" of an output feedback system to improve "system robustness" is an implicit way of handling system uncertainty (Chen, 1987). Indeed, it works quite well in some cases. We call this approach method 1.

Modern control theory, with its focus on pole placement, implicitly buffers the system from uncertain inputs by placing the system poles well to the left of the imaginary axis. For controllable systems, full state feedback allows for arbitrary placement of the controlled system poles. Alternately, the feedback gain may be determined by solving the matrix Riccati equation (Hollot and Barmish, 1980). We call this approach method 2.

The "second method of Lyapunov" has been used to provide an alternate approach to the design and analysis of control systems (Kalman and Bertram, 1960). Leitmann (1983) further developed this type of analysis for use with systems subject to uncertainty (Gutman and Leitmann, 1976; Leitmann, 1987). A recent version of two approaches (Soldatos, Corless, and Leitmann, 1990) uses the matrix Riccati equation to solve for the feedback gains for the linear portion of the controller, just as in method 2. However, the same gains are used to define a switching surface for the bang-bang part of the controller. The total controller is composed of the linear and bang-bang parts. We will call this approach method 3.

The final method uses the qualitative game theoretic necessary conditions to generate feedback strategies for w. This approach has the advantage of being applicable to nonlinear systems. Its disadvantage is that it can only be applied to one and two dimensional problems. We call this approach method 4.

The purpose of this chapter is to compare these different approaches to a two dimensional control problem. The general procedure for applying each of these methods will be discussed in detail.

6.3. An Inverted Pendulum

The problem will be one used by Solatos, Corless, and Leitmann (1990) in their recent paper on uncertain systems. The system is an inverted pendulum in which the nonlinear gravitational term has been replaced by an uncertain input. This results in a system of the form

$$\begin{aligned} \dot{x}_1 &= x_2 \\ \dot{x}_2 &= w + v \end{aligned} \tag{6.7}$$

which is equivalent to the one dimensional motion of a mass acted on only by forces w and v. If we set $v = 0$ and seek a minimum time control to the origin, we have reduced this to Bushaw's problem (Bushaw, 1958). The minimum time controller is bang-bang with at most one switch. The system may be driven in minimum time from every point in state space to the origin. Thus, the controllable set must be the entire state space. The playable set to the origin is also the entire state space. This follows from the fact that the game theoretic control for v is the opposite of that for w. Thus, an equivalent system under game theoretic control is defined by setting $r = w + v$, $|r| \leq w_m - v_m$. All of the different control approaches will be compared with this game theoretic result. Namely, the v-reachable set is zero and the playable set is the entire state space.

6.3.1 Method 1 - Output Feedback

In input-output format, the problem is given by

$$\ddot{y} = w + v. \tag{6.8}$$

The transfer function for the system is

$$G_p(s) = \frac{1}{s^2}. \tag{6.9}$$

Consider placing a phase lead compensator

$$H(s) = \frac{1 + \tau_e s}{1 + \tau_a s} \tag{6.10}$$

with $\tau_e \gg \tau_a$ in a control feedback loop as illustrated in Figure 6.1. The Laplace transform of the output is related to the Laplace transform of the command input U(s), and the uncertain input V(s) by

$$Y(s) = \frac{G_p(s)}{1 + KG_p(s)H(s)}[KU(s) + V(s)] \tag{6.11}$$

which is equivalent to

$$Y(s) = \frac{1 + \tau_a s}{\tau_a s^3 + s^2 + K\tau_e s + K}[KU(s) + V(s)]. \tag{6.12}$$

Equation (6.12) can be expressed as

$$\tau_a \dddot{y} + \ddot{y} + K\tau_e \dot{y} + Ky = Ku + K\tau_a \dot{u} + v + \tau_a \dot{v}. \tag{6.13}$$

For constant inputs, $u = \bar{u}$, $v = \bar{v}$, we have the steady state solution

$$y = \bar{u} + \frac{\bar{v}}{K}. \tag{6.14}$$

It follows that for high gain, the steady state error due to a constant uncertainty can be made small by making the gain large.

For $\tau_e \gg \tau_a$, the two dominant roots to the characteristic equation are approximated by

$$\lambda^2 + K\tau_e \lambda + K = 0. \tag{6.15}$$

If we choose $K = 10$ and $\tau_e = 0.3162$, then this system will be equivalent to a second order system with the characteristic equation

$$\lambda^2 + 2\xi\omega_n \lambda + \omega_n^2 = 0 \tag{6.16}$$

with $\xi = 0.5$ and $\omega_n^2 = 10$. We will consider this to be the nominal control design for this system when $v = 0$. The controller for this system is given by

$$W(s) = K\left[U(s) - \frac{1+\tau_e s}{1+\tau_a s} Y(s)\right] \tag{6.17}$$

which for small τ_a reduces to

$$W(s) = K\left[U(s) - (1+\tau_e s) Y(s)\right] \tag{6.18}$$

or equivalently in the time domain

$$w(t) = K\left[u(t) - y - \tau_e \dot{y}\right]. \tag{6.19}$$

Here we consider the command input is zero ($u(t) = 0$). In order to satisfy the maximum force requirement, equation (6.19) is modified using saturation control of the form

$$w(t) = \begin{cases} -w_m & \text{if } -K(y+\tau_e\dot{y}) < -w_m; \\ -K(y+\tau_e\dot{y}) & \text{if } |K(y+\tau_e\dot{y})| \le w_m; \\ w_m & \text{if } -K(y+\tau_e\dot{y}) > w_m. \end{cases} \tag{6.20}$$

The uncertainty, v, determined by solving (6.6) is determined to be of the form

$$v(t) = \begin{cases} v_m & \text{if } x_2 \ge 0; \\ -v_m & \text{if } x_2 < 0. \end{cases} \tag{6.21}$$

Figure 6.2 illustrates both the v-reachable set the domain of attraction obtained by solving (6.7) with the control w determined by (6.20) and the control for v determined by (6.21). For this example, we choose $w_m = 2$ and $v_m = 1$. The v-reachable sets (the smaller regions) are obtained by integrating (6.7) forward in time from an initial point near the origin. After a sufficiently long time the system trajectories approach the boundaries of the v-reachable set for values of $K = 10$ and 20 illustrated. The v-reachable set is shrunk by increasing K.

Figure 6.2 also shows the domain of attraction obtained by integrating (6.7) backward in time with u and v again determined by (6.20) and (6.21) but now with an initial point outside the v-reachable set. The domain of attraction is seen to increase with an increase in K. However, increasing K much beyond 20 will have little effect on the domain of attraction. The size of the domain of attraction is much more greatly effected by the value chosen for τ_e. Indeed much larger, but finite domain of attraction are possible. Any point outside of the domain of attraction cannot not driven to the origin under the control law specified by (6.20). Any point inside the domain of attraction can be guaranteed to be driven to be the boundary of the v-reachable set, but not necessarily to the origin.

6.3.2 Method 2 - Game Theoretic Matrix Riccati Equation

The method is described as follows: the system given by (6.7) can be rewritten as

$$\dot{\mathbf{x}}(t) = \mathbf{A}\mathbf{x}(t) + \mathbf{B}(w(t) + v(t)) \tag{6.22}$$

where

$$\mathbf{x} = \begin{bmatrix} x_1 \\ x_2 \end{bmatrix}, \mathbf{A} = \begin{bmatrix} 0 & 1 \\ 0 & 0 \end{bmatrix}, \mathbf{B} = \begin{bmatrix} 0 \\ 1 \end{bmatrix}.$$

The control w(t) is choosen to minimize the cost criterion:

$$J = \int_0^{t_f} (\mathbf{x}^T\mathbf{Q}\mathbf{x} + w^T R w - v^T \hat{R} v)dt, \tag{6.23}$$

where $\mathbf{Q}$ is an arbitrary positive semidefinite matrix, and R and $\hat{R}$ are arbitrary constants provided $\hat{R} > R$. Then the optimal control has a feedback form

$$w(t) = -\mathbf{B}^T\mathbf{S}\mathbf{x}(t) \tag{6.24}$$

where

$$\mathbf{Q} + \mathbf{SA} + \mathbf{A^T S^T} - \mathbf{SB}[\mathrm{R}^{-1} - \hat{\mathrm{R}}^{-1}]\mathbf{B^T S} = 0. \tag{6.25}$$

If we choose

$$\mathbf{Q} = \begin{bmatrix} 1 & 0 \\ 0 & 1 \end{bmatrix}, \quad \mathrm{R} = 1, \quad \hat{\mathrm{R}} = 2. \tag{6.26}$$

Substituting (6.26) to (6.25), we have

$$\mathbf{S} = \begin{bmatrix} 1.9566 & 1.4142 \\ 1.4142 & 2.7671 \end{bmatrix}$$

and

$$\mathrm{w(t)} = -1.4142\mathrm{x}_1 - 2.7671\mathrm{x}_2. \tag{6.27}$$

Since the control w is bounded, equation (6.27) must be modified to the form

$$\mathrm{w(t)} = \begin{cases} -\mathrm{w_m} & \text{if } -1.4142\mathrm{x}_1 - 2.7671\mathrm{x}_2 < -\mathrm{w_m}; \\ -1.4142\mathrm{x}_1 - 2.7671\mathrm{x}_2 & \text{if } |1.4142\mathrm{x}_1 + 2.7671\mathrm{x}_2| \leq \mathrm{w_m}; \\ \mathrm{w_m} & \text{if } -1.4142\mathrm{x}_1 - 2.7671\mathrm{x}_2 > \mathrm{w_m}. \end{cases} \tag{6.28}$$

Then we integrate (6.7) using (6.28) for w and (6.21) for v. By integrating forward in time starting near the origin we obtain the v-reachable set as shown in Figure 6.3. By integrating backward in time from outside the v-reachable set we obtain the domain of attraction as shown in Figure 6.4. The shape and size of both the v-reachable set and the domain of attraction depend on $\mathbf{Q}$, R and $\hat{\mathrm{R}}$; and different results may be obtained than are illustrated here. For example, if we choose $\mathbf{Q} = \mathbf{I}$, $\mathrm{R} = 0.5$ and $\hat{\mathrm{R}} = 1.0$, then the domain of attraction is smaller and the v-reachable set is larger than the results obtained by choosing (6.26).

6.3.3 Method 3 - Leitmann's Method

Instead of choosing an arbitrary **Q**, Soldatos, Corless, and Leitmann choses their parameters in the cost function (6.26) as

$$\mathbf{Q} = \begin{bmatrix} \alpha^2 & 0 \\ 0 & \alpha^2 \end{bmatrix}, \quad \alpha > 0, \quad \mathrm{R} = 1, \quad \hat{\mathrm{R}} = 0. \tag{6.29}$$

Then, the Riccati eqation

$$\mathbf{SA} + \mathbf{A^T S} - \mathbf{SBB^T S} + \mathbf{Q} = \mathbf{0} \tag{6.30}$$

has a unique positive definite solution **S**. For any $\epsilon > 0$, the proposed controller is given by

$$\mathrm{w(x)} = -\mathbf{B^T Sx} - \mathrm{v_m SAT}(\epsilon^{-1}\mathbf{B^T Sx}), \tag{6.31}$$

where SAT is a saturation function defined by

$$\mathrm{SAT(z)} = \begin{cases} \mathrm{z} & \text{if } \|\mathrm{z}\| \leq 1 \\ \|\mathrm{z}\|^{-1}\mathrm{z} & \text{if } \|\mathrm{z}\| > 1 \end{cases}$$

The first term of (6.31) is linear state variable feedback which will stablize the system in the LQ method. The second term of (6.31) is a bang-bang type control which is unique to Leitmann's method.

Substituting **A** and **S** into (6.30), the positive definite solution to Riccati equation (6.30) is given by

$$\mathbf{S} = \begin{bmatrix} s_{11} & s_{12} \\ s_{21} & s_{22} \end{bmatrix}$$

$$s_{11} = \alpha(\alpha^2 + 2\alpha)^{1/2}$$

$$s_{12} = s_{21} = \alpha$$

$$s_{22} = (\alpha^2 + 2\alpha)^{1/2}$$

Thus, the controller is obtained by

$$w(t) = -\alpha x_1 - (\alpha^2 + 2\alpha)^{1/2} x_2 - v_m \mathrm{SAT}(\varepsilon^{-1}(\alpha x_1 + (\alpha^2 + 2\alpha)^{1/2} x_2). \quad (6.32)$$

For this particular example, we choose $\varepsilon = 0.1$. In order to satisfy bounds on the control, (6.32) is subject to

$$w(t) = \begin{cases} w_m & \text{if } w(t) > w_m; \\ -w_m & \text{if } w(t) < -w_m. \end{cases} \quad (6.33)$$

We integrate (6.7) under the controller w(t) obtained by (6.32) and (6.33) (α = 0.10 and 0.05) with v(t) determined by (6.21). Again, starting near the origin and integrating forward in time we obtain the v-reachable set illustrated in Figure 6.5. Figure 6.6 shows that the domain of attraction. For a given ε the domain of attraction and the v-reachable set depends on the value of α as illustrated in Figures 6.5 and 6.6. Decreasing α increases both the v-reachable set and the domain of attraction. Note however decreasing ε can further decrease the v-reachable set.

6.3.4 Method 4 - Qualitative Game Theory

Qualitative game theory yields a control law for w. That is

$$w(t) = \begin{cases} -w_m & \text{if } x_2 \geq 0; \\ w_m & \text{if } x_2 < 0. \end{cases} \quad (6.34)$$

Then, the system is reduced to Bushaw's problem. The system can be rewritten as

$$\begin{aligned} \dot{x}_1 &= x_2 \\ \dot{x}_2 &= r \end{aligned} \quad (6.35)$$

where $r = w + v$, and $|r| \leq w_m - v_m$. According to the game theory, the v-reachable set is zero. However, applying this control law to the system (6.7) results

in a chattering solution to the origin along the x_1 axis. To avoid chattering, (6.34) is modified as follows:

$$w(t) = \begin{cases} -w_m \mathrm{sgn}(x_2); & \\ -2x_2/c_1 & \text{if } x_1 < 0 \text{ and } x_2 > 0 \text{ and } x_2 < c_1; \\ -2x_2/c_1 & \text{if } x_1 > 0 \text{ and } x_2 < 0 \text{ and } x_2 > -c_1; \\ -w_m & \text{if } x_1 < 0 \text{ and } x_2 > 0 \text{ and } x_2 < c_1 \text{ and } x_2 + c_2 x_1 > 0; \\ w_m & \text{if } x_1 > 0 \text{ and } x_2 < 0 \text{ and } x_2 > -c_1 \text{ and } x_2 + c_2 x_1 < 0, \end{cases} \tag{6.36}$$

where c_1 and c_2 are positive numbers. Figure 6.7 shows the control law defined in the state space. Any point in region I remains in I and will be ultimately driven to the origin along $\overline{ABO}$. And any point in region II remains in II and will be ultimately driven to the origin along $\overline{CDO}$. Trajectories from all other points ultimately enter region I or II. Thus, the domain of attraction is still the entire state space and the v-reachable set is still zero. The speed to the origin depends on c_1. The slope of $\overline{BOD}$ is c_2.

6.4. Tracking Problems

In the previous section, four methods are presented to eliminate uncertainties. Method 4 gives the best result based on a comparison the size of domain of attraction with the others. The procedure methods focused on the stabilization problems. Here, we will apply method 4 to the problem of tracking a system with uncertain inputs. In particular, this section addresses the problem of controlling a pure mass following a desired trajectory with an unknown input.

Consider a system

$$m\ddot{y} = u + w + v \tag{6.37}$$

where m = 0.05, $\ddot{y}$ is the acceleration, u is the command input, and w and v are defined by (6.2) and (6.3) with $w_m = 0.2$ and $v_m = 0.1$. Equation (6.37) can be expressed as

$$\begin{aligned} \dot{x}_1 &= x_2 \\ \dot{x}_2 &= (u + w + v)/m \end{aligned} \tag{6.38}$$

or

$$\dot{\mathbf{x}}(t) = \mathbf{A}\mathbf{x}(t) + \mathbf{B}(u(t) + w(t) + v(t)) \tag{6.39}$$

where

$$\mathbf{x} = \begin{bmatrix} x_1 \\ x_2 \end{bmatrix}, \mathbf{A} = \begin{bmatrix} 0 & 1 \\ 0 & 0 \end{bmatrix}, \mathbf{B} = \begin{bmatrix} 0 \\ 1/m \end{bmatrix}.$$

Let $\mathbf{x}^*$ be a vector which represents the desired output, so that the error e(t) is given by

$$\mathbf{e}(t) = \mathbf{x}(t) - \mathbf{x}^* \tag{6.40}$$

where $\mathbf{e} = [e_1\ e_2]^T$. The desired model can be expressed as

$$\dot{\mathbf{x}}^*(t) = \mathbf{A}\mathbf{x}^*(t) + \mathbf{B}u(t) \tag{6.41}$$

where

$$\mathbf{x}^* = \begin{bmatrix} x_1^* \\ x_2^* \end{bmatrix}.$$

Subtracting (6.41) from (6.39), we have

$$\dot{\mathbf{e}}(t) = \mathbf{A}\mathbf{e}(t) + \mathbf{B}(w(t) + v(t)) \tag{6.42}$$

The objective of the control w is to eliminate the effect of the uncertain input, v, such that the error will be zero all the time.

Suppose that the pure mass is moved to the right 5 meters in one second. The command input is given by

$$u(t) = \begin{cases} 1 & \text{if } 0 \le t \le 0.5; \\ -1 & \text{if } 0.5 < t \le 1.0. \end{cases} \tag{6.43}$$

And the control law based on method 4 is defined by

$$w(t) = \begin{cases} -0.2\text{sgn}(e_2); & \\ -0.2e_2/c_1 & \text{if } e_1 < 0 \text{ and } e_2 > 0 \text{ and } e_2 < c_1; \\ -0.2e_2/c_1 & \text{if } e_1 > 0 \text{ and } e_2 < 0 \text{ and } e_2 > -c_1; \\ -0.2 & \text{if } e_1 < 0 \text{ and } e_2 > 0 \text{ and } e_2 < c_1 \text{ and } e_2 + c_2e_1 > 0; \\ 0.2 & \text{if } e_1 > 0 \text{ and } e_2 < 0 \text{ and } e_2 > -c_1 \text{ and } e_2 + c_2e_1 < 0, \end{cases} \tag{6.44}$$

where $c_1 = 0.1$ and $c_2 = 1.0$ as shown in Figure 6.8. The control law for this uncertain input as before is defined by

$$v(t) = \begin{cases} -0.1 & \text{if } e_2 \geq 0; \\ 0.1 & \text{if } e_2 < 0. \end{cases} \tag{6.45}$$

Equation (6.39) is integrated both with $w = 0$ and w defined by (6.44). These results are compared with the desired trajectory obtained from (6.41) as illustrated in Figure 6.9 and 6.10. The dashed line in Figure 6.9 is the desired output, and the solid line is the displacement of the system with $w = 0$. The system is seen to diverge from the desired trajectory. Figure 6.10 shows that the system follows the desired trajectory exactly. The error is always zero.

6.5. Discussion

The methods dealing with the uncertainties have been discussed in previous sections. Method 4 can eliminate the uncertainties for either stabilizing the system or eliminating the error between the system and a desired model. Method 4 can be applied to a linear or nonlinear system. The domain of attraction obtained by method 4 is always closed to the playable set.

In this chapter, this method was applied to a two dimensional system. It is possible to design a control law based on the concepts of method 4 for a system of large dimension as long as we can find the switching surface. Then, we can build the control law based on game theories such that the v-reachable set will be zero.

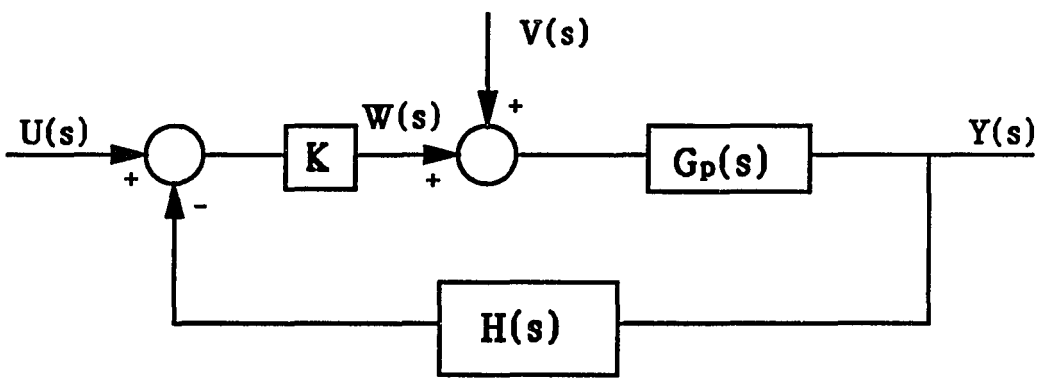

Figure 6.1 The Control System Design Using Output Feedback

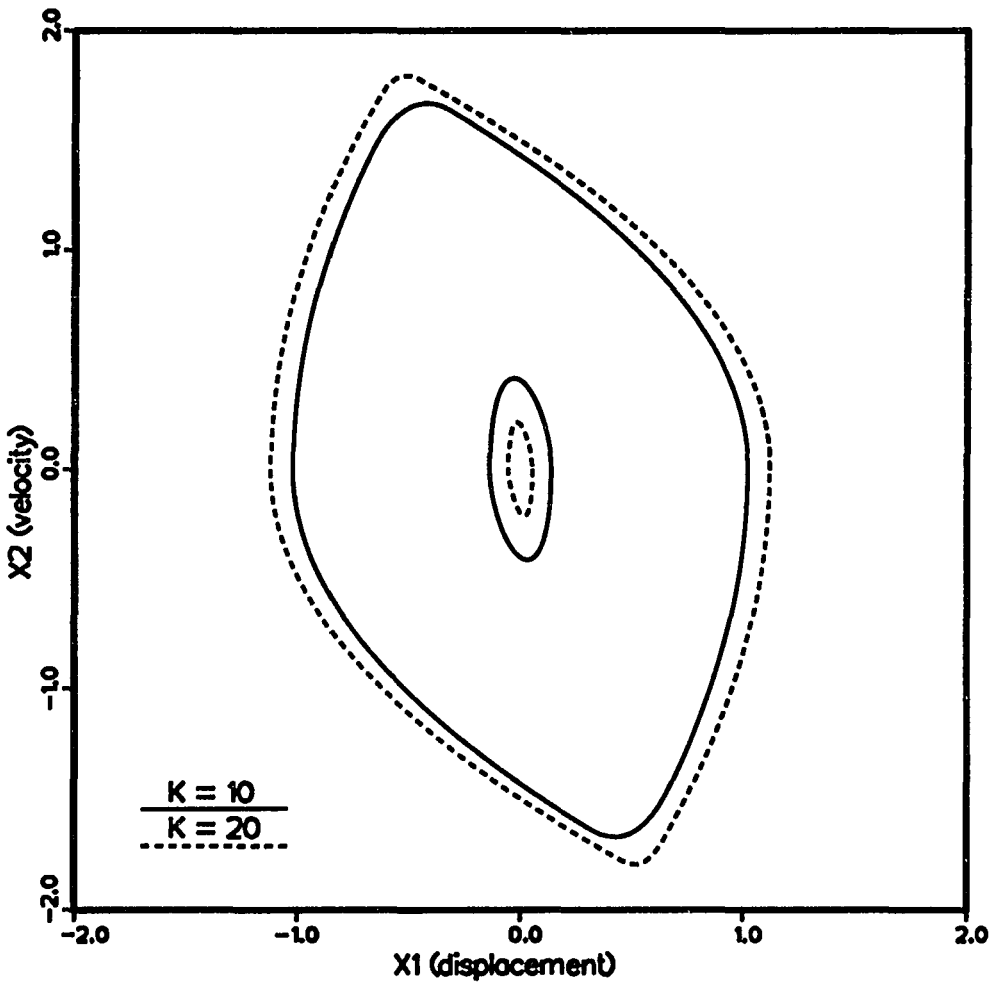

Figure 6.2 The V-reachable Set and Domain of Attraction Obtained by Using Output Feedback

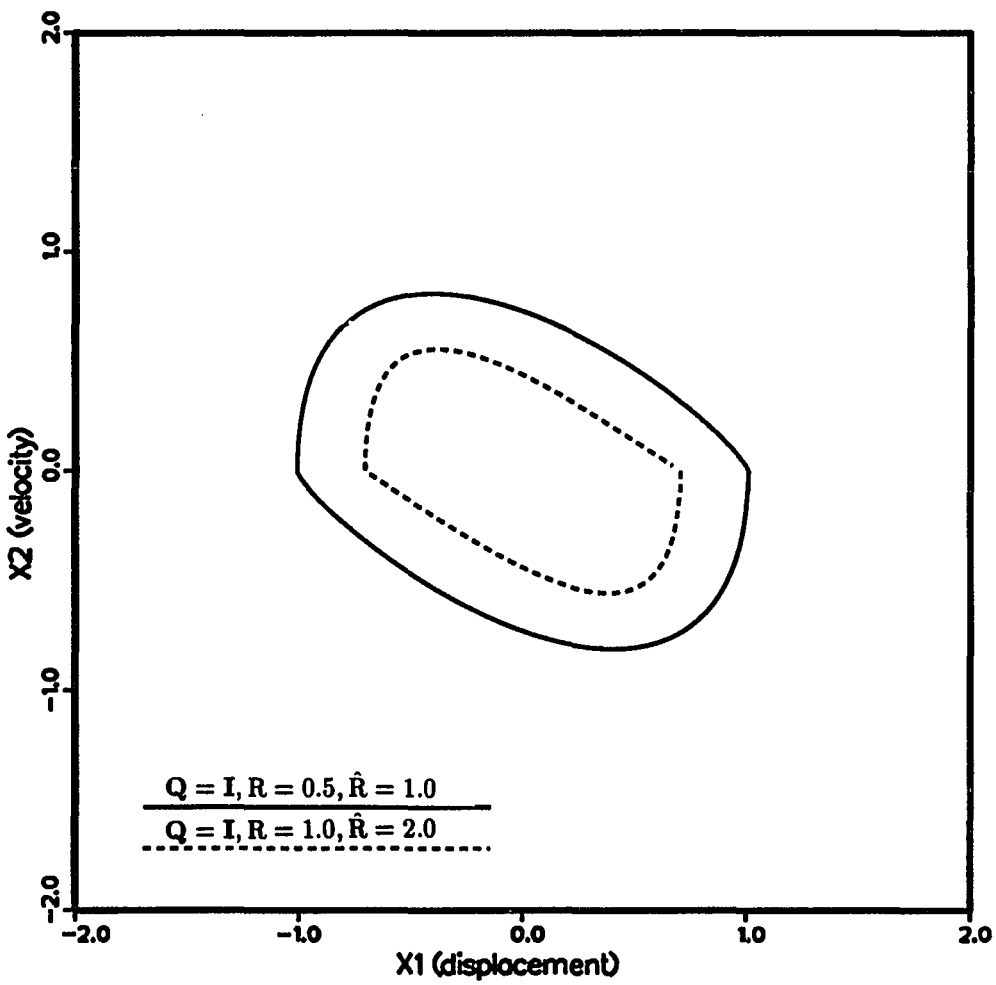

Figure 6.3 The V-reachable Set Obtained by Using LQ Design

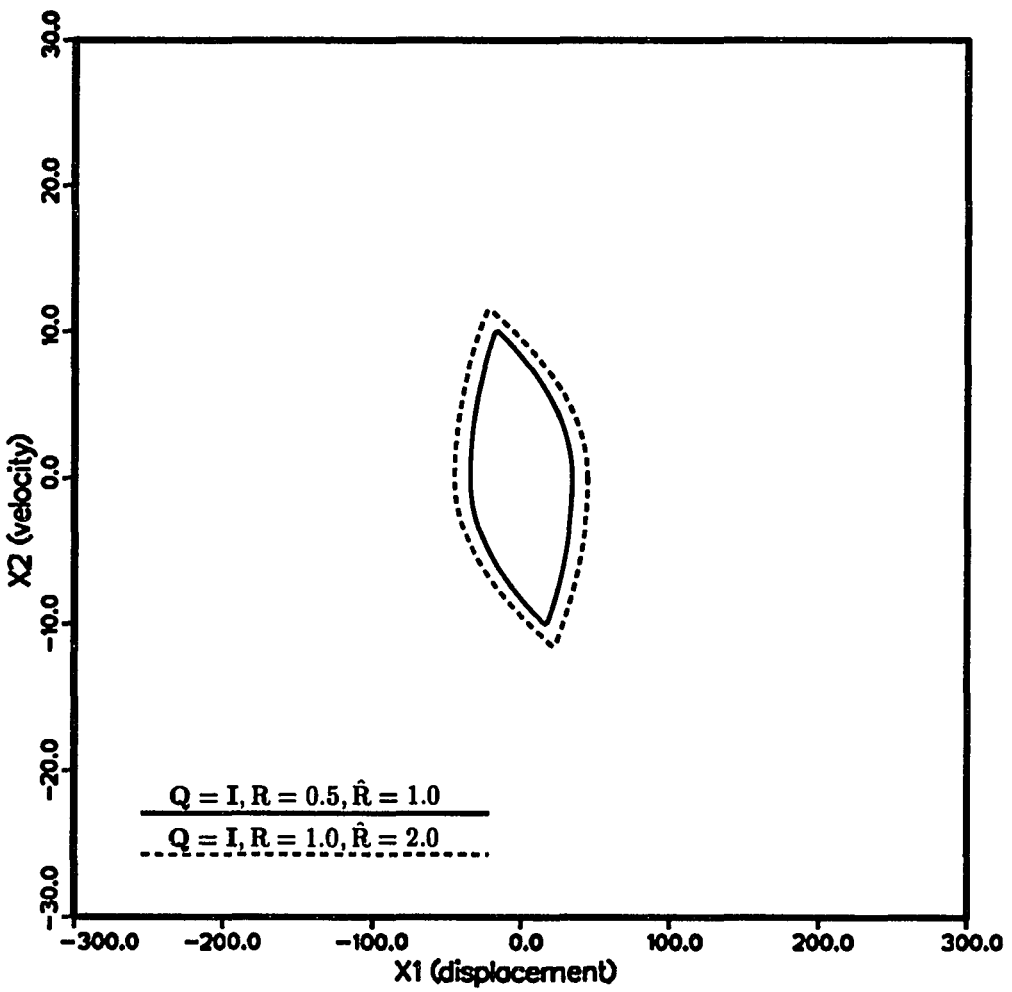

Figure 6.4 The Domain of Attraction Obtained by Using LQ Design

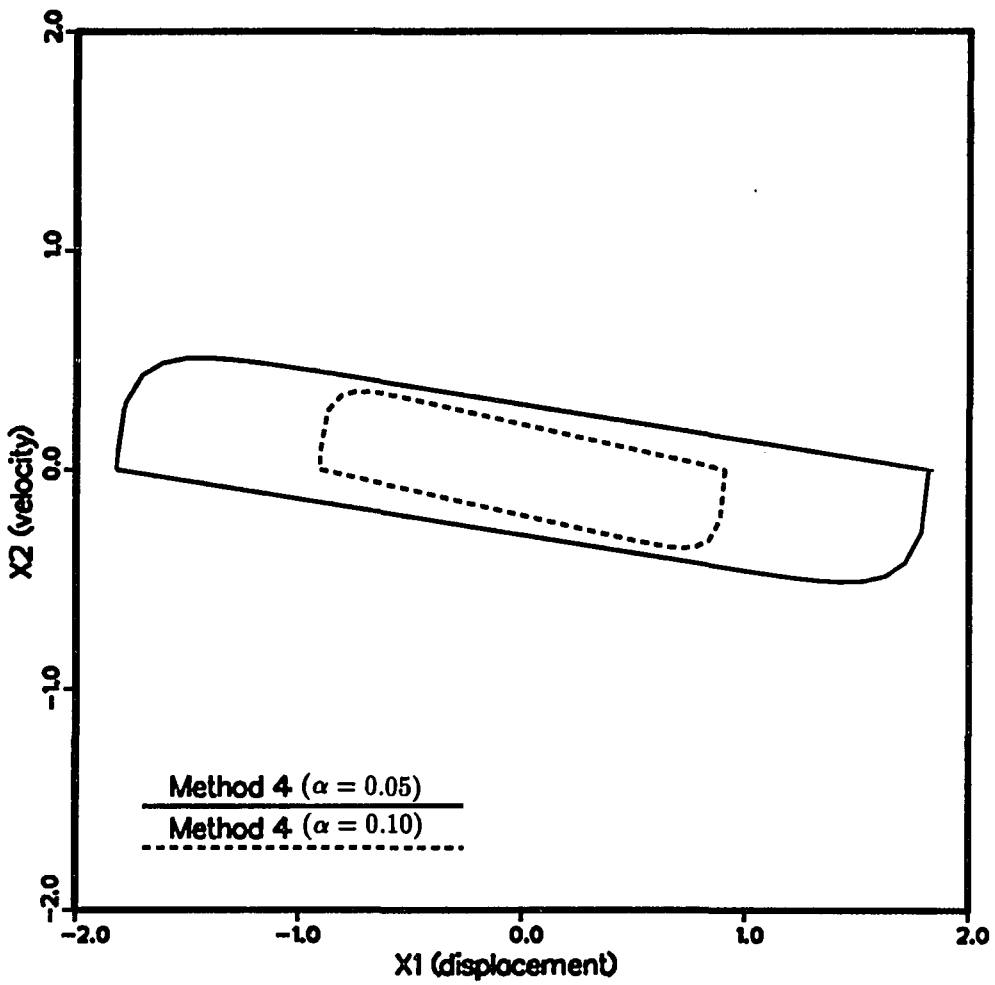

Figure 6.5 The V-reachable Set Obtained by Using Leitmann's Method

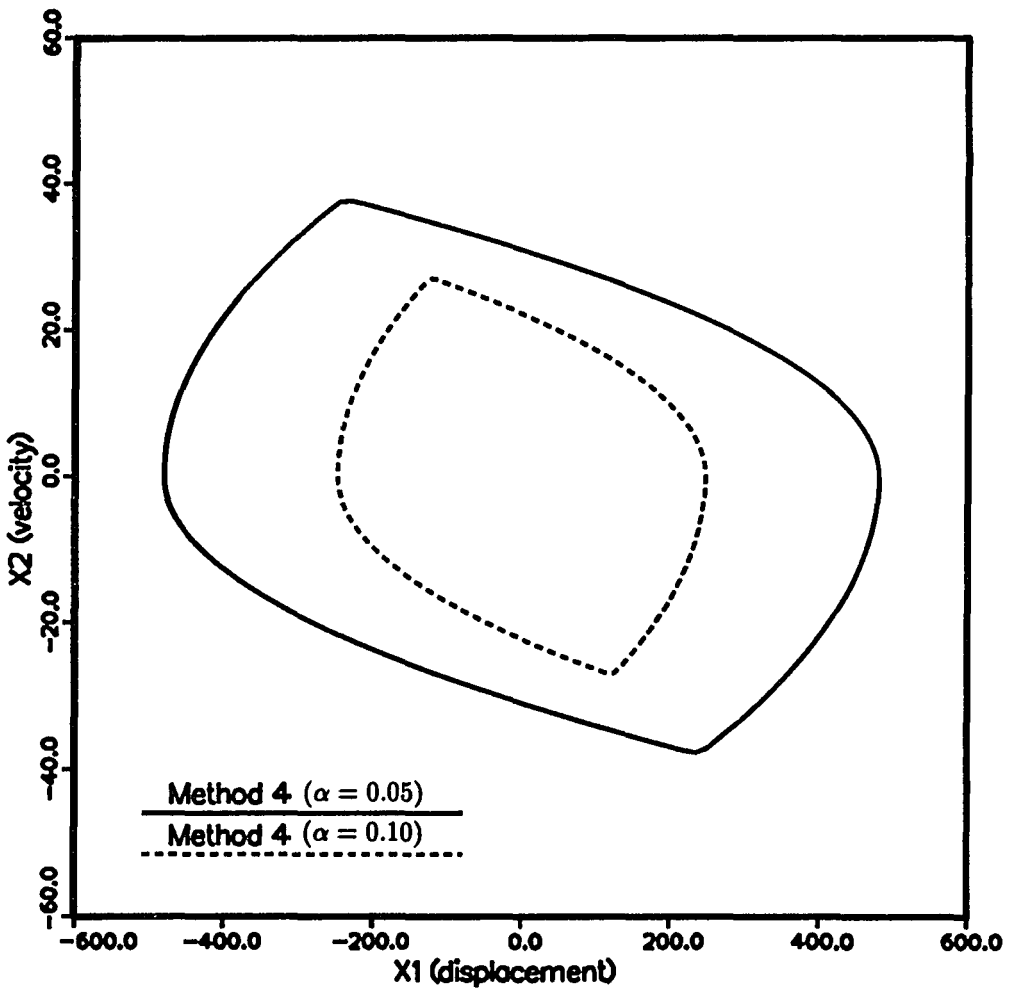

Figure 6.6 The Domain of Attraction Obtained by Using Leitmann's Method

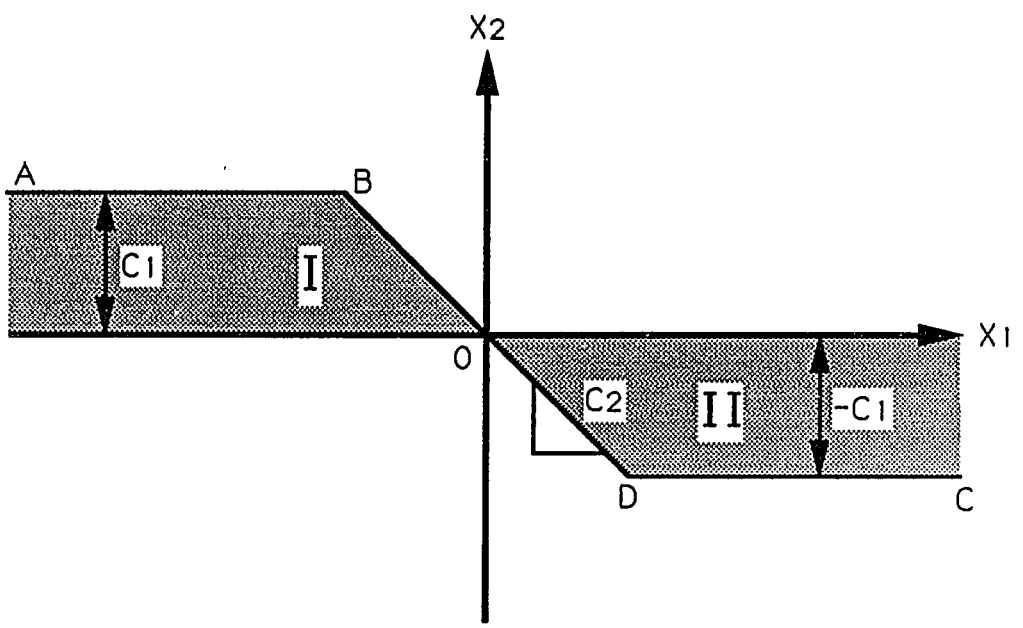

Figure 6.7 The Control Law Defined in the State Space

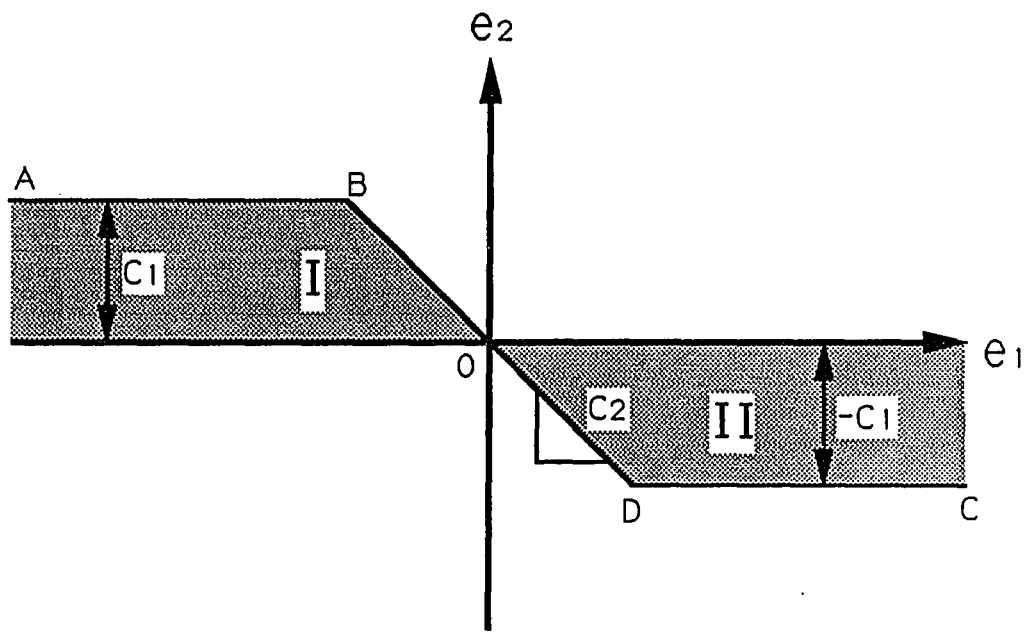

Figure 6.8 The Control Law Defined in the e Space

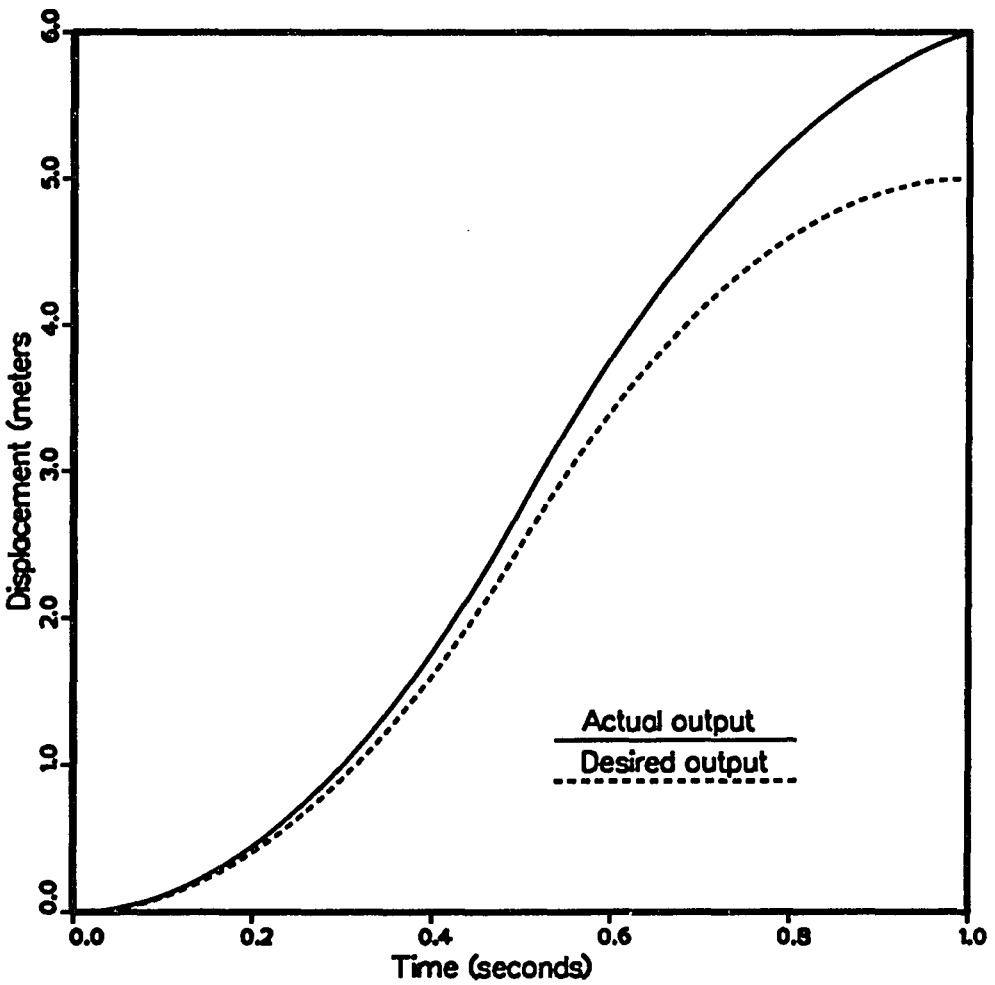

Figure 6.9 The Trajectory without Closed-loop Control and a Desired Output

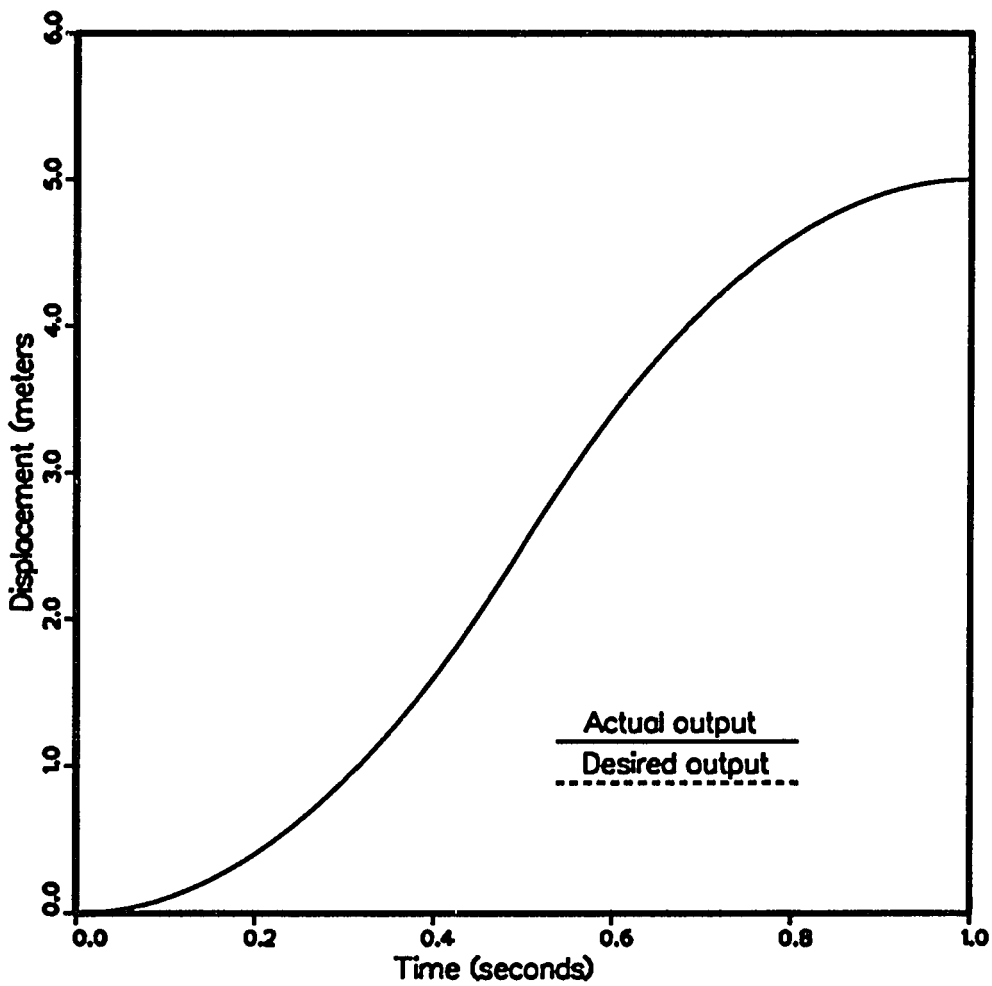

Figure 6.10 The Trajectory with Closed-loop Control

CHAPTER 7
CONCLUSIONS AND FUTURE WORK

A dynamic model for a thin flat plate has been presented. The model enables us to study the structure motion with different actuator-placement designs. Experiments on a flat plate were performed to validate the model.

The global motion of a flexible structure is treated as a nominal rigid body motion combined with an elastic motion. The elastic motion is assumed to be a small perturbation of the nominal rigid body motion. The small displacements measured with respect to the reference frame are discretized by a displacement-based finite element method. The modal displacements of the elements are used as generalized coordinates in deriving the equations of motion. Equations of motion are derived for the cases of prescribed rigid body motion as well as for prescribed external forces/torques through the application of Lagrange's equations [32].

The equations of motion, taking into account geometric nonlinearity for flexible structures, have not been presented here. The open-loop control design is based on small translation and small rotation assumptions. The closed-loop control design, which can be used to eliminate the nonlinearities, has been discussed in Chapter 6. Multibody systems consisting of interconnected rigid and deformable components that undergo large translational and rotational displacement have been studied extensively in recent years. The resulting mathematical model is highly non-linear because of the large body motion. Structural mechanics has come into wide use to denote the branch of study in which the deformation is the main concern. Equation (3.1) is not valid for large body translation and rotation since the mass

matrix will then no longer be time-invariant. Instead, a large number of elastic coordinates would have to be included in the mathematical model in order to accurately describe large deformations. The development of equations combining these effects and control system design (including open-loop and closed-loop) is left as a topic for future study.

To experimentally validate the proposed dynamic model, laboratory tests are performed on a flat plat. Using the validated, simulations are performed to point out the importance of actuator locations. The results obtained from numerical simulations are compared with those from experiments and found to show good agreement in most cases. The agreement for three actuators was not as good. The reasons are as follow: Firstly, the aerodynamic and amplifier dynamic are not taken into account in the simulation. Secondly, the damping ratio in each mode is assumed to be 2%. This may not be true in the plate. Finally, the thin plate is not very big and flexible enough to attach three actuators. The rigidity from the actuators will change the simulation, thus the actuators' dynamic should be taken into account.

There are a number of promising research directions [59-63] that can be taken using the proposed control approach. In order to mitigate the effect of rapid maneuvering of a flexible structure, it is proposed that extra actuators be employed. The number, location, and open-loop control law to be applied to each of the actuators can be determined by using the proposed methods. Both mode and energy suppression techniques can be used and can be examined in conjunction with passive damping, active damping, and nonlinear effects. Various combinations of open-loop and closed-loop along with passive damping may provide the best combination, considering factors such as the desirability to keep the control law to the actuators

simple and the desirability of using mostly passive damping in the post-maneuver control. The proposed approach to positioning a flexible structure discussed here provides an orderly way to investigate these problems.

A number of advantages to the proposed control system approach are: (1) Actuator number and placement is an integral part of the total control design. (2) Separation of the maneuvering control and closed-loop control is natural and should lead to a reliable design. (3) The potential exists for a proper control design with a minimum of state information required. It is likely that the open-loop maneuvering with passive post maneuver damping along with post-maneuver closed-loop control based on position feedback can provide satisfactory performance. Position information would be required from only a few actuator locations. (4) The potential exists for relatively simple maneuvering control. There may be no need for rapidly changing variable actuators. (5) If the maneuvering command can be maintained open-loop and if a sufficient number of actuators can be employed (using energy or mode suppression) to provide motion which reasonably mimics rigid body motion, then the resulting motion will be close to minimum time. Any shaping of the (usually bang-bang) open-loop minimum time control will result in a loss to this performance index. (6) Additional actuators can provide backup in case of actuator failure.

APPENDIX A

THE D/A BASIC CODE

```
900  PRINT "DDAA.BAS is for D/A conversion series."
920  PRINT "*************************************************************************"
925  PRINT "This program transforms Decimal digital values into Hexadecimal one"
930  PRINT : PRINT
1000 PRINT "The range of voltage is from -10 to 10 volts."
1010 PRINT
1060 PRINT "This example is designed for the DT2801, DT2801-A, or DT2818"
1070 PRINT "If used with a DT2801/5716, DT2805/5716 or a DT2808 "
1080 PRINT "lines 1300 and 1950 must be modified to correctly convert"
1090 PRINT "the Analog Data Values into single precision values."
1120 '
1160 '   All variables should be given initial values
1170 '   before being used in PCLAB calls.
1175 'SISO program. !!!
1180 '
1195 DIM YO%(6000),Y(6000)
1200 INPUT "Enter the wanted output times ( < 6000) = ";NUMBER.OF.VALUES%
1205 ERROR.VALUE% = 0
1206 '
1208 OPEN "AADD.DAT" FOR INPUT AS #2
1210 FOR K = 0 TO NUMBER.OF.VALUES%-1
1211 INPUT #2, Y(K)
1213 NEXT K
1215 FILES = "DDAA.DAT"
1216 OPEN "O",1,FILES
1220 CALL SET.ERROR.CONTROL.WORD(ERROR.VALUE%)
1260 HIGH.V! = +10!              ' Highest voltage in range.
1270 LOW.V!  = -10!              ' Lowest voltage in range.
1280 RANGE! = HIGH.V! - LOW.V!   ' Total voltage range.
1290 '
1300 NOC! = 4096!
1310 ' For 1420 a DT2801/5716 and DT2805/5716:   NOC! = 65536!
1320 ' For DT2808: NOC! = 1024!
1330 '
1340 LSB! = RANGE!/NOC!          ' Voltage of Least Significant Bit.
1350 '
1360 '  The following section sets up the A/D.
1370 '
1390 '
1550 INPUT " Enter the desired Gain (1,2,4 or 8) ",GAIN%
1560 '
1580 '
1590 SCALED.LSB! = LSB! / GAIN%          ' Calculate scaled LSB.
1600 SCALED.LOW! = LOW.V! / GAIN%        ' Calculate scaled LOW voltage.
1610 '
1620 ' Next set up the internal clock.
1630 '
1640 INPUT " Enter the output frequency ( 25. - 12000.) ",REQUESTED.FREQ
1650 CLOCK.DIVIDER% = (800000! / REQUESTED.FREQ) - .5
1655 CALL SET.CLOCK.DIVIDER (CLOCK.DIVIDER%)
1660 ACTUAL.FREQ = 800000! / CLOCK.DIVIDER%
1670 PRINT " Actual frequency is ";ACTUAL.FREQ;" Hertz"
1680 '
2160 '    Set up the control parameters for DAC.
2165 '
2170 INTERNAL.CLOCK% = 0         'Code 0, for internal clock mode.
2175 OUTPUT.MODE% = -1               'Specifies DAC at Channel 0 & 1.
2190 '
2192 'PRINT "*** Starting time for ready to D/A : ",TIMER
2194 CALL SETUP.DAC(INTERNAL.CLOCK%,OUTPUT.MODE%)
```

```
2195 '
2210 FOR I% = 0 TO NUMBER.OF.VALUES%-1
2220 YO%(I%) = (Y(I%)-SCALED.LOWI)/SCALED.LSBI
2230 NEXT I%
2233 'PRINT "     Stopping Time for ready to D/A : ";TIMER : PRINT
2235 PRINT "Press RETURN key to begin D/A conversion of acquired values.";
2236 INPUT A$ : IF A$ = " " THEN GOTO 2236
2238 PRINT : PRINT "Beginning D/A conversion....."
2240 NOV% = NUMBER.OF.VALUES%/2 - 1
2250 CALL DISABLE.SYSTEM.CLOCK                ' Turn off PC's time of day clock.
2260 CALL DAC.SERIES(NOV%,YO%(0))
2350 CALL ENABLE.SYSTEM.CLOCK
2395 PRINT "D/A conversion is completed."
2440 'FOR K1 = 0 TO NUMBER.OF.VALUES%-1
2455 'PRINT #1,YO%(K1)
2460 'NEXT K1
2500 '
2530 INPUT "Go again (Y/n)";ANS$
2540 IF ANS$ = "N" GOTO 2600
2550 IF ANS$ = "n" GOTO 2600
2560 INPUT "Reset parameters - No. of samples, gain, freq. (y/N)";ANS2$
2570 IF (ANS2$ <> "Y") AND (ANS2$ <> "y") GOTO 2194
2580 CLOSE #1
2585 CLOSE #2
2590 GOTO 1200
2600 PRINT "END OF FORCE.BAS."
2700 PRINT "END OF FORCE.BAS."
```

APPENDIX B

THE A/D BASIC CODE

```
REM
REM $INCLUDE: 'PCLDEFS.BI'
REM
'
'   Data Collection program for use with Data Translation DT2801-A A/D card
'   Modification of PCEX02.BAS.
'   June 1989
'
'   Routines:  SETUP.ADC, SET.CLOCK.FREQUENCY, DISABLE.SYSTEM.CLOCK,
'   ADC.SERIES, ENABLE.SYSTEM.CLOCK, ANALOG.TO.VOLTS
'
DIM ANALOG.ARRAY%(19999)
status% = 0
'
status% = SET.ERROR.CONTROL.WORD(status%)
'
'  The following section sets up the A/D.
'
TIMING.SOURCE% = 0          ' Software trigger, internal clock.
'
' Define channel scan.
'
input.channels:
PRINT
INPUT "Enter the first channel in the scan :", start.chan%
INPUT "Enter the last channel in the scan :", end.chan%
'
IF (start.chan% <= end.chan%) GOTO calculate.scan.count
PRINT "In this program the starting channel number cannot be"
PRINT "greater than the ending channel number."
GOTO input.channels
'
calculate.scan.count:
max.points% = 20000 / (end.chan% + 1) - start.chan%
PRINT "Enter the number of data points per channel (<"; max.points%; : INPUT "):",
IF NUM% > max.points% GOTO calculate.scan.count
scan.length% = (end.chan% + 1) - start.chan%
number.of.values% = NUM% * scan.length%
number.of.scans% = (number.of.values% / scan.length%) - 1
INPUT "Enter the desired Gain (1,2,4,8,10,100 or 500):", gain%
'
' Next set up the internal clock.
'
SETUP.CLOCK:
INPUT "Enter the Frequency :", TPP!
REQUESTED.FREQ! = TPP! * scan.length%
'
redo:
status% = SETUP.ADC(TIMING.SOURCE%, start.chan%, end.chan%, gain%)
IF status% = 0 GOTO trig
PRINT "*** Illegal channels or gain specified.": GOTO input.channels
'
' This performs the actual data collection.
'
trig:
INPUT "Trigger (Y/n)?", x$
IF x$ = "N" OR x$ = "n" THEN GOTO collect
INPUT "Channel ?", trigchan%
level = 10 / 4096
```

```
level = level / gain%
PRINT "level (1 = "; : PRINT USING "#.#####"; level; : INPUT " V):", triglevel%
value% = 0
status% = ADC.VALUE(trigchan%, gain%, value%)
trig1% = value% + triglevel%
trig2% = value% - triglevel%
'
' Check for trigger
'
check:
status% = ADC.VALUE(trigchan%, gain%, value%)
IF value% < trig1% AND value% > trig2% THEN GOTO check
PRINT "trigger": GOTO aquire
'
' Collect data
'
collect:
INPUT "hit return to start data collection:", x$
aquire:
status% = SET.CLOCK.FREQUENCY(REQUESTED.FREQ!)
status% = DISABLE.SYSTEM.CLOCK          ' Turn off PC's time of day clock.
status% = ADC.SERIES(number.of.values%, ANALOG.ARRAY%(0))
status% = ENABLE.SYSTEM.CLOCK           ' Turn on PC's time of day clock.
IF status% <> 0 THEN PRINT "Error during acquisition. ", status%
'
' Save data
'
SAVE.SCAN:
PRINT
INPUT "save (Y/n)?", x$
IF x$ = "n" OR x$ = "N" THEN GOTO AGAIN
FOR k = 0 TO scan.length% - 1
CH% = k + start.chan%
PRINT "Enter file name for channel "; CH%; " (C/R to skip)"; : INPUT ":", file$
IF file$ = "" THEN GOTO NEXT1
OPEN "O", #1, file$
'
' Compute starting point of scan in array
'
FOR scan% = 0 TO NUM% - 1
SP% = scan% * scan.length%
'
' Calculate the channel number and effective voltage for each value in
' the scan.
'
CHANNEL% = CH% + start.chan%
'
status% = ANALOG.TO.VOLTS(ANALOG.ARRAY%(SP% + CH%), gain%, VOLTAGE!)
'
PRINT #1, USING " #.####¬¬¬¬ "; VOLTAGE!;
IF (scan% + 1) / 5 = INT((scan% + 1) / 5) THEN PRINT #1,
NEXT scan%
CLOSE #1
NEXT1:
NEXT k
'
' Repeat process?
'
AGAIN:
PRINT
INPUT "Again (Y/n)?", x$
IF x$ = "n" OR x$ = "N" GOTO the.end
INPUT "change parameters (y/N)?", x$
IF x$ = "y" OR x$ = "Y" GOTO input.channels ELSE GOTO redo
the.end:
END
```

REFERENCES

1. Shrivastava, S. K., Manoharan, M. G., and Ried, R. C., " Control Structure Interactions in Large Space Structures: Analysis Using Energy Approach," Journal of Aeronautical Society of India, Vol. 35, No. 2, May 1983, pp. 59-67.
2. Joshi, S. P., Vincent, T. L., and Lin, Y. C., "Control for Energy Dissipation in Structure," Journal of Guidance, Control, and Dynamics, Vol. 13, No. 4, 1990, pp. 751-753.
3. Vincent, T. L., Joshi, S. P., and Lin, Y. C., "Positioning and Active Damping of Spring-Mass System," Journal of Dynamic Systems, Measurement, and Control, Vol. 3, December 1989, pp. 592-599
4. Vincent, T. L., Joshi, S. P., and Lin, Y. C., "Positioning and Active Damping of Flexible Beams," Journal of Guidance, Control, and Dynamics, Vol. 13, No. 4, 1990, pp. 714-724.
5. Vincent, T. L., Lin, Y. C., and Joshi, S. P., "Controlling a Flexible Plate to Mimic a Rigid One," in Advances in Control and Dynamic Systems, Vol. XXXIV, Part 2, edited by C. T. Leondes, Academic Press, June 1990, pp. 87-135.
6. Goh, C. J. and Caughey, T. K., "A Quasi-Linear Vibration Suppression Technique for Large Space Structure via Stiffness Modification, " International Journal of Control, Vol. 41, No. 3, 1985, pp. 803-811.
7. Skelton, R. E. and DeLorenzo, M., "Space Structure Control Design by Variance Assignment," Journal of Guidance, Vol. 8, No. 4, July-August 1985, pp. 454-462.
8. Joshi, S. M., "A Controller Design Approach for Large Flexible Space Structure," NASA Cr-165717, May 1981.
9. Gajic, Z., "Decentralization of a Linear-Quadratic Control Problem by a Fixed Point Algorithm," Proceedings of 24th Conf. on Decision and Control, Ft. Lauderdale, FL, Dec. 1985, pp. 1463-1467.

10. Hughes, P. C., et. al., "Controllability and Observability for Flexible Spacecraft," Journal of Guidance and Control Vol. 3, 1980, pp. 707-716.
11. Skelton, R., and Chiu, D., "Optimal Selection of Inputs and Outputs in Linear Stochastic System," J. Astronautical Sciences, Vol. 31, 1983, pp. 399-414.
12. Skelton, R., and Delorenzo, M. L., "Selection of Noisy Actuators and Sensors in Linear Stochastic Systems," Large Scale System , Vol. 4, 1983. pp. 109-136.
13. Skelton, R., and Delorenzo, M. L., "Space Structure Control Design by Variance Assignment," Journal of Guidance and Control, Vol 8, 1985, pp. 454-462.
14. Skelton, R., and Norris, G. A., "Selection of Sensors and Actuators in the Presence Of Correlated Noise," Control Theory and Advanced Technology, Vol. 4, 1988, pp. 53-71.
15. Viswanathan, C. N., "Aspects of Control of Large Flexible Spacecraft," doctor dissertation, Columbia University, 1980.
16. Longman, R. W., and Alfriend, K. T., "Actuator Placement from Degree of Controllability Criteria for Regular Slewing of Flexible Spacecraft," Acta Astronautica, Vol. 8, 1981, pp. 703-718.
17. Juang, J. N., and Rodriguez, G., "Formulation and Applications of Large Structure Actuators and Sensors Placements," Proceedings, 2nd VPI and SU/AIAA Symposium on Dynamics and Control of Large Flexible Spacecraft, 1979.
18. Martin, P. C., "Optimal Allocation of Actuators for Distributed-Parameter Systems," ASME Trans. J. Dynamic Systems, Measurement, and Control, Vol. 100, 1978, pp. 227-228.
19. Lindberg, R. E., "Actuator-Placement Considerations for the Control of Large Space Structures," doctoral dissertation, Columbia University, 1983.
20. Barret, M. F., "Robust Control for Large Space Antennas," Proceedings, NASA/DOD Control/Structure Interaction Technology, Norfolk, Virgina, Nov. 18-20, 1986.

21. Hale, A. L., "Large Spacecraft Pointing and Shape Control," Proceedings, NASA/DOD Control/Structure Interaction Technology, Norfolk, Virgina, Nov. 18-20, 1986.

22. Velde, W. E. V. and He, J., "Design of Space Structure Control Systems Using On-Off thrusters," Journal of Guidance, Vol. 6, No. 1, Jan.-Feb. 1983, pp. 53-60.

23. Balas, M. J., "Direct Velocity Feedback Control of Large Space Structure," Journal of Guidance and Control, Vol. 2, No. 3, May-June 1979, pp. 252-253.

24. Martinovic, Z. N., Haftka, R. T., Hallauer Jr, W. L. and Schamel II, G. C., "A Comparison of Active Vibration Control Techniques: Output Feedback vs Optimal Control," AIAA-87-0904, AIAA/ASME/ASCE/AHS 28th Structure, Structural Dynamics and Materials Conf., Monterey, April 1987, Part 2A, pp. 610-621.

25. Meirovitch, L., Baruh, H., and Oz, H.,"A Comparison of Control Techniques for Large Flexible Systems," Journal of Guidance, Vol. 6, No. 4, July-August 1983, pp. 302-310.

26. Meirovitch, L. and Baruh, H., "Control of Self-Adjoint Distributed-Parameter System," Journal of Guidance, Vol. 5, No. 1, Jan-Feb. 1982, pp. 60-66.

27. Sun, C. T., Kim, B. J. and Bogdanoff, J. L., "On the Derivation of Equivalent Simple Models for Beam and Plate-Like Structure in Dynamic Analysis, Proceedings AIAA Dynamic Specialists Conference, Atlanta, Georgia, April 1981, pp. 523-532.

28. Zienkiewicz, O. C., The Finite Element Method, McGraw-Hill Book Company, 1977.

29. Berry, D. T., Yang, T. Y. and Skelton, R. E., "Dynamic and Control of Lattice Beams Using Simplified Finite Element Models," Journal of Guidance, Vol. 8, No. 5, Sep.-Oct., 1985, pp. 612-619.

30. Przemmieniecki, J. S., Theory of Matrix Structural Analysis, Dover, New York, 1985.

31. Meirovitch, L., Computational Methods In Structural Dynamics, Sijthoff and Noordhoff, The netherlands, 1989.
32. Shabana, A. A., Dynamics of Multibody System, John Wiley and Sons, New York, 1989.
33. James, M. L., et. al., Vibration of Mechanical and Structural Systems, Happer and Row, Publisher, New York, 1989.
34. Greenwood, D. T., Principles of Dynamics, Prentice-Hall, Inc., Englewood Cliffs, N.J., 1988.
35. Penzien, J., Dynamics of Structures, McGraw-Hill, New York, 1975.
36. Meirovitch, L., and Baruh, H., " The Implementation of Modal Filters for Control of Structures," Journal of Guidance and Control, Vol. 8, 1985, pp. 707-716.
37. Schaechter, D. B., and Eldred, D. B., "Experimental Demonstration of the Control of Flexible Structures " Journal of Guidance, Vol. 7, 1984, pp. 527-534.
38. Bayard, D. S., et. al., "Optimal Experiment Design for Indentification of Large Space Structures," Automatica, Vol. 24, 1988, pp. 357-364.
39. Bayard, D. S., et. al., "Frequency Domain Indentification on a Large Flexible Structure," Proceedings, 27th IEEE Conference on Decision and Control, Austin, Texas, 1988.
40. Schafer, B., and Holzach H., "Experimental Research on Flexible Beam Modal Control," AIAA Paper 84-1020, 1984.
41. Montgomery, R. C., "Performance Bound for Testing a Failure Accommodation System for a Flexible Grid," Proceedings, 23rd Conference on Decision and Control, Las vegas, NV, 1984.
42. Honer, G. C., and Inman, D. J., "Microprocessor Controlled Force Actuator," Journal of Guidance, Control and Dynamics, Vol. 11, 1988, pp. 230-236.
43. Juang, J., "Rapid Muti-Flexible-Body Maneuvering Experiments," Proceedings, 27th IEEE Conference on Decision and Control, Austin, Texas, 1988.

44. Greeley, S. W., et. al., "Experimental Demostration of the Maximum Entropy/Optimal Projection Design Theory for Active Vibration Control," Proceedings, 27th IEEE Conference on Decision and Control, Austin, Texas, 1988.

45. Ozguner, U. and Yurkovish, S., "Decentralized Control Experiments on NASA's Flexible Grid," Technical Report CRL-1003-W86-R, Control Research Laboratory, The Ohio State University, 2015 Neil Ave, Columbus, OH 43210, Feb. 1986.

46. Politansky, H., and Pilkey, W. D., "Suboptimal Feedback Vibration Control of a Beam with a Proof-Mass Actuator," Journal of Guidance, Vol. 12, 1989, pp. 691-697.

47. Gorman, D. J., Free Vibration Analysis of Rectangular Plates, Elsevier North Holland, Inc., New York, 1982.

48. Blevin, R. D., Formulas for Natural Frequency and Mode Shape, Van Nostrand Reinhold, New York, 1979.

49. Leissa, A. W., "The Free Vibration of Rectangular Plates," Journal of Sound Vibration, Vol. 31, 1973, pp. 257-293.

50. Astrom, K. J., and Wittenmark, B., Adaptive Control, Addison-Wesley Publishing Company, New York, 1989.

51. Kientzy, D., and Richardson, M., "Using Finite Element Data to Set Up Modal Tests," Sound and Vibration, June 1989, pp. 16-23.

52. Chen, Y. H., "Robust Output Feedback Controller: Direct Design," Int. Journal Control, Vol. 46, No. 1083, 1987.

53. Gutman, S., and Leitmann, G., "Stabilizing Feedback Control for Dynamic Systems with Bounded Uncertainty,"Proceedings IEEE Conf. Decision Control, 1976.

54. Hollot, C. V., and Barmish, B. R.,"Optimal Quadratic Stabilizability of Uncertain Linear Systems,"Proceedings 18th Allerton Conf. Communications, Control Computing, 1980.

55. Athans, M., and Falb, P. L., Optimal Control, McGraw-Hill, New York, 1966.

56. Leitmann, G., "Deterministic Control of Uncertain System via a Constructive Use of Lyapunov Stability Theory," 14th IFIP Conference on System Modelling and Optimization, Leipzig, German Democratic Republic, July 3-7, 1989.

57. Ambrosino, G., Celentano, G., and Garofalo, F., "Robust Model Tracking Control for a Class of Nonlinear Plants," IEEE Trans. Automatic Control, AC-30, No. 275, 1985.

58. Chen, Y. H., "Deterministic Control for a New Class of Uncertain Dynamic systems," IEEE Trans. Automatic Control, AC-32, No. 73, 1987.

59. Venkayya, V. B., and Tischler, V. A., "Frequency Control and the Effect on Dynamic Response of Flexible Structure," AIAA Journal, Vol. 11, 1985, pp. 1768-1774.

60. Sridhar, B., et. al., "Design of a Precision Pointing Control System for the Space Infrared Telescope Facility," IEEE Control Systems Magazine, 1986, pp. 28-34.

61. Burdisso, R. A., and Haftka, R. T., "Optimal Location of Actuators for Correcting Distortions in Large Truss Structures," AIAA Journal, Vol. 27, 1990, pp. 1406-1411.

62. Wie, B., et. al., "New Approach to Attitude/Momentum Control for the Space Station,"Journal of Guidance, Vol. 12, 1989, pp. 714-722.

63. Balas, M. J., "Trends in Large Space Structure Control Theory: Fondest Hopes, Wildest Dreams," IEEE Transactions on Automatic Control, Vol. AC-27, No. 3, June 1982, pp. 522-535.